COO 1195-125

THE REACTION p p→p p $\pi^+\pi^-$ AT 7.9 BeV/c

BY

DONALD FRANK GRETHER
B.A., Miami University, 1962
M.S., University of Illinois, 1964

THESIS

Submitted in partial fulfillment of the requirements
for the degree of Doctor of Philosophy in Physics
in the Graduate College of the
University of Illinois, 1968

Urbana, Illinois

DISCLAIMER

COO 1195-125

THE REACTION p p→p p $\pi^+\pi^-$ AT 7.9 BeV/c

BY

DONALD FRANK GRETHER
B.A., Miami University, 1962
M.S., University of Illinois, 1964

THESIS

Submitted in partial fulfillment of the requirements
for the degree of Doctor of Philosophy in Physics
in the Graduate College of the
University of Illinois, 1968

Urbana, Illinois

THE REACTION p p → p p π^+ π^- AT 7.9 BeV/c

Donald Frank Grether, Ph.D.
Department of Physics
University of Illinois, 1968

The reaction p p → p p π^+ π^- has been studied at an incident momentum of 7.9 BeV/c using the Brookhaven 80 inch hydrogen bubble chamber. Approximately 3600 events of the reaction were identified; the cross section was determined to be $2.54 \pm .13$ mb.

The reaction is found to be dominated by production of the quasi-three body final state N^{*++} p π^-. A simple one pion exchange model is compared to the data and is shown to give generally good results for invariant mass distributions for the entire final state, and for mass and angular distributions for the quasi-three body state. Discrepancies between the data and the model are found to be primarily associated with enhancements in the N^{*++} π^- of p π^+ π^- mass distributions at about 1425 MeV and 1700 MeV. Examination of the 1425 MeV enhancement indicates an apparent interference process rather than an incoherent sum of one pion exchange background and resonance production; the enhancement could not be identified as the N*(1470), the P_{11} wave resonance of π^- p phase shift analysis.

Examination of the $\pi^+ \pi^-$ mass distribution gives some indication for production of the ρ meson, but no indication of other $\pi \pi$ resonances. No evidence is found for resonances with Baryon number = 2.

ACKNOWLEDGEMENTS

I would like to express my appreciation to Professor Robert D. Sard, my advisor, for his interest and support during this research.

Many of the physicists at Illinois gave advice and assistance at various stages of the experiment. I thank them all. I am particularly indebted to Mr. Jerald J. Wray for his extensive and invaluable contributions to the lengthy process of converting the raw data to a form suitable for analysis.

For their capable efforts and spirit of cooperation, I thank the Scanners, Measurers, Ionizers, Bookkeepers, Engineers and Programers associated with this experiment.

Finally, I am sincerely grateful to my wife, Becky, and to our parents for their understanding and encouragement throughout my years of graduate study.

TABLE OF CONTENTS

I. INTRODUCTION

As part of an investigation at the University of Illinois of proton-proton interactions at 7.9 BeV/c, we report on the final state p p π^+ π^-. The results of a study of the final states involving strange particles have been reported elsewhere.[1,2]

The general features of the p p π^+ π^- final state at 7.9 BeV/c are consistent with those reported in investigations at 4.0 BeV/c,[3] 5.5 BeV/c,[4] 6.6 BeV/c,[5] 8.1 BeV/c,[6] and 10.0 BeV/c.[7,8] The final protons and proton-pion combinations are peripheral in nature. The p π^+ invariant mass distribution shows strong production of N^{*++} (1236); the p π^- distribution shows resonant structure at the invariant masses of the first three resonant peaks observed in the π^- p scattering cross section. The p π^+ π^- distribution shows some evidence for resonance production, particularly around 1700 MeV. Any contribution to the final state from channels involving resonances with Baryon number = 2 or meson resonances (e.g. the ρ) is small, if present.

The absence of strongly competing channels allows a relatively clean separation of the quasi-three body final state $N^{*++}(1236)\ p\ \pi^-$. A simple one pion exchange model is compared to our data at 7.9 BeV/c and is shown to give generally good results for invariant mass distributions for the entire final state, and for mass and angular distributions for the quasi-three body state. Differences between the data and the model are shown to be primarily associated with the resonance(s) at 1700 MeV in the $p\ \pi^+\pi^-$ (and $N^{*++}\ \pi^-$) mass distribution and with a possible resonance at about 1425 MeV that appears as an enhancement in the $N^{*++}\ \pi^-$ mass distribution. This enhancement has been attributed to a kinematic effect arising from one pion exchange (Deck effect) at 6.6 BeV/c[5] and at least in part to the N* (1470), the P_{11} wave resonance of phase shift analysis, at 8.1 BeV/c[6] and 10.0 BeV/c.[7,8] The enhancement in our data is examined in detail and found to not correspond to an incoherent sum of one pion exchange and resonance production. We are not able to interpret the enhancement as partially due to production of the N* (1470).

Examination of the p p, p p π^+, and p p π^- mass distributions yields no evidence for resonances with Baryon number ≤ 2. In particular, no evidence is seen for the

candidate for a p p π^+ resonance at 2520 MeV reported at 4.0 BeV/c.[3] A small enhancement in the π^+ π^- mass distribution at roughly 700 MeV is investigated and found to possibly correspond to the ρ meson.

II. EXPERIMENTAL PROCEDURE

A. Raw Data

The data are from an exposure of the Brookhaven 80 inch hydrogen bubble chamber to a separated beam of protons from the Alternating Gradient Synchrotron. The nominal beam momentum was 8 BeV/c; the actual momentum at the center of chamber was later determined to be 7.87 BeV/c (Section II, H). The film, taken in July, 1964, consisted of some 37,800 pictures divided more or less evenly among 41 rolls. Thirteen of these rolls were judged to be of inferior quality and were not used. The present experiment dealt with about 25,000 pictures from the remaining 28 rolls.

B. Relationship to the Strange Particle Analysis

Between July, 1964 and the summer of 1965 the film was scanned and measured for strange particle events with visible decays. These events were analyzed by M. W. Firebaugh.[1,2] Many of the scanning and measuring procedures of the experiment reported here were adopted from those of Firebaugh. The properties of the magnetic field and of the liquid hydrogen were determined in his work.

THIS PAGE
WAS INTENTIONALLY
LEFT BLANK

frame number, the type of event (4 or 6 prong), the region number, the sequence number, flag information and occasionally a sketch of the event. The region number localized the vertex to one of four regions of the chamber as seen in view 3 (Figure 1). For frames with more than one event* sequence numbers were assigned to the vertices of the events, numbering from the upstream to the downstream end of the chamber. The flag information consisted of numeric codes indicating the presence of Dalitz pairs, "kinks" (scatters) or other interactions on secondary tracks, etc. This information helped to identify events as well as to alert the measurer to, for example, the presence of a scatter on a secondary track so that he would not measure past the scatter.

Of the 28 rolls, 23 were scanned once. The remaining 5 rolls were scanned twice in order to calculate efficiencies. The scanning produced 19,461 4 prong events and about 1/6 as many 6 prongs. The scanning efficiency for the 4 prong events was calculated assuming that events missed in one of the scans were uncorrelated with those missed in the other. The calculated efficiency was essentially 100% for

---

*There were, on the average, 4 events for every 5 frames. Statistical fluctuations made it not uncommon to find 2-5 events/frame.

Figure 1

Definition of the scanning fiducial volume, the cross section fiducial volume, and the regions. The fiducials (and thus volumes and regions) are shown projected to the center plane of the chamber along the light ray to camera 3.

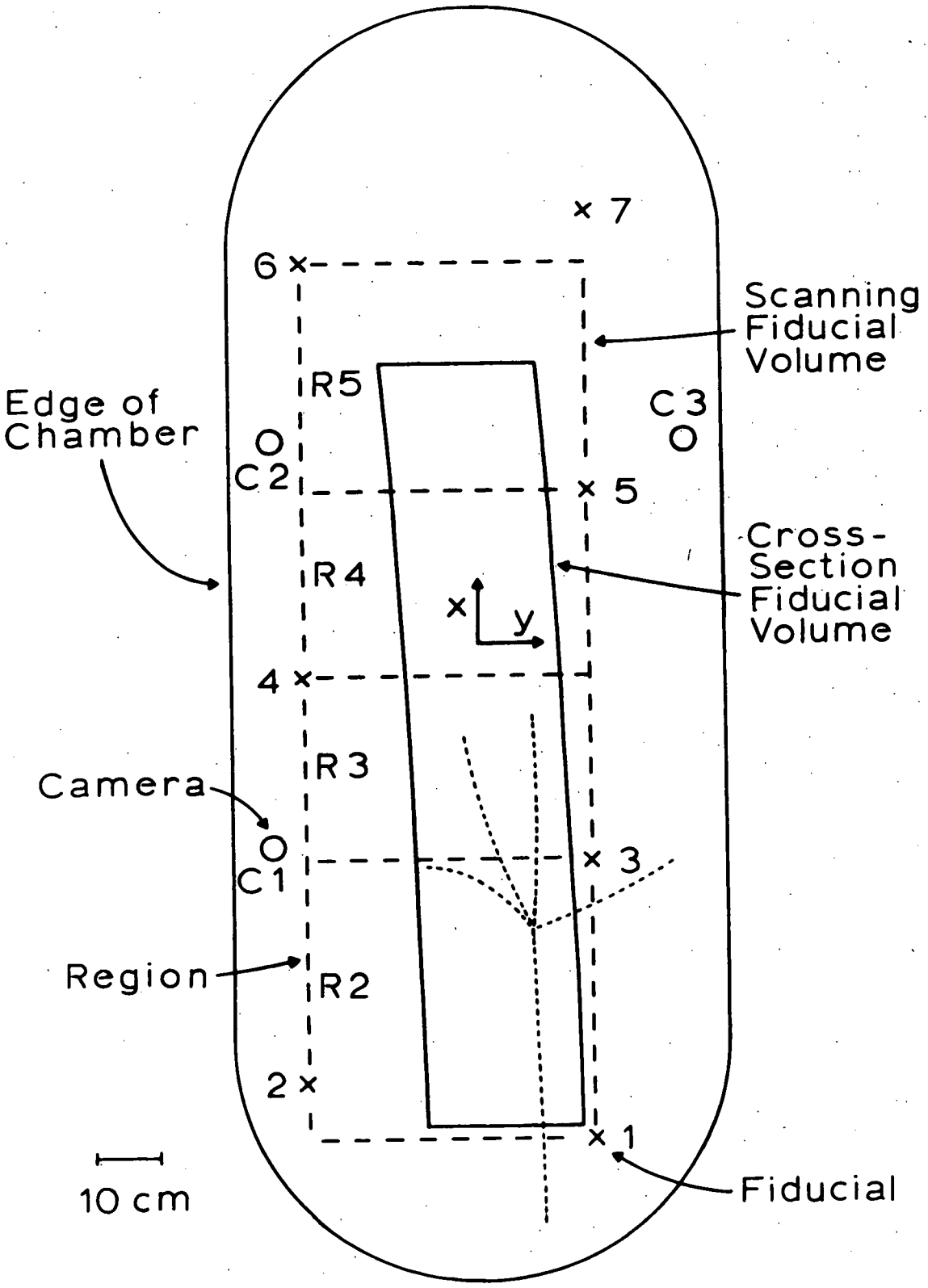
× 7
6 ×
Scanning
Fiducial
Volume
R5
C3
O
Edge of
Chamber
O
C2
× 5
Cross-
Section
Fiducial
Volume
R4
x
y
4 ×
R3
Camera
O
C1
× 3
Region
R2
2 ×
× 1
Fiducial
10 cm

the 5 double scanned rolls with an inferred efficiency of 98% for the single scanned rolls.

D. Measurement

The measuring was done by non-physicists on conventional digitized measuring projectors. An Itek-Hermes was used for the bulk of the measuring; a few hundred of the events were measured on a NRI-MPS3. These machines have fixed optics and a moveable stage digitized by encoders to least count 1 micron. Measurers viewed the film at a magnification that gave an image close to life size, and at this magnification were capable of an accuracy of about 50 microns in real space. Indicative information (roll number, frame number, etc.), x,y coordinates of fiducials and x,y coordinates of points along the tracks were recorded on punched cards in a form suitable for computer analysis. Three fiducials (2,4,7) were measured in each of the three views. Each track was measured in two views, as required by the spatial reconstruction program.

The scanners made no attempt to determine whether an event could be successfully measured. The measurers, however, were permitted to reject an event under certain conditions. The primary cause of rejected events was the "flare", the reflection of the bubble chamber flash tube

into the camera lenses. An event was rejected if the flare obscured a track in one of the views needed for reconstruction of that track. An event could also be rejected if, for example, the tracks were very faint or the vertex was obscured by beam tracks. Of the scanned 4-prongs 6.5% were rejected and thus not measured. The 6-prongs were measured in about 2/3 of the film. They will not be considered further.

E. Spatial Reconstruction and Kinematic Fitting

The events were reconstructed by the program EUCLID, and the program ILLFIT was used for kinematic fitting. Both programs were developed at Illinois by Professor G. Ascoli and are discussed in references 1 and 9. We consider here aspects of these programs relevant to later discussion.

The input to EUCLID consists of the x,y coordinates of the fiducials and points along the track, and the bubble chamber constants. EUCLID outputs for a given track and mass hypothesis the parameters ϕ, $\tan\lambda$, k at the vertex and an error matrix for the uncertainties in these parameters. The coordinate system is shown in Figure 1 (the z axis points into the chamber). ϕ is the angle between the x axis and the projection of the track in the x,y plane,

λ is the angle between the track and the x,y plane and $k = 1/p \cdot \cos \lambda$ where p is the magnitude of the vector momentum.

ILLFIT subjects an event to various hypotheses consistent with conservation of charge, baryon number and strangeness. Given the hypothesized mass, ϕ, $\tan\lambda$, k and the error matrix for each measured track, ILLFIT adjusts the parameters in a least squares sense to determine any unmeasured variables (such as for a neutral particle) as well as to satisfy the constraints imposed by conservation of four momentum. ILLFIT outputs the fit values for ϕ, $\tan\lambda$, k for each track and an error matrix that takes into account the correlations between tracks. A χ^2 is obtained as a measure of the amount of adjustment relative to the estimated errors necessary to satisfy the constraint equations. ILLFIT also calculates the "missing momentum" and "missing mass."

$$\vec{P}_m = \vec{P}_b - \Sigma \vec{P}_i$$

$$E_m = M_t + E_b - \Sigma E_i$$

$$M_m^2 = E_m^2 - P_m^2$$

where $\vec{P}_m$ and E_m are the missing variables, M_m the missing

mass, M_t the target mass, and $\vec{P}_b$ and E_b ($\vec{P}_i$ and E_i) the measured momentum and energy for the beam (secondary tracks). A correct hypothesis involving no neutral particles would be expected to have missing variables and mass equal to zero within the errors. A correct hypothesis involving a neutral particle would be expected to have a missing mass equal, within errors, to the rest mass of the neutral particle.

Table 1 lists the hypotheses tested in this experiment. Fit numbers 1,3 and 5 are the appropriate ones for the final state of interest, p p π^+ π^-. For most events these hypotheses are constrained by all four conservation of momentum equations and are known as "4-C" fits. Some events have a secondary interaction so close to the vertex that only the direction of the interacting track may be determined well and the magnitude of the momentum (and hence k) is either unknown or known only to within a large error. If the track had only two measured points (undetermined momentum) or if

$$(\delta k)^2/k^2 > .5$$

then k was treated as an unknown. The event is "constraint reduced"; one constraint equation is effectively

Table 1

Fit Number	Track 2	3	4	5	1-C Fit Neutral	mm Hypothesis Neutrals
1	p	p	π^+	π^-	-	-
2	p	p	π^+	π^-	π^o	2 π^o
3	p	π^+	p	π^-	-	-
4	p	π^+	p	π^-	π^o	2 π^o
5	π^+	p	p	π^-	-	-
6	π^+	p	p	π^-	π^o	2 π^o
7	p	π^+	π^+	π^-	n	n + π^o
8	π^+	p	π^+	π^-	n	n + π^o
9	π^+	π^+	p	π^-	n	n + π^o
10	π^+	π^+	π^+	π^-	-	2n

removed to determine the unknown variable and the 4-C fit becomes a 3-C fit.

Fit numbers 2, 4 and 6-9 are for the hypotheses with one neutral particle. Before attempting a fit ILLFIT requires that the missing mass be "reasonable." Specifically, no fit is tried if

$$\left|(M_m^2 - M^2)/\delta M_m^2\right| > 6$$

where M is the mass of the hypothesized neutral. Effectively three of the constraint equations are used to determine the parameters of the neutral and these hypotheses are thus 1-C fits. Constraint reduced events cannot be fit to hypotheses with one neutral.

For Fit numbers 2, 4 and 6-10 we associate hypotheses with two or more neutral particles. There are insufficient constraint equations to allow a fit and these hypotheses are called "missing mass" or "mm." Table 1 gives the two neutral particles of minimum rest mass for each mm hypothesis. For post-ILLFIT analysis it was considered desirable to obtain some quantitative criteria for judging the kinematic probability of a mm hypothesis. Let M_0 be the sum of the rest masses of the 2 neutrals and consider $\vec{P}_m$ to be the momentum of the neutral system. Then $E_0 = (\vec{P}_m^{\,2} + M_0^2)^{\frac{1}{2}}$ is

the minimum energy needed to make the hypothesis kinematically possible. To account for errors we construct a mm probability, P_{mm}. Let $x = E_m - E_0$ then

$$P_{mm} = 1 \ , \ x \geq \delta x$$

$$P_{mm} = e^{-(x - \delta x)^2/(\delta x)^2} \ , \ x < \delta x$$

P_{mm} is "reasonable" in the sense that it gives a high probability if the missing energy, E_m, is close to or greater than the minimum energy required and gives a low probability if E_m is much less than E_0.

Not all measurements could be successfully reconstructed by EUCLID. The failures could usually be attributed to measurer's errors. Typically, 20% of a measurer's events failed. All events were measured until they either reconstructed or had failed to reconstruct after three measurements. Of the measured events 3.6% had failed to reconstruct after these three tries.

Of the events that were both measured and successfully reconstructed (17,532 events) 1.2% had all fits rejected by ILLFIT and no missing mass hypothesis considered kinematically "reasonable" ($x/\delta x \geq -6$). A sample of these events was examined in some detail. It was found that for most of

the events in the sample the problem could be attributed to measuring errors that had escaped the checks in the reconstruction program.

F. Ionization

Ionization information can be used to supplement the output of ILLFIT in designating an event as belonging to a particular final state. The first 20% of the events measured were "ionized." A discussion of the application of the ionization to the separation of hypotheses is given in the next section. We discuss here the method of obtaining the information.

Each event was ionized on the scanning table by two non-physicists working independently. Each "ionizer" made visual estimates of the ionization of the secondary tracks relative to the minimum ionizing beam tracks. Experience indicated that the ionizers could reliably separate protons from π's and K's on tracks with momentum less than 1300 MeV/c and π's from K's on tracks with momentum less than 700 MeV/c. A track was considered as not ionized if the two ionizers disagreed. The accuracy of the ionization was checked in two ways. First, the per-cent of ionized tracks for which both ionizers are wrong was calculated, given the per-cent of tracks on which the ionizers disagreed and under the assumption that mistakes are uncorrelated. This check

indicated that the ionizers were both wrong on .25% of the ionized tracks. For the second check the ionizers' results were compared to those of a physicist on a sub-sample of events. This check indicated that the ionizers were both wrong on about 1% of the ionized tracks. We accept this latter percentage as the more realistic.

G. Selection of Hypotheses

For this experiment it was considered necessary only to select events belonging to the final state p p π^+ π^-. We identified an event to be of this final state if it had at least one 4-C fit with $\chi^2 \leq 1.85$ or 3-C fit with $\chi^2 \leq 16.3$. These cutoffs correspond to a theoretical χ^2 probability of .1%. The measured events yielded 3598 events satisfying the above criterion, 3449 4-C and 149 3-C. We considered an event to be ambiguous between two 4-C (or 3-C) fits if at least one of the fits met the above criterion and the χ^2 probabilities for the two fits were within a factor of 10. There were 118 such events. They are characterized by being ambiguous with respect to the exchange of proton and π^+ mass assignments of two tracks of nearly equal magnitude of momentum. In 53 of the ambiguous events these tracks had low enough momentum to allow

ionization to select the correct fit.* For the remaining events the fit with the smallest χ^2 was chosen. Extrapolation from the ionized events predicts that for 1/3 of the non-ionizable events (less than 1% of the 3598 4-C and 3-C events) the wrong fit has been chosen.

We now consider several sources of contamination from events that have been identified as p p π^+ π^- by the above criterion but that actually belong to some other final state. We begin by discussing ambiguities between the selected fit and other hypotheses. We define an event to be ambiguous between the selected fit and a second hypothesis if the ratio of χ^2 probability (or mm probability) of the second hypothesis to that of the selected fit is greater than 1/10.

The largest class of ambiguities is between a 4-C fit to p p π^+ π^- and 1) a 1-C π^o fit, or two π^o mm hypothesis, with a proton and π^+ interchanged (e.g. fit 1 and fit 4), 2) a 1-C neutron fit, or neutron plus π^o mm hypothesis, with a proton changed to a π^+ (e.g. fit 1 and fit 7). To study these ambiguities we examined the events in the ionized part of the film. Disregarding the ionization, of the 674

---

*The author ionized the ambiguous events in the 80% of the film not ionized by non-physicists.

4-C events 177 were ambiguous. Of these ambiguous events the ionization information uniquely selected the 4-C fit in 153, ruled out the 4-C fit in two and could not resolve the ambiguity in the remaining 22. Allowing for a 1% error in the identification by ionization of the uniquely selected events* and assuming that the unresolved events are distributed in the same way as the resolved ones, we estimate that the 1-C and mm states considered here represent a contamination of not more than 1% of the total sample of 4-C events.

A less tractable type of ambiguity is that between a 4-C fit and the 1-C π^o fit with no permutation of masses (e.g. fit 1 and fit 2) since the ambiguity cannot be resolved by ionization. The number of events with an ambiguity of this type constitutes 3% of the total number of 4-C events. These events typically have a high momentum (4-7 BeV/c) secondary track with a relatively high error (greater than 2% compared to the more usual 1%). We conjecture that these events are essentially all 4-C events and that the high error in momentum permits the π^o fit. If this conjecture is wrong and if we should choose the fit

---

*The ionization of the 2 non 4-C events was verified by the author.

with the highest χ^2 probability then this ambiguity represents a contamination of 1.5%.

Not all of the 4-prong events can be attributed to the final states of Table 1. In particular strange particle final states with undetected decays can give the 4-prong topology. From reference 1 we estimate that about .3% of the scanned 4-prongs are from the 4 body states p K^+ Σ^+ $\pi\pi$, p K^+ π^+ Σ^- with undetected decays (mostly decays of Σ^+s along the line of flight) and that less than 3% are from states with 5 or more bodies with undetected Σ, Λ^o and K^o decays (e.g. p K^+ π^+ π^- Λ^o). These latter states should contribute essentially nothing to the contamination since we have shown that the far more numerous 5 or more body states of Table 1* rarely fake a fit to p p π^+ π^-. If, at worst, all of the 4 body strange particle states fake p p π^+ π^-, the resulting contamination would be about 1%. Reference 1 does not allow a reliable estimate of the number of p p K^+ K^- events because of the low detection efficiency for charged K's in a bubble chamber. To study contamination from these events we refit the ionized events identified as p p π^+ π^- to the p p K^+ K^- hypothesis.

---

*The p p π^+ π^- events constitute roughly 1/5 of the measured events. Thus, by default, the other non-strange final states account for about 4/5 of the events.

Out of the 674 events, 7 were ambiguous with this latter hypothesis. Ionization selected the p p π^+ π^- fit in 4, the p p K^+ K^- in 1 and could not resolve 2. We conclude that the strange particle events are not a significant source of contamination.

Since constraint reduced events have no 1-C fits or missing mass calculations the 3-C events cannot be checked for contamination from 5 or more body states as could the 4-C. We did not exclude the 3-C events because constraint reduction has some tendency to occur on high momentum tracks. Thus the constraint reduced events are not an unbiased sample. To examine the possibility that the 3-C fits are to some large extent extraneous we artificially contraint reduced 438 random events. Of these, 94 had a 4-C fit with χ^2 less than 18.5 all but one of which reduced to the corresponding 3-C fit with χ^2 less than 16.3. Of the remaining 344 events, 3 had a 3-C fit with χ^2 less than 16.3 upon constraint reduction. We conclude that out of the 610 actual constraint reduced events only a few of the 149 identified as p p π^+ π^- are extraneous.

From the above considerations we estimate that the overall contamination of the 3598 events identified as p p π^+ π^- is 2 $\mp$ 2%.

In the preceding discussion we defined ambiguity on the basis of the theoretical χ^2 probability. This probability is correct in a strict sense only if the experimental χ^2 distribution agrees with the theoretical prediction. If the errors have been uniformly underestimated (or overestimated) by a factor of "a" then we expect

$$\chi^2_{\text{true}} = \chi^2_{\text{exp}}/a^2.$$

For the 4-C events the experimental distribution was fitted (least squares) to the theoretical prediction using a^2 as an adjustable parameter. The fitted value was $a^2 = 1.47$. In Figure 2 we show the experimental distribution and the theoretical curve for the fitted value of a^2. The discrepancy between the general shape of the distribution and the theoretical curve indicates that the errors are not altogether uniformly underestimated.

If we apply the above value of a^2 to both the 4-C and 3-C fits then the χ^2_{exp} cutoffs of 18.6 and 16.3 are cutoffs of 12.65 and 11.1 for χ^2_{true} with corresponding probabilities of 1.3% and 1.1%. In the above study of ambiguities we defined a 1-C fit to be ambiguous with a 4-C fit if the ratio of probabilities using χ^2_{exp} was greater than 1/10. To examine what effect the correction

Figure 2

χ^2 distribution for the 3449 4-C events identified as p p π^+ π^-. The smooth curve is discussed in the Text.

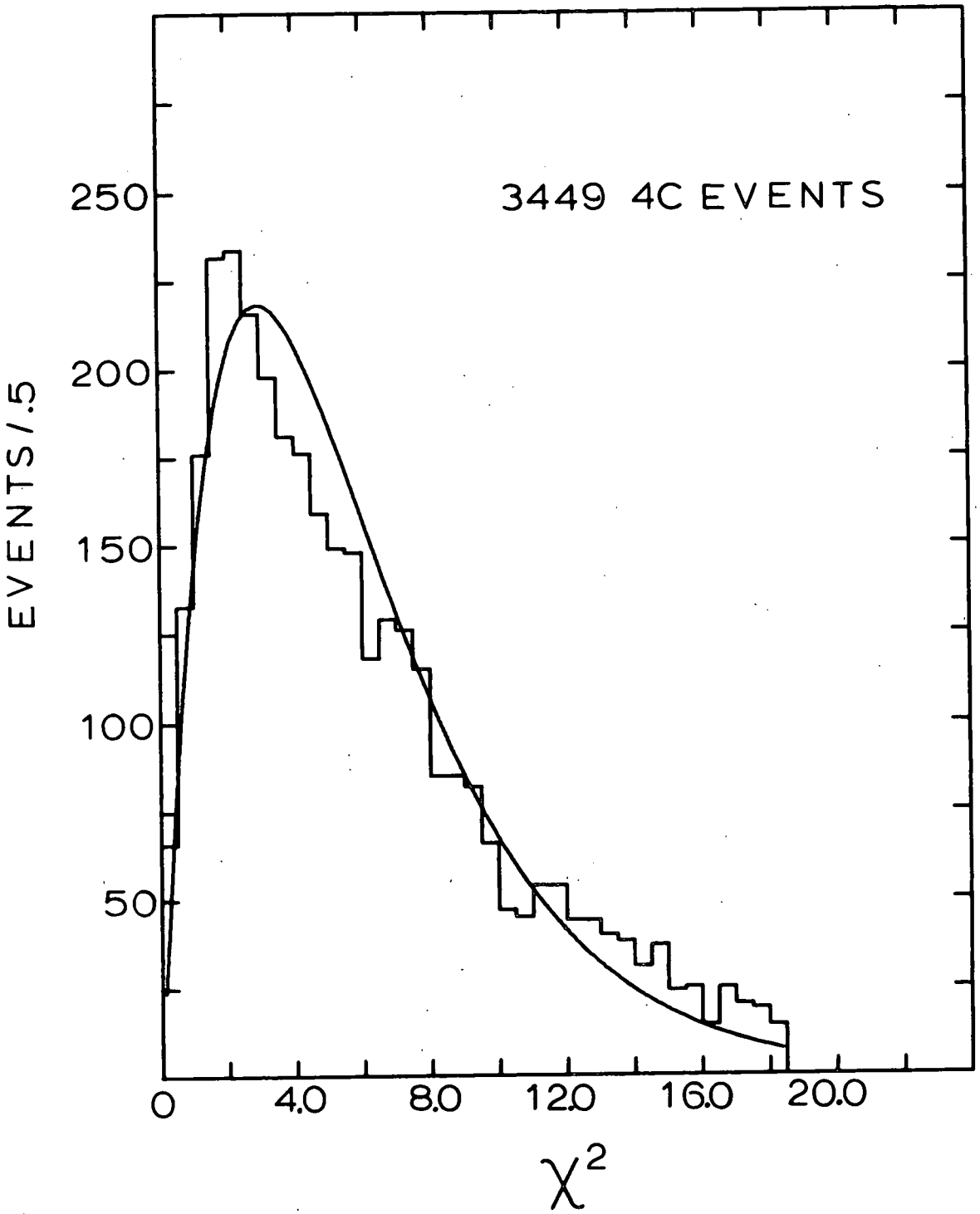
3449 4C EVENTS
EVENTS/.5
250
200
150
100
50
0
4.0
8.0
12.0
16.0
20.0
χ^2

factor a^2 would have on this definition we assume that the value 1.47 applies to the 1-C fits (as well as to the 4-C fits). Then, using χ^2_{exp} and a ratio of 1/10 corresponds to using χ^2_{true} and a ratio that varies from 1/5 to essentially 1/10 as χ^2_{true} for the 4-C fit varies from 0 to 12.65. This variation would not effect to any large extent our estimates of the amount of contamination.

For cross-section purposes it is necessary to correct for the number of events missed by the χ^2 cutoff. Experimentally, there were 249 events with a 4-C fit with χ^2 between 18.5 and 40.0, or 7.2% of the number with χ^2 less than 18.5. The theoretical prediction for $a^2 = 1.47$ is 1.4%. We attribute the discrepancy to both the non-uniform underestimate of the errors and contamination. We correct the cross-section by $5 \pm 3\%$.

H. Beam Momentum

The beam momentum was obtained for 250 events with unambiguous 4-C fits to p p π^+ π^-. These events were fitted again with k of the beam track treated as an unknown. For each event ILLFIT thus solved for k of the beam at the vertex, subject to three constraint equations (3-C fit). For a beam track $\cos\lambda$ is nearly equal to 1 and thus solving for k is essentially equivalent to solving for the beam

momentum. For each event the resulting beam momentum was extrapolated to the center of the chamber, allowing for energy loss. The beam momenta were then weighted by the inverse square of the error assigned by ILLFIT. The weighted average was $7.875 \pm .005$ BeV/c. The weighted rms width of the distribution was .088 BeV/c.

III. CROSS SECTION

The cross section for the final state p p π^+ π^- was obtained for only those events inside a "cross section" fiducial volume. This volume, shown in Figure 1, is internal to the scanning fiducial volume so that mistakes made by the scanners in assigning vertices to the scanning volume would not effect the cross section calculation. The sides have the orientation and curvature of the beam tracks to facilitate calculation of the total track length.

The cross section is given by the standard formula:

$$\sigma = (M_H / (\rho L_T)) N$$

where

M_H = mass of the hydrogen atom = 1.673×10^{-24} gm

ρ = density of the hydrogen[1] = .0629 gm/cm^3

L_T = total beam track length

N = corrected number of events

The total track length was determined from a count of beam tracks in every 10th frame in view 3. The tracks were counted on a line that passed thru fiducial 3 and that was

limited by the sides of the cross section fiducial volume. We estimate that the count is accurate to within $\pm$ 2%. The attenuation of the beam tracks is given by:

$$dI(x)/dx = -I(x)\sigma_T\rho/M_H = -I(x)\lambda$$

where

I = number of beam tracks

σ_T = the total pp cross section = 40.0 mb[10]

From this equation we calculate

$$L_T = 10 \cdot I_3 \cdot (e^{\lambda L_3}/\lambda) \cdot (1 - e^{-\lambda L})$$

where

I_3 = number of beam tracks at fiducial 3
= $30569(1 \pm .02)$

L = length of a beam track in the fiducial volume
= 120.2 cm

L_3 = length of a beam track from the upstream end of the fiducial volume to fiducial 3
= 41.7 cm

We then calculate that

$$\sigma = 7.43\ (1 \pm .02) \times 10^{-4} \cdot N\ (mb)$$

The number of 4-C and 3-C events inside the cross section fiducial volume totals 2899. We correct this number by the values given earlier for 1) scanning efficiency, 2) events not measured, 3) events which failed to reconstruct, 4) events with all fits rejected and no reasonable mm hypothesis, 5) contamination, 6) the χ^2 cutoff. The correction factor is then $1.18\ (1 \pm .04)$ where the error estimate comes from the uncertainty in the contamination and the χ^2 cutoff. Including the statistical uncertainty in the uncorrected number of events, we obtain

$$\sigma = 2.54 \pm .13 \text{ mb.}$$

This value may be compared to cross sections obtained for the same final state in experiments at nearby beam momenta: $2.6 \pm .3$ at 6.6 BeV/c,[5] $2.42 \pm .10$ at 8.1 BeV/c,[6] and $2.4 \pm .2$ at 10 BeV/c.[8]

IV. ANALYSIS

A. Production Cosines

One of the most striking features of the final state p p π^+ π^- is the peripheral nature of the protons and proton-pion combinations. We discuss this feature in terms of the "production cosine", defined in the overall center-of-mass as the cosine of the angle between the three-momentum vector of a particle (or combination of particles) and that of an incident proton. Since there are two incident protons, two production cosines may be calculated for each particle or combination. Figure 3 shows the distributions of positive production cosines for the final protons, p π^+ combinations, π^+'s and π^+ π^- combinations. By conservation of momentum the p π^- distribution is identical to that of p π^+ , p π^+ π^- to that of the protons, etc. The π^- distribution (not shown) is similar to that of π^+. Also shown are the proton and p π^+ distributions when the proton in combination with the π^+ is in the mass band of the N*(1236) (defined as $1.15 \leq M(p\ \pi^+) \leq 1.30$ BeV/c)*. The

---

Here and in subsequent analyses we adopt the convention of plotting two quantities (e.g. p π^+ production cosines) from a single event when both quantities meet a selection criterion (e.g. p π^+ in N mass band).

Figure 3

(a) Unshaded. Production cosine for all p π^+ combinations.

Shaded. Production cosine for those p π^+ combinations in the N^{*++} mass band.

(b) Unshaded. Production cosine for all protons.

Shaded. Production cosine for those protons which, in combination with the π^+, are in the N^{*++} mass band.

(c) Production cosine for all π^+'s.

(d) Production cosine for all π^+ π^- combinations.

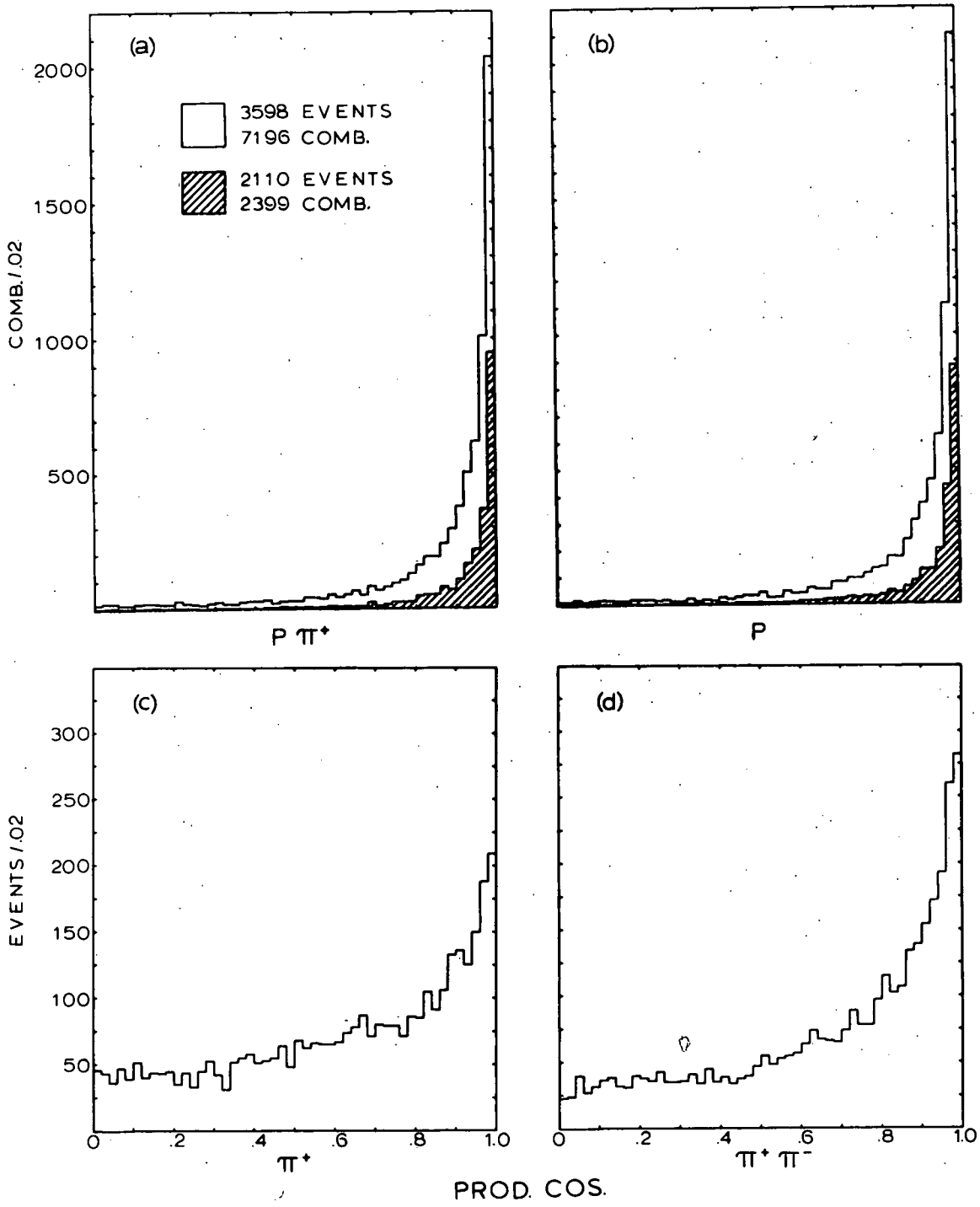
(a)
3598 EVENTS
7196 COMB.
2110 EVENTS
2399 COMB.
COMB./.02
2000
1500
1000
500
P π⁺
(b)
P
(c)
EVENTS/.02
300
250
200
150
100
50
0
.2
.4
.6
.8
1.0
π⁺
(d)
π⁺ π⁻
PROD. COS.

sharp peaking of the proton and proton-pion distributions towards large production cosine is suggestive of a peripheral production mechanism. In subsequent analysis we take advantage of this peripherality by identifying a final proton (or proton-pion combination) as having originated from the initial proton to which it has the positive production cosine (or, equivalently, the smallest Δ^2, the square of the four-momentum transfer).

B. One Pion Exchange Model

The suggestion that the data results from a production mechanism yielding peripheral protons and proton-pion combinations invites comparison of the data to a one pion exchange model (OPEM). The two possible Feynman diagrams for the exchange of a single pion are shown in Figure 4. Calculations of these diagrams have met with some success when applied to the state p p π^+ π^- at several incident momenta (2.0 and 2.85 BeV/c,[11] 4 BeV/c,[3] and 10 BeV/c[7,8]). Calculations of similar diagrams have been compared to the three and four body strange particle states at our momentum[1,2] with generally good results.

We use the calculation of diagram (a) of Figure 4 as given by Ferrari and Selleri.[12]

Figure 4

The two possible Feynman diagrams for the exchange of a single pion in the reaction

$$p\ p \rightarrow p\ p\ \pi^+\ \pi^-$$

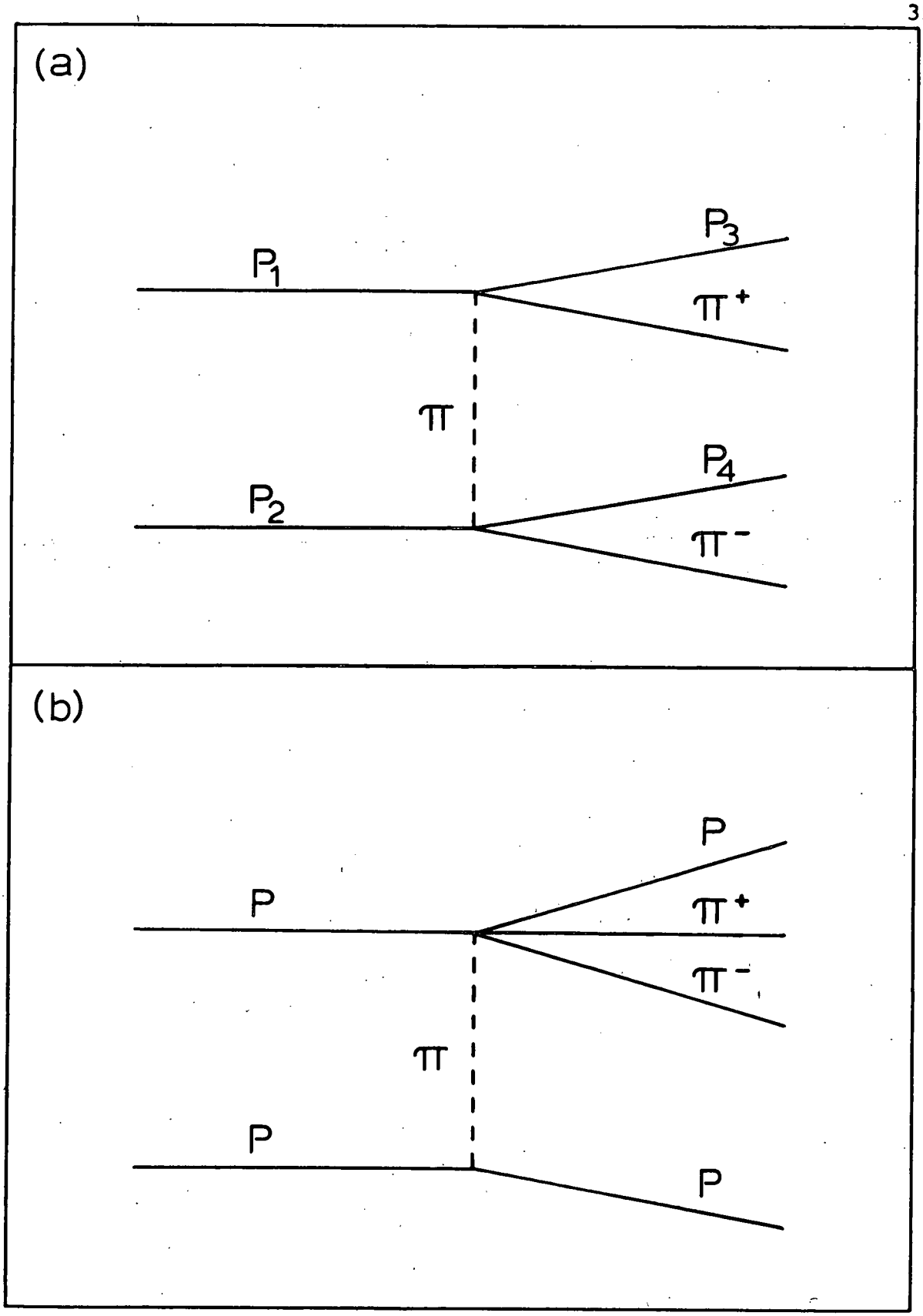
(a)
P1
P2
P3
P4
π
π+
π−
(b)
P
P
P
P
π
π+
π−

$$(1)\quad \frac{d\sigma}{d\omega^+ d\Omega^+ d\omega^- d\Omega^- d\Delta^2} = \left(\frac{1}{16\pi^3 F^2}\right) x \left(2(\omega^-)^2 P^+ \frac{d\sigma^+}{d\Omega^+}(\omega^+,\Omega^+)\right)$$
$$x\left(\frac{R(\omega^{\pm},\omega^-,\Delta^2)}{(\Delta^2 + m^2)^2}\right) x \left((2(\omega^-)^2 P^- \frac{d\sigma^-}{d\Omega^-}(\omega^-,\Omega^-))\right)$$

where + (-) refers to the $\pi^+ p$ ($\pi^- p$) vertex and

m (M) = mass of a pion (proton)

$F^2 = (P_1 \cdot P_2)^2 - M^4$ = flux factor

P_1, P_2 = four momentum of the incident protons

ω = π p invariant mass

P = magnitude of three-momentum of the outgoing proton in the π p rest frame.

$\frac{d\sigma}{d\Omega}(\omega,\Omega)$ = the physical π p elastic scattering differential cross section in the π p rest frame.

Δ^2 = the square of the four momentum transfer from an incident proton to a final proton-pion combination.

$R(\omega^+,\omega^-,\Delta^2)$ is a form factor.

The form factor "R" is as developed by Ferrari and Selleri[13] can be written as

$$(2)\quad R(\omega^+,\omega^-,\Delta^2) = \left(K'(\Delta^2)\ K(\Delta^2)\ Q(\omega^+,\Delta^2)\ K(\Delta^2)\ Q(\omega^-,\Delta^2)\right)^2$$

where K' is an unknown form factor for the pion propagator, K is an unknown form factor at each proton-pion vertex, and Q is a form factor that corrects the physical proton-pion cross section so that it corresponds to the off-the-mass-shell scattering of the exchanged pion. Q has been calculated[13,14,15] but with various results and then only for values of ω near the N*(1236) where one partial wave dominates. Empirical forms have been given[13,14] for the products $K'K^2$ and $K'K^2Q$ (ω outside the N*(1236) region).

A cross section for diagram (b) may be expressed in terms of the physical but experimentally unattainable process

$$\pi^o\ p \rightarrow \pi^+\ \pi^-\ p$$

and unknown form factors.[11] Actual calculations[3,11] have invoked isotopic spin arguments to relate the above process to the $\pi\ \pi$ N states of $\pi^{\pm}p$ inelastic scattering. In addition these calculations are made assuming that the empirical form factors obtained for virtual pion-proton elastic scattering apply to virtual pion-proton inelastic scattering.

---

*The result obtained by Ferrari and Selleri in reference 13 has been criticized by Jackson.[15] Selleri[14] has defended the result of reference 13 while deriving a less approximate version.

In subsequent analysis we compare the data to a calculation for diagram (a) only. This calculation provides a quite reasonable description of the background and thus we feel justified in neglecting diagram (b) and its associated complexity and uncertainty. However, in view of our neglect of this latter diagram (as well as other possible exchange diagrams) detailed considerations of equation (2) are of questionable value. We substitute the simple form factor

$$R(\Delta^2) = (A / (A + \Delta^2))^2 \tag{3}$$

with "A" treated as an adjustable parameter. (A similar form was used by Ferrari[11] at 2.0 and 2.85 BeV/c; at 4 BeV/c[3] and 10 BeV/c[7,8] the form given by our equation (2) was used.)

Equation (1) was evaluated by Monte-Carlo methods using pion-proton differential elastic scattering cross section data available in the literature (some details are given in Appendix A). A set of "events" was generated randomly* that, taken as a whole, satisfied equation (1). In comparing the data to the model the Monte-Carlo events

---

*A computer program was used that was adopted from one written at Illinois by U. E. Kruse and B. Terreault.

were subjected to the same selection criteria as the real events. Thus for the model we "forget" which proton in an event is at the upper vertex of diagram (a) and which at the lower.

C. The Proton-Pion System

To examine the extent to which the OPEM describes the data we discuss in this section the data in terms of variables appropriate to the model. These variables are the Δ^2, mass, and angular distributions of the proton-pion combinations.

1. The p π^+ Mass Distribution

The strong production of the $N^{*++}(1236)$ dominates the p p π^+ π^- final state at the incident beam momentum of this experiment. This strong production is seen in Figure 5a, a histogram of all p π^+ invariant mass combinations. Superimposed on the histogram are the predictions of Lorentz invariant phase space and of the OPEM, both normalized to the number of experimental combinations. The OPEM prediction is for the form factor of equation (3) with $A = 3(\text{BeV}/c)^2$. As discussed below, this value was chosen to bring the model's Δ^2 distribution to the p π^+ combinations in the N* mass band into rough agreement with

that of the data. For events with a p π^+ in the N^{*++} the other p π^+ invariant mass contributes to the background of the distribution in Figure 5a. Thus the data appear consistent with most of the events having a proton in the N^{*++}. To obtain an estimate of the number of N^{*++} events, a simple Breit-Wigner resonance form was fitted to the p π^+ distribution with the background approximated by phase space. The fit resulted in $45 \pm 1\%$ of the combinations being assigned to the resonance, corresponding to about 90% of the events having a p π^+ combination in the N^{*++}.

The height of the N^{*++} peak may be enhanced relative to the background by selecting the more peripheral p π^+ combinations. Figure 5b shows the distribution for $|\text{prod. cos } (p\ \pi^+)| \geq .96$. This selection criterion is satisfied by at least one p π^+ combination in 2216 events and by both combinations in 826 of these events.

The predominance over background of the N^{*++} peak and the further enhancement of the peak resulting from the cut on the prod. cosine allow a relatively clean selection of events belonging to the quasi-three body state N^{*++} p π^-. These events are of particular interest since the protons may be "labelled." That is, the proton (designated p_a)

Figure 5

(a) Mass distribution for all $p\,\pi^+$ combinations. The solid curve is the prediction of the OPEM; the dashed curve is Lorentz invariant phase space. Both curves are normalized to the number of experimental combinations.

(b) Mass distributions for those $p\,\pi^+$ combinations with $|\text{prod. cos}| \geq .96$. The curve is the prediction of the OPEM normalized to the number of experimental combinations.

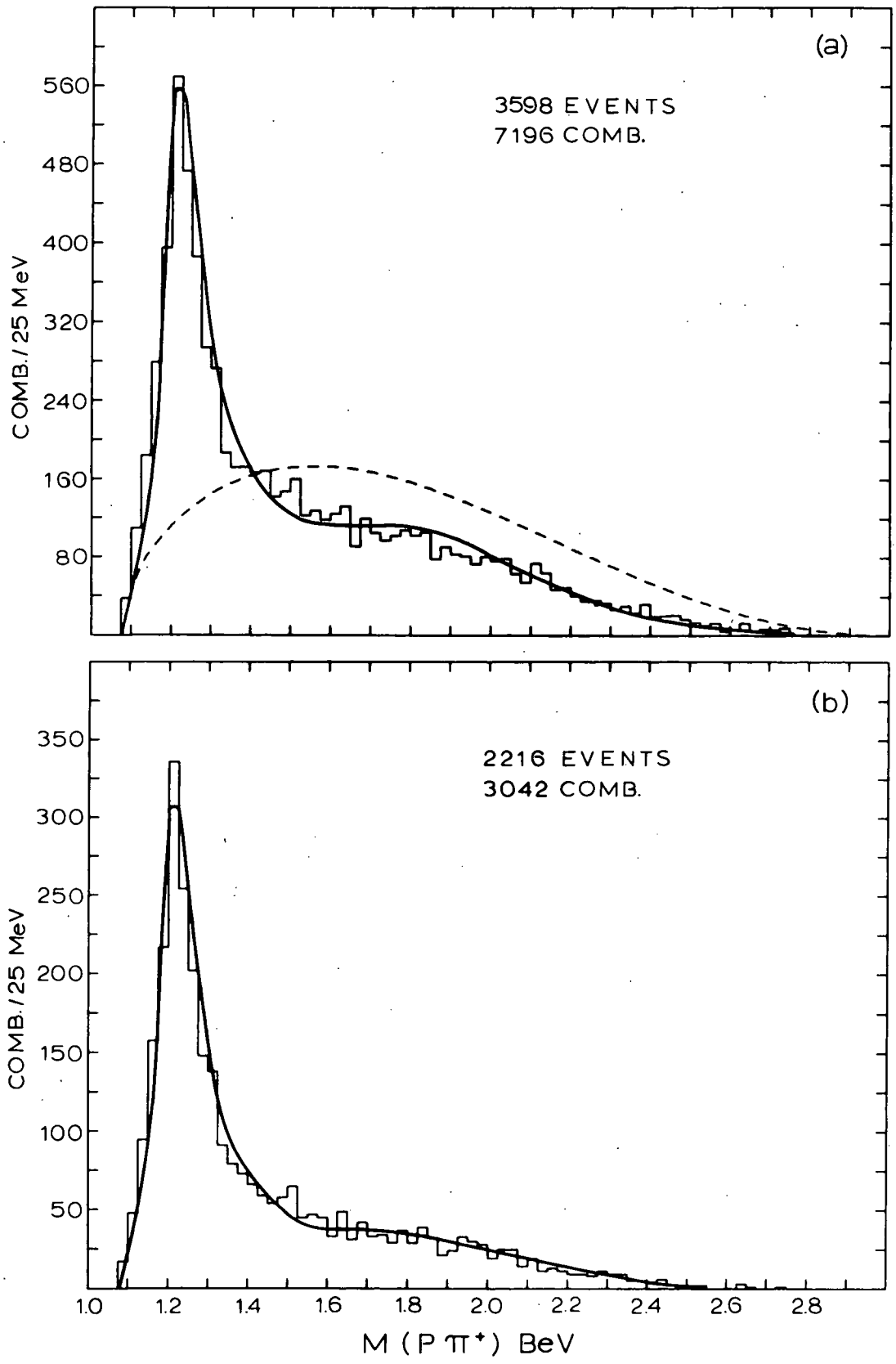
(a)
3598 EVENTS
7196 COMB.
560
480
400
320
240
160
80
COMB./25 MeV
(b)
2216 EVENTS
3042 COMB.
350
300
250
200
150
100
50
COMB./25 MeV
1.0
1.2
1.4
1.6
1.8
2.0
2.2
2.4
2.6
2.8
M (P π⁺) BeV

that in combination with the π^+ is in the N* mass band ($1.15 \leq M(p_a\pi^+) \leq 1.30$ BeV) may be identified with the upper vertex of Diagram (a) (Figure 4) and the remaining proton (designated p_b) with the lower vertex. The N* mass band selection criterion is satisfied by at least one p π^+ combination in 2110 events and by both combinations in 289 (or 14%) of these events. 1218 of the 2110 events satisfy the additional criterion of $|\text{prod. cos } (p_a\pi^+)| \geq .96$; for 97 (or 8%) of the events, both combinations satisfy this latter criterion. For the "double" N^{*++} events (both p π^+ combinations in the N^{*++} mass band) we expect that at most one of the combinations results from the decay of a N^{*++}. At least one combination is "wrong" in the sense that, although it satisfies the selection criterion, it does not result from the decay of a N^{*++}. The above numbers of double N^{*++} events imply that of the 2399 combinations that satisfy the mass criterion at least 289 (12%) are wrong, and that of the 1315 combinations that satisfy the additional selection on production cosine at least 97 (7%) are wrong. The OPEM predicts 11% and 7% respectively. The total percent of wrong combinations is greater than the percent calculated from the double N^{*++} events since there will be events for which only one p π^+

combination satisfies the selection criterion but this combination does not result from a N^{*++}. This total may not be obtained directly but may be estimated from the OPEM since the $p_4\pi^+$ combinations (see Figure 4a) constitute the wrong combinations. For the model 22% of the combinations satisfying the selection on mass and 18% of the combinations satisfying the additional cut on production cosine are wrong. These percents are probably reasonable estimates since, as indicated in Figure 5, the OPEM approximates fairly well the height of the N^{*++} peak relative to the background. In addition the percent of double N^{*++} predicted by the model (given above) agrees well with that of the data.

The $p\ \pi^+$ mass distribution shows no evidence for the production of higher, Ispin = 3/2 resonances. The second resonance seen as a peak in π^+ p elastic scattering, the $N^*_{3/2}(1950)$ (Γ = 220 MeV, $J^P = 7/2^+$, F_{37} wave of phase shift analysis)*, appears in the OPEM curve (Figure 5a) as a broad shoulder near 1900 MeV. The absence of a comparable shoulder in the data indicates that this

---

For N resonances we give the Ispin as a subscript and the mass value as obtained from reference 16 in parentheses. Other parameters (e.g. spin), if given, are also from reference 16.

resonance is not produced as strongly as predicted by the model (if at all). The p π^+ mass distribution shows no enhancements at the masses of other Ispin = 3/2 resonances.[16,17]

2. The p π^- Mass Distribution

The p π^- invariant mass distribution for all combinations (Figure 6a) shows three peaks which we interpret as corresponding to the peaks observed in π^- p elastic scattering. The OPEM curve reflects these resonant peaks; the first two are the $N^*_{3/2}(1236)$ and $N^*_{1/2}(1525)$ (Γ = 115 MeV, $J^P = 3/2^-$, D_{13} wave of phase shift analysis). The third peak corresponds to a region in which several phase shifts resonate. Considered "well established"[16,17] resonances are the $N^*_{1/2}(1680)$(Γ = 170 MeV, $J^P = 5/2^-$, D_{15}) the $N^*_{1/2}(1690)$ (Γ = 130 MeV, $J^P = 5/2^+$, F_{15},) and the $N^*_{3/2}(1640)$ (Γ = 180 MeV, $J^P = 1/2^-$, S_{31}). Possible resonances are the $N^*_{3/2}(1690)$ (Γ = 280 MeV, $J^P = 3/2^+$, P_{33}) and the $N^*_{3/2}(1690)$ (Γ = 280 MeV, $J^P = 3/2^-$, D_{33}). The $p_b \pi^-$ distribution (Figure 6b) shows these same peaks but enhanced relative to the background, consistent with the behavior of the OPEM. This "double Isobar" production (simultaneous production of N^{*++} and N^{*o}) argues in favor of a dominant contribution from

Figure 6

(a) Mass distribution for all $p\,\pi^-$ combinations. The solid curve is the prediction of the OPEM (A = 3) and the dashed curve is phase space, both normalized to the number of experimental combinations.

(b) The $p_b\pi^-$ mass distribution. p_b is the other proton when one proton is in the $N^{*++}(1236)$ mass band ($1.15 \leq M(p_b\pi^+) \leq 1.30$). The shaded histogram is for those $p_b\pi^-$ combinations for which $|\text{prod. cos}\,(p_a\pi^+)| \geq .96$. The curves are the corresponding OPEM predictions, normalized to the number of experimental combinations.

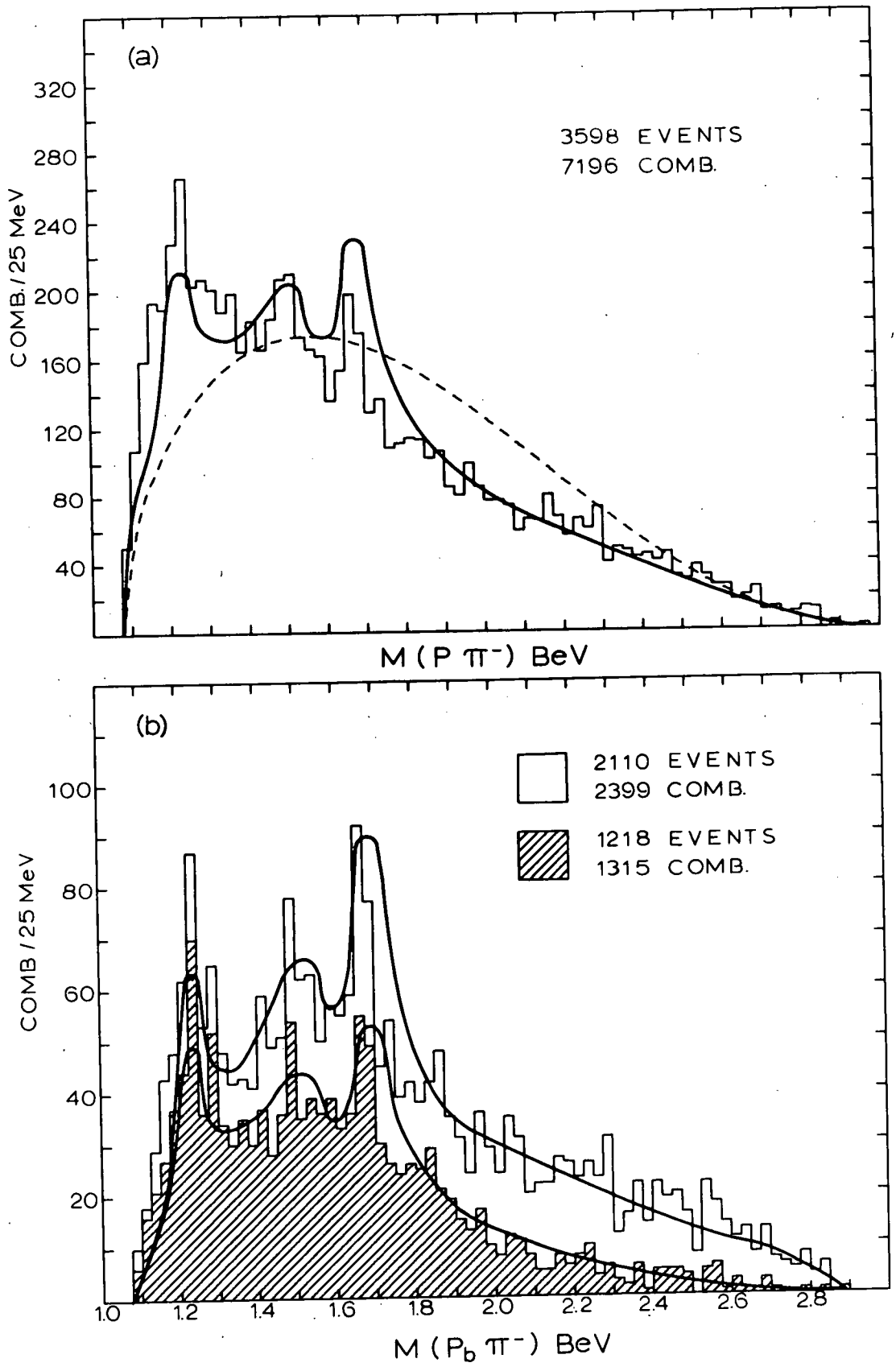
(a)
3598 EVENTS
7196 COMB.
COMB./25 MeV
320
280
240
200
160
120
80
40
M (P π⁻) BeV
(b)
2110 EVENTS
2399 COMB.
1218 EVENTS
1315 COMB.
COMB / 25 MeV
100
80
60
40
20
1.0
1.2
1.4
1.6
1.8
2.0
2.2
2.4
2.6
2.8
M (Pb π⁻) BeV

diagram (a) (Figure 4) as opposed to diagram (b). That is, although diagram (b) could give both N^{*++} and N^{*o} production it cannot do so simultaneously.

The OPEM predicts the three resonant peaks seen in the data and, particularly for the $p_b\pi^-$ combinations, describes fairly well the general shape of the mass distributions. There are, however, discrepancies. For the data the overall distribution (Figure 6a) shows a rather broad excess of events (relative to the model) in the mass region 1.1 to 1.4 BeV. In Section D we show evidence for resonance production in the $p\ \pi^+\ \pi^-$ mass distribution from roughly 1.3 to 1.8 BeV. The above excess may be traced to this resonance production since the $p\ \pi^-$ invariant mass from these resonances is kinematically restricted to low values. The overall distribution also has a depletion of events in the third resonance region ($\sim$1680 MeV) for which we can offer no simple explanation. Both the excess of events in the region of the N*(1236) and the depletion in the third resonance region are present in the $p_b\pi^-$ distribution, but to a lesser extent than in the overall distribution.

We see no evidence for resonance production above 1700 MeV. Neither the overall $p\ \pi^-$ nor the $p_b\pi^-$ mass

distribution shows enhancements at the masses of known Ispin = 3/2 or Ispin = 1/2 resonances.[16,17]

3. The Δ^2 Distribution.

The experimental Δ^2 distributions for all p π^+ combinations and for those in the N*(1236) mass band are compared to the predictions of the OPEM in Figure 7. For each proton-pion combination the smaller of the two possible Δ^2 is plotted. The comparison to the model is made for no form factor and for the form factor of equation (3) with A = 1 and A = 3. For ease of comparison the model's curves have been normalized to the number of experimental combinations. The OPEM with the form factor of equation (3) is not able to reproduce the sharpness of the overall experimental distribution. A value of A = 3 provides fair agreement between the data and the model for the $p_a \pi^+$ distribution and we use this value in comparing the model to the experimental mass and angular distributions.

The general agreement between the experimental proton-pion mass distributions and the model make it attractive to assume that some significant part of the data results from one pion exchange. This assumption, however, does not necessarily imply that the prediction

Figure 7

(a) Δ^2 distribution for all p π^+ combinations. The OPEM curves are given for no form factor and for the form factor of equation (3) with A = 1 and A = 3. The curves are normalized to the number of experimental combinations.

(b) Δ^2 distribution for those p π^+ combinations in the N^{*++} mass band. The curves are as in (a).

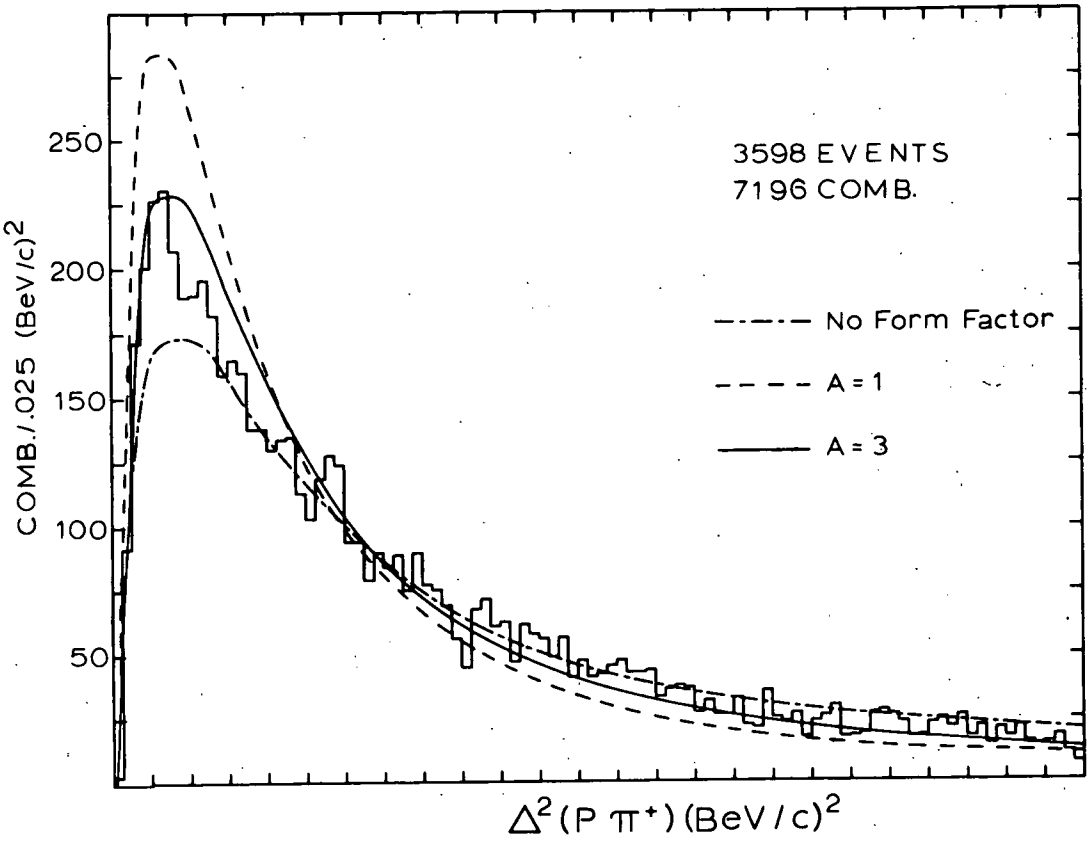
3598 EVENTS
7196 COMB.
No Form Factor
A = 1
A = 3
COMB./.025 (BeV/c)²
250
200
150
100
50
Δ²(P π⁺) (BeV/c)²

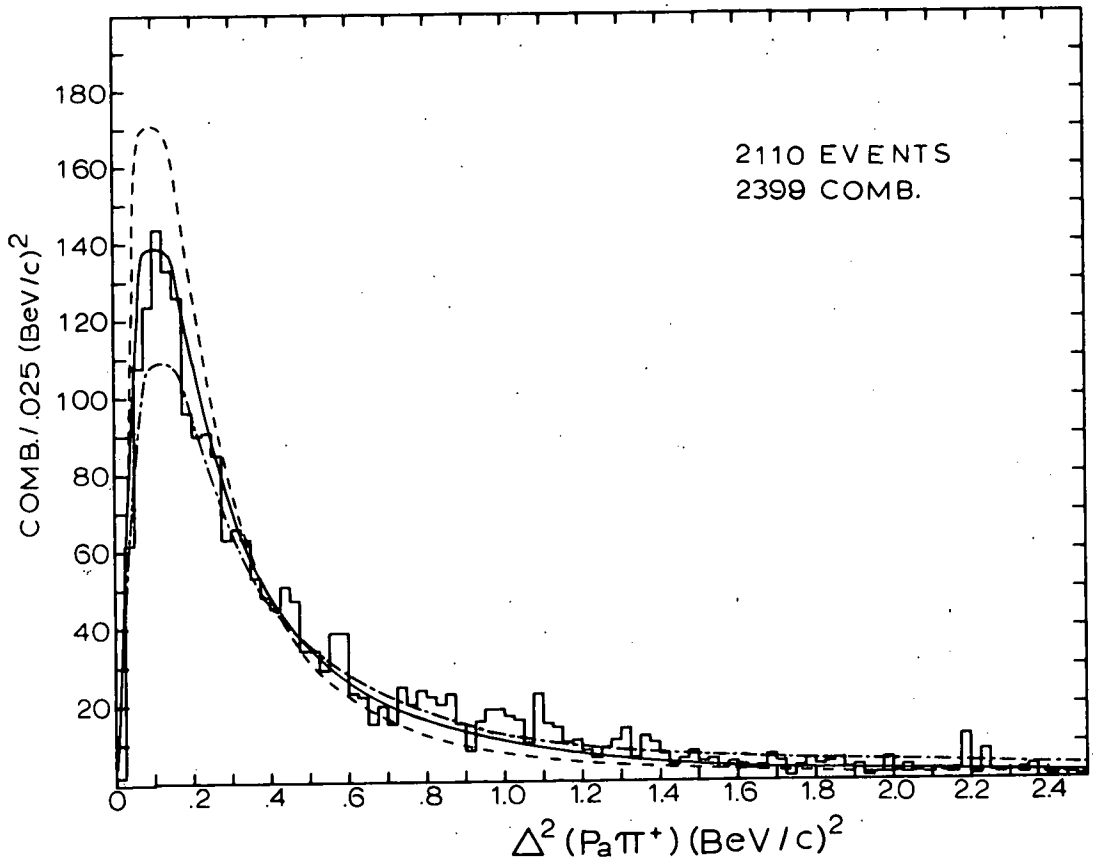
2110 EVENTS
2399 COMB.
COMB./.025 (BeV/c)²
180
160
140
120
100
80
60
40
20
0
.2
.4
.6
.8
1.0
1.2
1.4
1.6
1.8
2.0
2.2
2.4
Δ²(Pa π⁺) (BeV/c)²

of the model should agree with the experimental Δ^2 distribution since other production processes may contribute to the experimental distribution. Thus, as mentioned in Section B, considerations of more complicated form factors (that might give better agreement with the data) are of questionable value. We also mention that the value $A = 3$ for the form factor of equation (3) may not be an appropriate choice for whatever fraction of the data may be attributed to one pion exchange.

4. Angular Distributions

The remaining variables appropriate to the OPEM may be expressed as angular distributions of the proton-pion combinations at each vertex. Since a given proton may be reliably identified with a given vertex only for the events in the quasi-three body final state N^{*++} $p_b\pi^-$ we restrict the discussion to these events. The angles considered are defined in a standard manner as shown in Figure 8a. For a hypothetical event Figure 8b illustrates these angles for the $p_b\pi^-$ combination as well as the momentum vectors for various particles as seen in the $p_b\pi^-$ rest frame.

Figure 8

(a) Definition of the angles discussed in the text. "in" and "out" refer to the incident and outgoing protons. $(\overrightarrow{p_{out}\pi})$ specifies the direction of transformation from the overall center of mass to the $p_{out}\pi$ rest frame.

(b) The angles defined as in (a) for the $p_b\pi^-$ system for a hypothetical event. Also shown are various momentum vectors transformed to the $p_b\pi^-$ rest frame. $p_\alpha(p_\beta)$ is the incident proton with the positive production cosine to the $p_a\pi^+$ ($p_b\pi^-$) system.

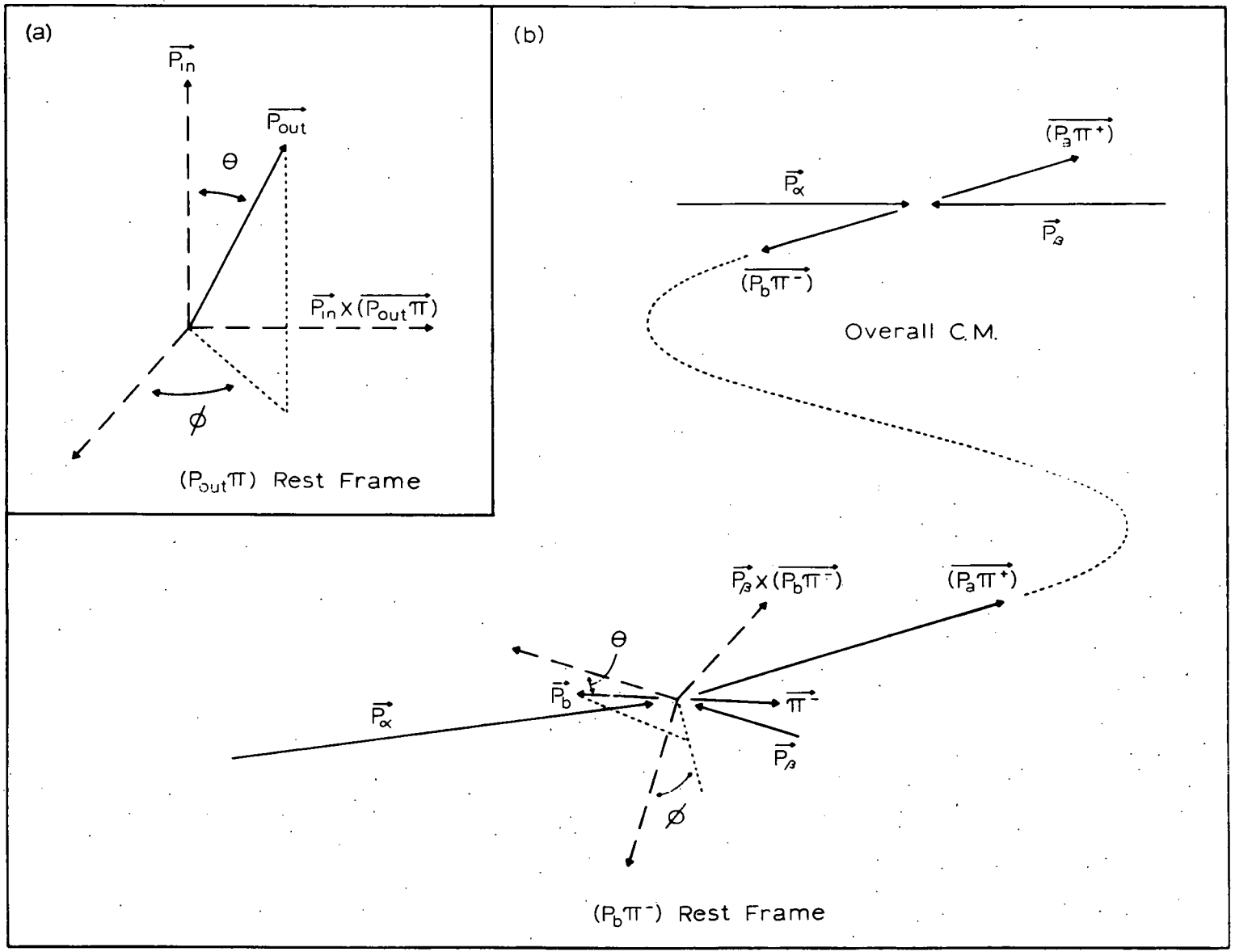
(a)
$\vec{P}_{in}$
$\vec{P}_{out}$
Θ
$\vec{P}_{in} \times (\vec{P}_{out}\pi)$
φ
$(P_{out}\pi)$ Rest Frame
(b)
$(\vec{P_a\pi^+})$
$\vec{P}_\alpha$
$\vec{P}_\beta$
$(\vec{P_b\pi^-})$
Overall C.M.
$\vec{P}_\beta \times (\vec{P_b\pi^-})$
$(\vec{P_a\pi^+})$
Θ
$\vec{P}_b$
$\vec{P}_\alpha$
$\vec{\pi}^-$
$\vec{P}_\beta$
φ
$(P_b\pi^-)$ Rest Frame

The angular distributions for $p_a\pi^+$ are compared to the predictions of the OPEM in Figure 9a and 9b. A selection of pure N^{*++} ($p_3\pi^+$ combinations) from the model would have a distribution of cos θ as observed in π^+ p elastic scattering. That is, a nearly symmetric distribution going approximately as $1 + 3\cos^2\theta$. The ϕ distribution would be isotropic as required by the exchange of a spinless pion. The model's deviation from symmetry in cos θ and isotropy in ϕ results from the inclusion of the wrong p π^+ combinations ($p_4\pi^+$) whose invariant mass happens to be in the N^{*++} mass band. The experimental cos θ distribution resembles the OPEM prediction but is noticeably flatter near cos $\theta = \pm 1$. The agreement with the model is better for those events satisfying the cut on production cosine, suggesting that the cut reduces the relative contribution from processes other than from the one pion exchange diagram that we are considering. The ϕ distribution for the data has a larger deviation from isotropy than predicted by the model but is in qualitative agreement. Again, the agreement is improved with the selection on production cosine.

The $p_b\pi^-$ angular distributions are displayed in Figure 9c and 9d for all combinations. Since for π^- p

Figure 9

Angular distributions for those events in the quasi-three body final state:

$$N^{*++} \; p_b\pi^-$$
$$\hookrightarrow \; p_a\pi^+$$

The shaded histograms are for the additional requirement $|\text{prod. cos } (p_a\pi^+)| \geq .96$. The smooth curves are the OPEM (A = 3) predictions normalized to the number of combinations in the corresponding experimental distributions.

(a) Cos θ for $p_a\pi^+$.

(b) ϕ for $p_a\pi^+$.

(c) Cos θ for $p_b\pi^-$.

(d) ϕ for $p_b\pi^-$.

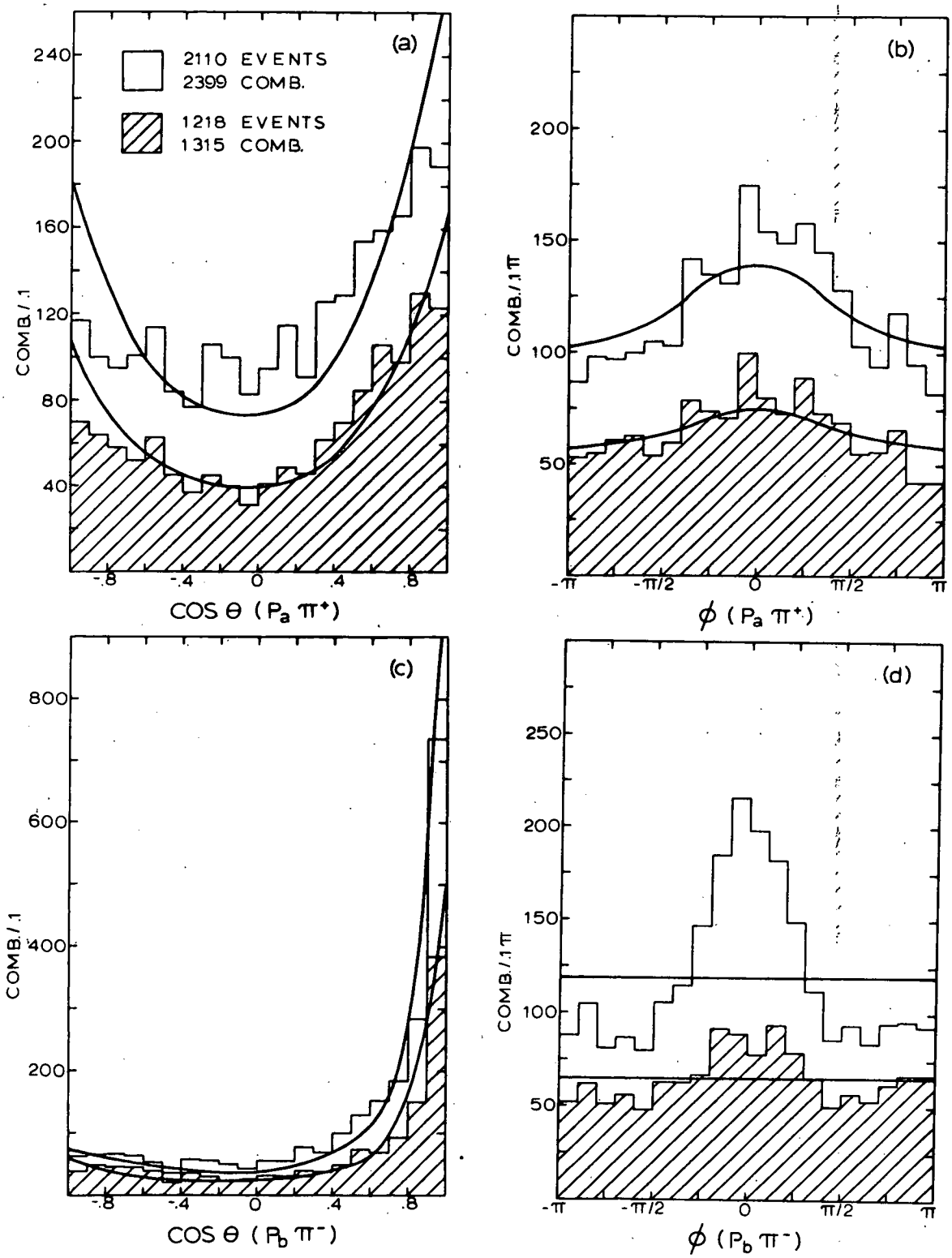
(a)
2110 EVENTS
2399 COMB.
1218 EVENTS
1315 COMB.
COMB./.1
COS Θ ($P_a \pi^+$)
(b)
COMB./.1π
φ ($P_a \pi^+$)
(c)
COMB./.1
COS Θ ($P_b \pi^-$)
(d)
COMB./.1π
φ ($P_b \pi^-$)

elastic scattering the cos θ distribution is a function of the invariant mass, we display in Figure 10 the cos θ distributions for various mass intervals. The data and the model agree reasonably well, with the largest discrepancy between the model and the data in the region of the $N^{*0}(1236)$ ($1.15 \leq M(p_b\pi^-) \leq 1.30$ BeV). For completeness we mention that for the model the wrong $p_b\pi^-$ combinations ($p_3\pi^-$) tend to populate the cos θ region near +1. For the model the ϕ distribution is isotropic for both the correct and wrong combinations. The experimental ϕ distribution is essentially flat outside the region $-\pi/2$ to $\pi/2$ but shows a marked peaking in that region. Of all the discrepancies between the data and the model in the distributions examined so far, the peaking in ϕ is the most clear-cut. Thus we use this peaking to place an upper limit on the amount of the data (for the quasi-three body state) that may be attributed to the simple one pion exchange diagram that we have considered. This upper limit, taken as twice the number of combinations outside the region $-\pi/2$ to $\pi/2$, is 1806 combinations (75.3% of the total number of combinations) for the selection on mass of $p\,\pi^+$ alone and 1150 combinations (87.5%) for the additional selection

Figure 10

The cos $\theta(p_b\pi^-)$ distributions for various $p_b\pi^-$ mass regions. The shaded distributions are for the cut on production cosine. The OPEM curves are normalized to the total number of experimental combinations (not to the number in each mass region).

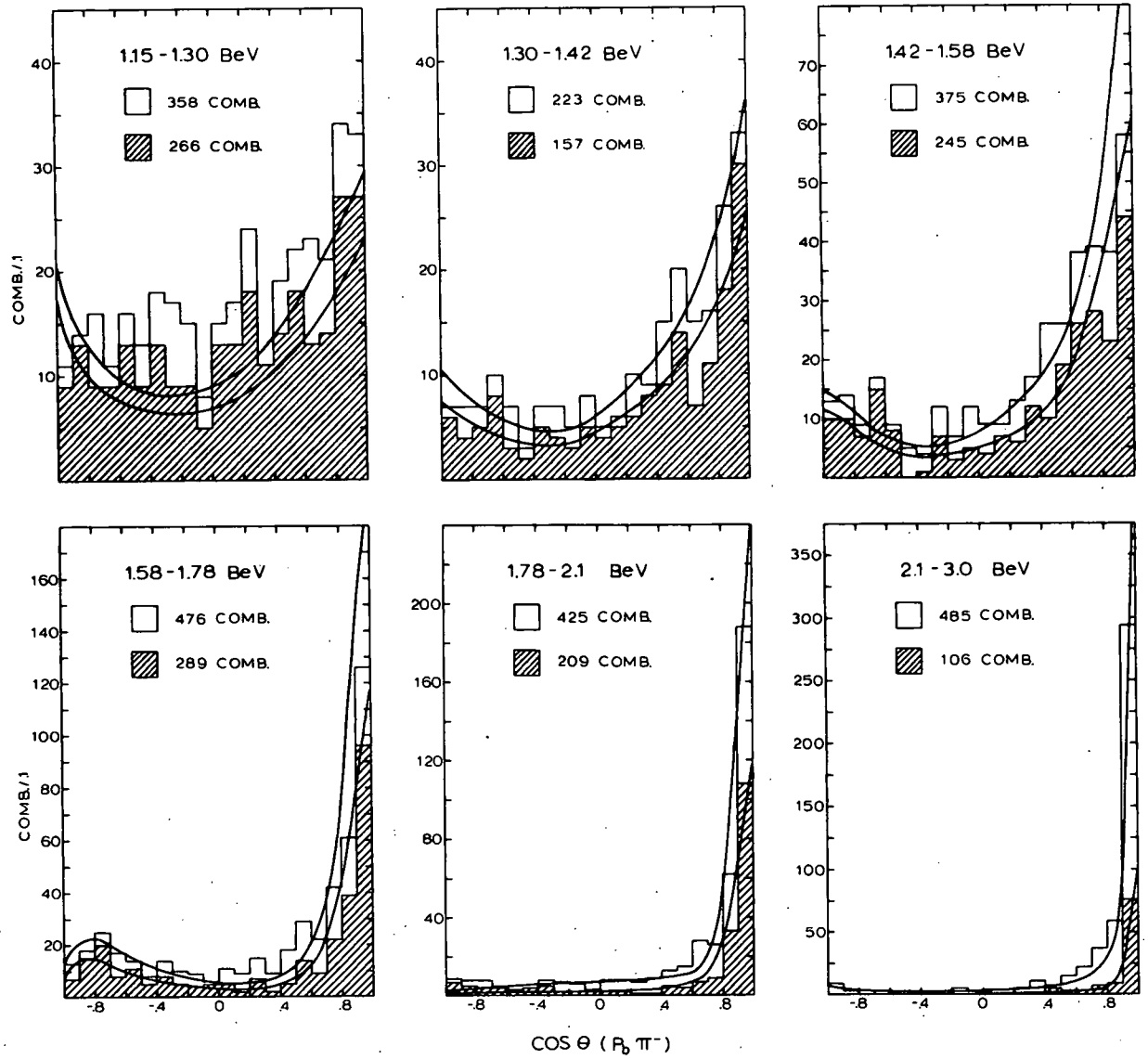
1.15 - 1.30 BeV
358 COMB.
266 COMB.
1.30 - 1.42 BeV
223 COMB.
157 COMB.
1.42 - 1.58 BeV
375 COMB.
245 COMB.
1.58 - 1.78 BeV
476 COMB.
289 COMB.
1.78 - 2.1 BeV
425 COMB.
209 COMB.
2.1 - 3.0 BeV
485 COMB.
106 COMB.
COMB./.1
COS Θ ($P_b \pi^-$)

on production cosine. As has been previously noted, the relative contribution that may be attributed to one pion exchange is greater for the cut on production cosine. The dependence of the peaking in ϕ on the $p_b\pi^-$ invariant mass is shown as a scatter plot in Figure 11. The excess of events between $-\pi/2$ and $\pi/2$ is distributed throughout the $p_b\pi^-$ mass range except in the region of the N*(1236) where the distribution is fairly isotropic. In the next section we show that the peaking in ϕ may be understood as a kinematic reflection of resonance production in the $p\,\pi^+\,\pi^-$ system.

D. The $p\,\pi^+\,\pi^-$ System

1. Relationship to the OPEM

The comparison of the data to a OPEM in the previous section indicated that a significant fraction of the data is consistent with the exchange of a single pion. Thus the distributions of other variables (e.g. $p\,\pi^+\,\pi^-$ mass) may be expected to be to a large extent the result of kinematic reflections of one pion exchange. The production of a resonance should appear as an enhancement above this one pion exchange background. In accordance with the above discussion we now compare the $p\,\pi^+\,\pi^-$ mass distribution to the background prediction of the OPEM.

Figure 11

(a) The mass of $p_b\pi^-$ plotted against $\phi(p_b\pi^-)$.

(b) The same as in (a), but for the additional requirement that $|\text{prod. cos } (p_a\pi^+)| \geq .96$.

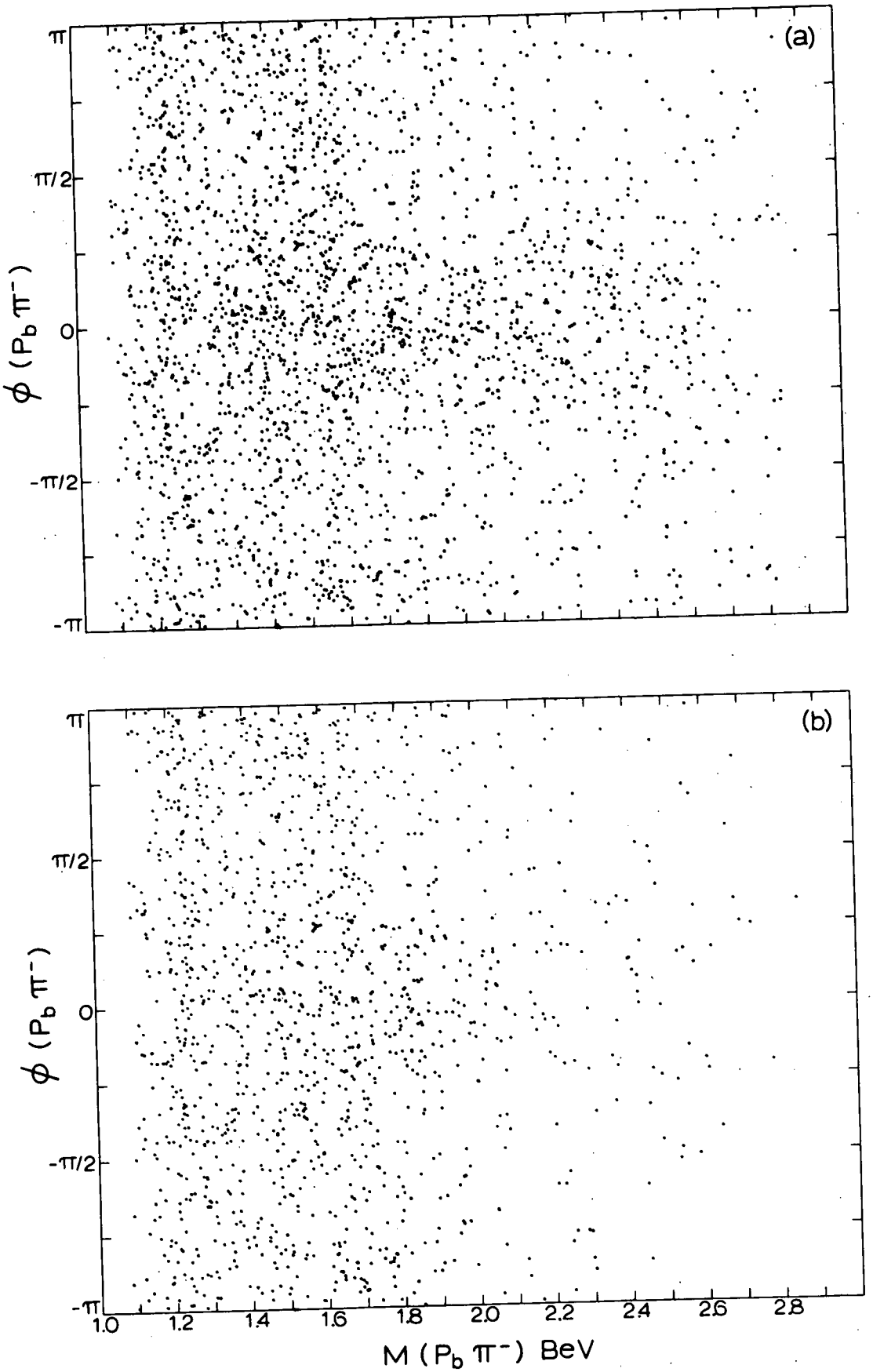
(a)
π
π/2
0
-π/2
-π
φ (P_b π⁻)
(b)
π
π/2
0
-π/2
-π
φ (P_b π⁻)
1.0
1.2
1.4
1.6
1.8
2.0
2.2
2.4
2.6
2.8
M (P_b π⁻) BeV

The p π^+ π^- invariant mass distribution for all combinations is shown in Figure 12a, together with the predictions of phase space and the OPEM. As suggested above, the OPEM describes the general shape of the mass distribution. In particular, the shift towards low mass relative to phase space is predicted. The most prominent deviation from the OPEM curve and the general trend of the distribution is an enhancement between roughly 1.65 and 1.775 BeV. This enhancement has been reported in the p p π^+ π^- final state at incident proton beam momenta of 5.5,[4] 8.1,[6] and 10.0 BeV/c.[7,8] As discussed in Section IV, C, 2 there are some three to five partial waves that resonate in this mass region, all of which have inelastic decay modes. It is reasonable to assume that some combination of these resonances leads to the peak observed in the p π^+ π^- mass distribution.

The general shape of the N^{*++} π^- mass distribution (Figure 12b) is fairly well predicted by the OPEM. The region above 1.8 BeV seems particularly well described by the model. The tendency of the data to peak at low invariant mass is predicted by the model but this low mass region does have structure above the OPEM curve. For the distribution without the cut on production

Figure 12

(a) Mass distribution for all p π^+ π^- combinations. The solid curve is the OPEM prediction (A = 3). The dashed curve is phase space. Both curves are normalized to the number of experimental combinations.

(b) The $p_a\pi^+$ π^- mass distribution where $p_a\pi^+$ is in the N^{*++} mass band. The shaded histogram is for the additional restriction $|\text{prod. cos } (p_a\pi^+)| \geq .96$. The curves are the corresponding OPEM predictions normalized to the number of experimental combinations.

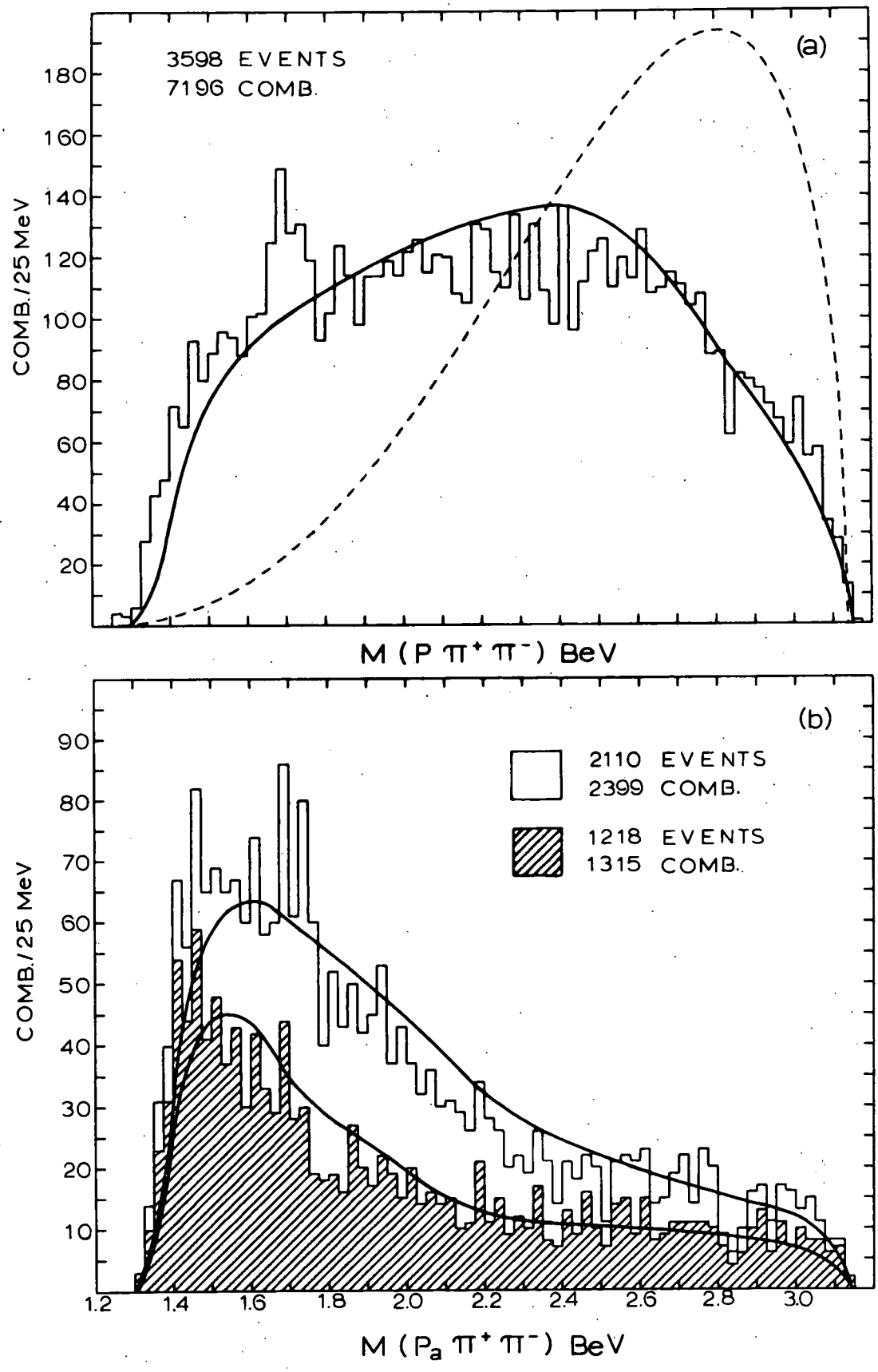
3598 EVENTS
7196 COMB.
(a)
COMB./25 MeV
M (P π⁺ π⁻) BeV
(b)
2110 EVENTS
2399 COMB.
1218 EVENTS
1315 COMB.
COMB./25 MeV
M (Pa π⁺ π⁻) BeV

cosine (unshaded histogram) a remnant of the enhancement at 1700 MeV is present as well as an excess of events in the region 1350 - 1600 MeV. The cut on production cosine (shaded histogram in Figure 12b) essentially eliminates the peak at 1700 MeV, leaving only an enhancement in the 1350 - 1500 MeV region above the OPEM background prediction. The existence of a resonance at low mass (e.g. the peak at 1700 MeV) does not necessarily imply the decay mode

$$N^{*+} \rightarrow N^{*++}(1236)\ \pi^-$$

since for such a resonance the p π^+ invariant mass is kinematically restricted to low values. For simplicity, however, we will refer to the mass distributions of Figure 12b as $N^{*++}\ \pi^-$.

The peaking of the OPEM in the low $N^{*++}\ \pi^-$ mass region results primarily from a kinematic reflection of the π^- p scattering at the lower vertex of Diagram (a) (Figure 4) together with the peripheral nature of the proton-pion combinations. This type of kinematic reflection resulting from one pion exchange was originally described by Deck[18] in an attempt to explain the A_1 meson. The effect may be understood by examining

Figure 8b. Because of the peripheral nature of the interaction the p_β vector and the N^{*++} vector (consider $p_a\pi^+$ to be in the N^{*++}) point more or less in opposite directions in both the overall center of mass and the $p_b\pi^-$ rest frame. For the N^{*++} π^- system to have small invariant mass it is then necessary that the π^- be produced backwards with respect to p_β, corresponding to large, positive values of $\cos\theta(p_b\pi^-)$. The inclusion of physical π^- p elastic scattering data in the model gives a $\cos\theta(p_b\pi^-)$ distribution that consists predominately of just such values, as shown in Figure 9c. This predominance of large, positive values then leads to the peaking at low N^{*++} π^- mass. Of course a low mass resonance decaying into N^{*++} π^- is constrained to produce values of $\cos\theta$ that are large and positive. Thus, although the data agree with the model in peaking towards such values of $\cos\theta(p_b\pi^-)$, we cannot exclude the possibility that some of the peaking results from resonance production.

The excess of events above the OPEM curve between 1350 and 1500 MeV suggests the possibility of a contribution from resonance production in addition to the one pion exchange background. Two candidates from phase

shift analysis are the $N^*_{1/2}(1470)$ ($J^P = 1/2^+$, $\Gamma = 210$ MeV, P_{11}) and the $N^*_{1/2}(1525)$. The N*(1525), discussed previously, decays into N π π 45% of the time, the N*(1470) 35% of the time. Since the data peak below 1500 MeV the N*(1470) is perhaps the more logical candidate. We defer a more detailed discussion of this resonance to section IV, D, 2. For definiteness we will refer to the N^{*++} π^- enhancement between 1350 and 1500 MeV as the 1425 MeV enhancement.

The relationship between the 1425 MeV enhancement, one pion exchange, and possible resonance production has been investigated in the p p π^+ π^- final state in several experiments other than the one reported here. At neighboring beam momenta are the experiments reported by Gellert et al. at 6.6 BeV/c,[5] Guyader et al. at 8.1 BeV/c,[6] and Almeida et al. at 10 BeV/c.[7,8] Gellert et al. conclude that the peaking expected from one pion exchange is a sufficient explanation of the enhancement. This conclusion was not based upon a comparison to a model calculation but rather primarily upon a comparison of the cos $\theta(\bar{p}_b\pi^-)$ distribution of the data to the distribution observed in π^- p elastic scattering. (The definition of $p_b\pi^-$ was similar to the one used in this

experiment with the cut on production cosine to the N^{*++}. The comparison was made in terms of a moments analysis of the cos θ distribution as a function of π^- p invariant mass, corresponding roughly to a comparison of the shaded distributions in Figure 10 to the OPEM predictions.) Guyader et al. and Almeida et al. compare the data to a model calculation similar to the one of this experiment. They observe a similar disagreement between the model and the data to that shown in Figure 12b. This disagreement plus some arguments based on various angular distributions (we discuss these arguments later) lead both Guyader et al. and Almeida et al. to the conclusion that the enhancement is not entirely kinematic in origin. Both attribute at least part of the enhancement to the N*(1470). Given these conflicting conclusions it is of interest to examine further the relationship of the 1425 MeV N^{*++} π^- enhancement to the OPEM and to possible resonance production.

The Δ^2 distribution to the N^{*++} is the only variable of the OPEM adjusted (aside from normalization) to agree with the data. In Figure 13 we show that the failure of the model to explain the peaking around 1425 MeV may not be attributed to a wrong choice of the adjustable

parameter A. The $N^{*++}\ \pi^-$ mass distribution is replotted and compared to the prediction of the model for A = 3, A = 1 and for no form factor (equivalent to A = ∞). Each curve has been normalized to the number of events between 1.8 and 2.4 BeV, the mass region of best agreement between the data and the model. For the overall $N^{*++}\ \pi^-$ distribution (Figure 13a) the high mass region is relatively insensitive to A, the low mass region relatively sensitive. Although the model does not reproduce the peaking at either 1425 or 1700 MeV for any of the values of A, the amount of the data that might be ascribed to resonance production is very dependent upon the choice of A. For the distribution with the cut on production cosine (Figure 13b) the prediction of the model is essentially independent of the choice of A. We use this distribution to determine the statistical significance of the 1425 MeV enhancement since the value obtained will not depend strongly on A. We take the enhancement to lie in the interval $1.35 \leq M(p_a\pi^+\ \pi^-) \leq 1.475$ BeV (the upper limit has been chosen to avoid to some extent a possible contribution from the N*(1525)). This mass region contains 95 events above the OPEM background (A = 3) of 116 events, a 6 standard deviation effect.

Figure 13

(a) A comparison of the $p_a\pi^+$ π^- mass distribution ($p_a\pi^+$ in the N^{*++} mass band) to the OPEM for various values of the adjustable parameter A. The various curves are normalized to the number of experimental combinations in the mass region 1800 - 2400 MeV.

(b) Same as (a) but with the additional restriction that $|\text{prod. cos } (p_a\pi^+)| \geq .96$.

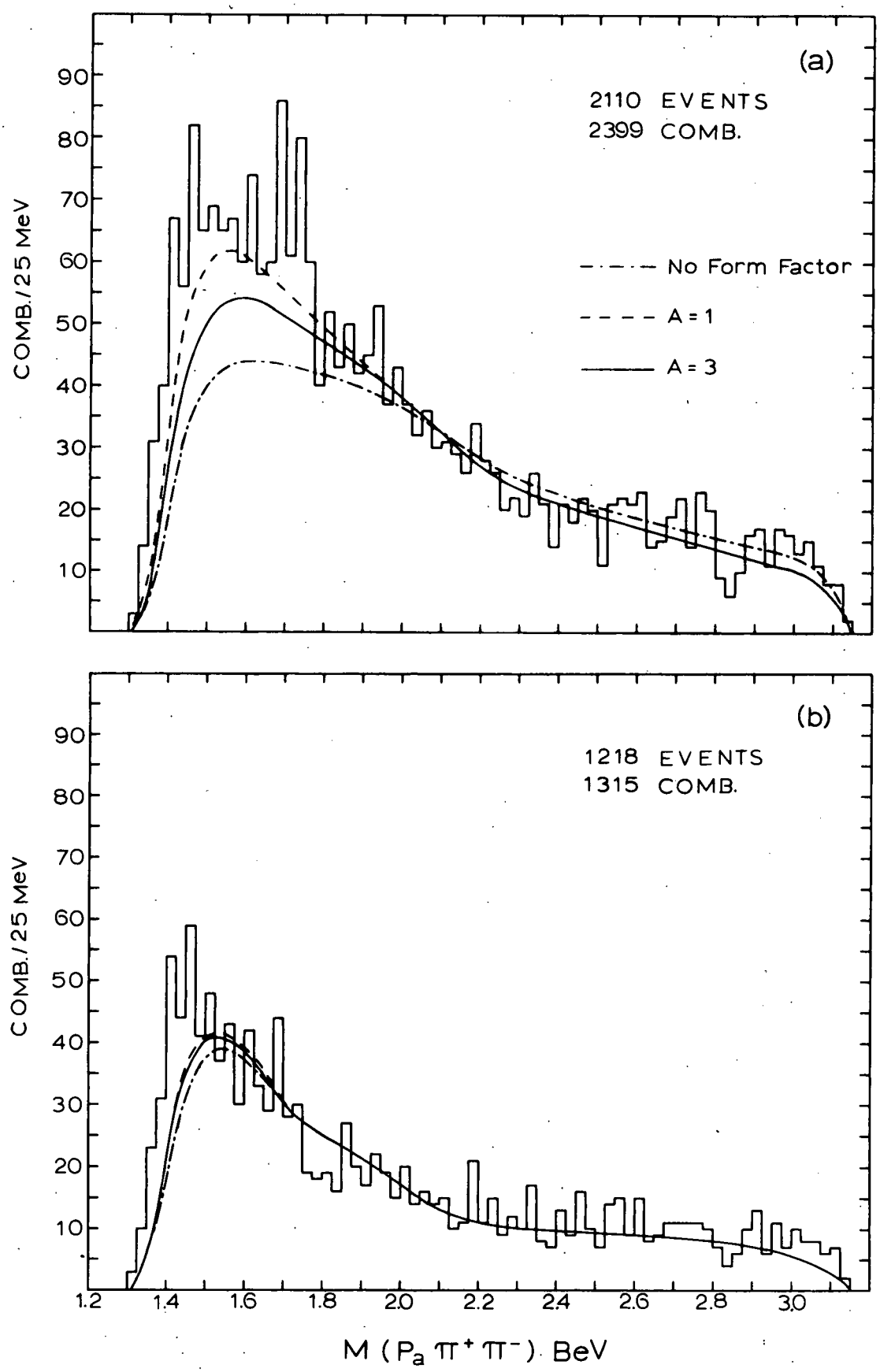
(a)
2110 EVENTS
2399 COMB.
No Form Factor
A = 1
A = 3
(b)
1218 EVENTS
1315 COMB.
COMB./25 MeV
10
20
30
40
50
60
70
80
90
1.2
1.4
1.6
1.8
2.0
2.2
2.4
2.6
2.8
3.0
M ($P_a \pi^+ \pi^-$) BeV

In addition to the previously discussed kinematic dependence of $N^{*++}\ \pi^-$ mass and $\cos\theta(p_b\pi^-)$, the mass is correlated with $\phi(p_b\pi^-)$. This latter correlation may also be understood by examination of Figure 8b. Consider, for a given $\cos\theta$, a rotation of the π^- vector about the p_β vector corresponding to a change of ϕ from 0 to π. The π^- will be maximally aligned with the N^{*++} (minimum $N^{*++}\ \pi^-$ mass) for $\phi = 0$ and minimally aligned (maximum $N^{*++}\ \pi^-$ mass) for $\phi = \pi$. This correlation may be observed experimentally as shown in Figure 14. As discussed in Section IV, C, 4 and shown in Figure 9d, the $\phi(p_b\pi^-)$ distribution peaks above the flat distribution expected for one pion exchange between $-\pi/2$ and $+\pi/2$. Figure 14a shows that for the overall sample of N^{*++} events values of ϕ between $-\pi/2$ and $\pi/2$ occur almost exclusively for $N^{*++}\ \pi^-$ mass less than about 1800 MeV. This is just the region of enhancement above the OPEM prediction (Figure 13a). For the cut on production cosine to the N^{*++}, Figure 14b shows that values of ϕ between $-\pi/2$ and $+\pi/2$ occur primarily for $N^{*++}\ \pi^-$ mass less than about 1500 MeV, again the region of enhancement above the OPEM prediction (Figure 13b) The peaking in $\phi(p_b\pi^-)$ may thus be explained as

Figure 14

(a) $\phi(p_b\pi^-)$ plotted against $p_a\pi^+\pi^-$ mass, with $p_a\pi^+$ in the N^{*++} mass band.

(b) Same as (a) but with the additional restriction $|\text{prod. cos}\,(p_a\pi^+)| \geq .96$.

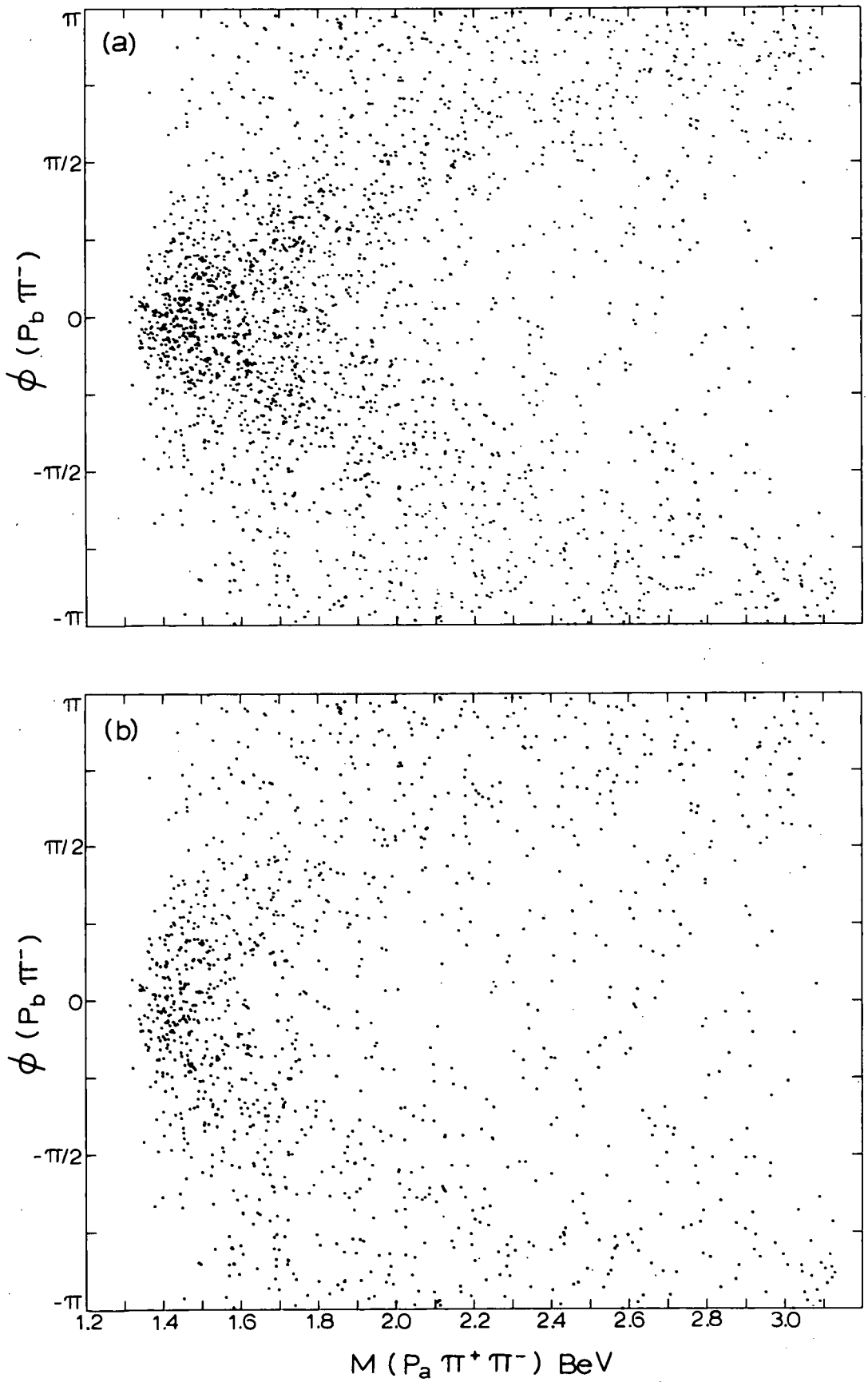
(a)
(b)
π
π/2
0
-π/2
-π
φ (P_b π⁻)
1.2
1.4
1.6
1.8
2.0
2.2
2.4
2.6
2.8
3.0
M (P_a π⁺ π⁻) BeV

resulting from resonance production at low $N^{*++}\pi^-$ mass.*

Earlier we observed that, as shown in Figure 11, the $\phi(p_b\pi^-)$ distribution was fairly isotropic for the $p_b\pi^-$ mass in the region of the $N^{*0}(1236)$. Thus for these double N*(1236) events ($p_a\pi^+$ and $p_b\pi^-$ in the N*(1236) mass band) we would expect no enhancement at low $N^{*++}\pi^-$ mass if our correlation of peaking in $\phi(p_b\pi^-)$ near zero and $N^{*++}\pi^-$ resonance production is correct. Figure 15 displays the $N^{*++}\pi^-$ mass distributions both for the double N* events and for the double N* events removed. As expected there is no evidence for an enhancement in the distributions for the double N* events. The distributions are quite flat and in agreement with the shape predicted by the OPEM. The peaking above the OPEM curve is seen only in the distributions with the double N* events removed.

The N^{*++} decay angular distributions relevant to one pion exchange were examined in Section IV, C, 4 and found to be in general agreement with the OPEM

---

*Almeida et al. in reference 7 report a similar peaking. They point out that the peaking is not consistent with a simple OPEM but do not relate the peaking to $N^{*++}\pi^-$ resonance production.

Figure 15

Mass distributions for $p_a\pi^+\pi^-$ with $p_a\pi^+$ in the N^{*++} mass band and with $p_b\pi^-$ both in and out of the $N^{*0}(1236)$ mass region. The solid curves are the OPEM (A = 3) predictions normalized to the 1.8 - 2.4 BeV mass region.

(a) Mass of $p_b\pi^- \geq 1.35$ BeV.

(b) Mass of $p_b\pi^- < 1.35$ BeV.

(c) Same as (a) but with $|\text{prod. cos } (p_a\pi^+)| \geq .96$.

(d) Same as (b) but with $|\text{prod. cos } (p_a\pi^+)| \geq .96$.

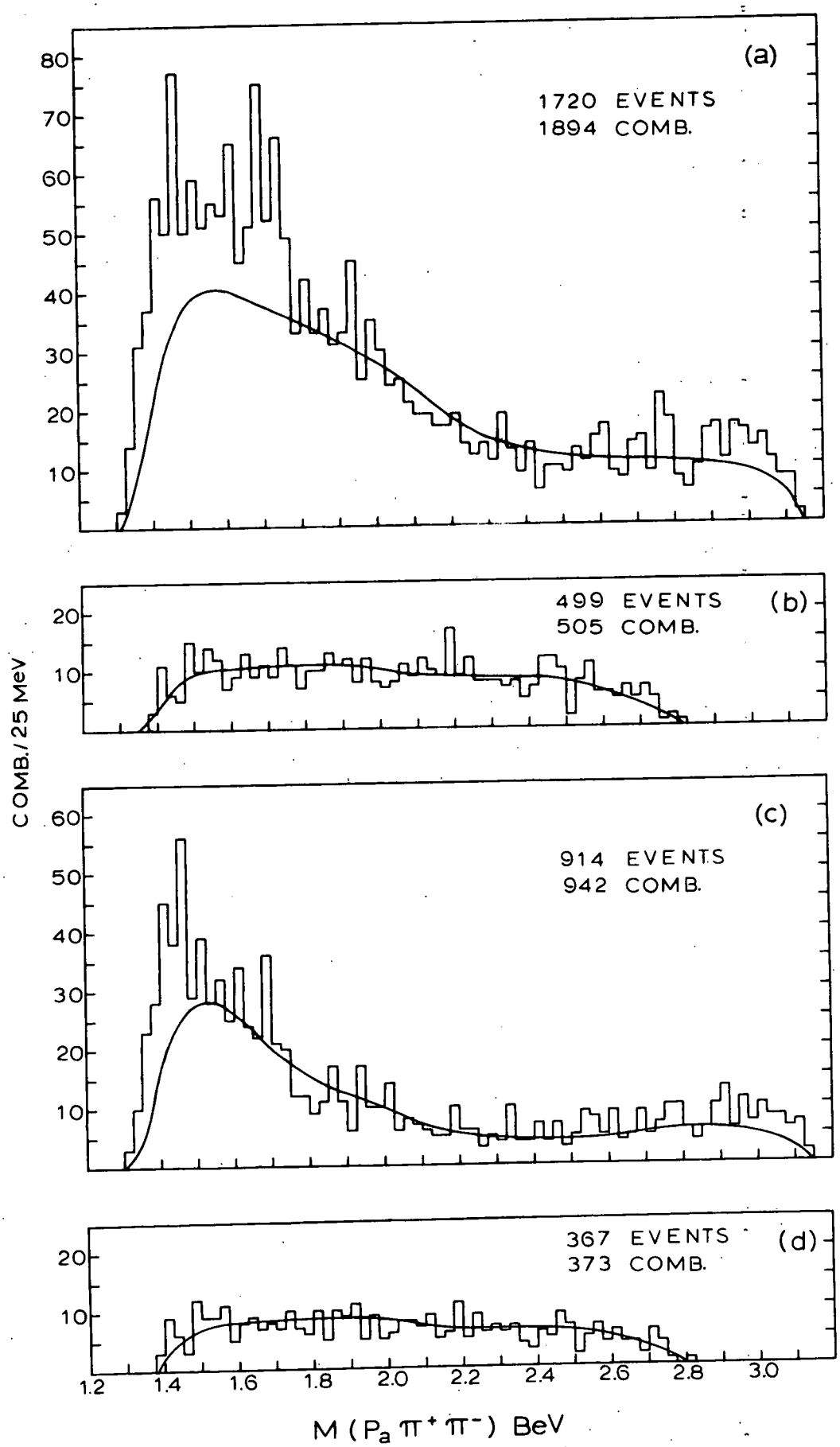
(a)
1720 EVENTS
1894 COMB.
(b)
499 EVENTS
505 COMB.
(c)
914 EVENTS
942 COMB.
(d)
367 EVENTS
373 COMB.
COMB./25 MeV
M ($P_a \pi^+ \pi^-$) BeV

prediction for the sample with the cut on production cosine to the N^{*++}. We now examine these angular distributions for various N^{*++} π^- mass regions. The N^{*++} decay angles are of course not kinematically related to the N^{*++} π^- mass as are $\cos\theta(p_b\pi^-)$ and $\phi(p_b\pi^-)$. For N^{*++}'s formed by one pion exchange the $\phi(p_a\pi^+)$ distribution will be flat and the $\cos\theta(p_a\pi^+)$ distribution will go approximately as $1 + 3\cos^2\theta$ for any N^{*++} π^- mass region. However it is useful to examine these angular distributions, especially for the 1425 MeV region, since a N^{*+} resonance decaying into N^{*++} π^- (or into p π^+ π^-) will not in general give the decay distributions expected from one pion exchange.

The N^{*++} decay distributions for the N^{*++} π^- mass region 1350 - 1475 MeV are shown in Figure 16; the distributions for the regions 1475 - 1800 MeV and above 1800 MeV are shown in Figure 17. The smooth curves are the predictions of the OPEM (A = 3) normalized to the 1.8 - 2.4 BeV region of the appropriate N^{*++} π^- mass distribution. The decay distributions for the region above 1800 MeV with the cut on production cosine (shaded histograms, Figures 17c and d) agree quite well with the OPEM predictions. This agreement is reasonable since this region appears to be free from

Figure 16

Distribution of decay angles (as defined in Figure 8) for $p_a\pi^+$ with $p_a\pi^+$ in the N^{*++} mass band and 1.35 BeV $\leq$ M $(p_a\pi^+ \pi^-) \leq$ 1.475 BeV. The shaded distributions are for the cut on the production cosine to $p_a\pi^+$. The smooth curves are defined in the text.

(a) cos $\theta(p_a\pi^+)$

(b) $\phi(p_a\pi^+)$

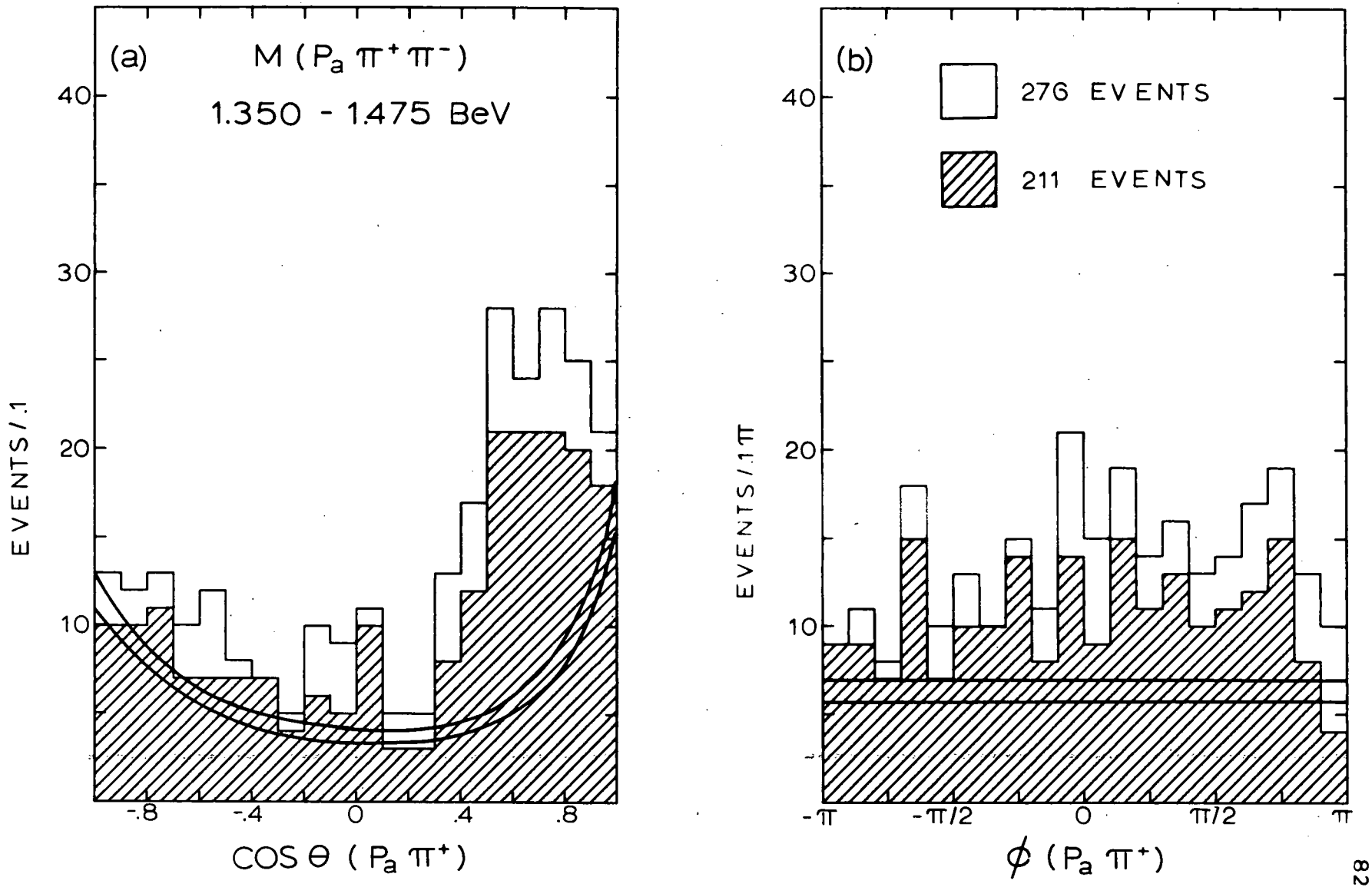
(a)
M ($P_a \pi^+ \pi^-$)
1.350 - 1.475 BeV
EVENTS / .1
40
30
20
10
-.8
-.4
0
.4
.8
COS Θ ($P_a \pi^+$)
(b)
276 EVENTS
211 EVENTS
EVENTS / .1π
40
30
20
10
-π
-π/2
0
π/2
π
φ ($P_a \pi^+$)

Figure 17

Distributions of decay angles for $p_a\pi^+$ with $p_a\pi^+$ in the N^{*++} mass band and selections on the mass of $p_a\pi^+\ \pi^-$. The shaded distributions are for the cut on production cosine to $p_a\pi^+$. The smooth curves are defined in the text.

(a) $\cos\theta(p_a\pi^+)$ for $1.475 \leq M(p_a\pi^+\ \pi^-) \leq 1.8$ BeV.

(b) Corresponding $\phi(p_a\pi^+)$.

(c) $\cos\theta(p_a\pi^+)$ for $M(p_a\pi^+\ \pi^-) \geq 1.8$ BeV.

(d) Corresponding $\phi(p_a\pi^+)$.

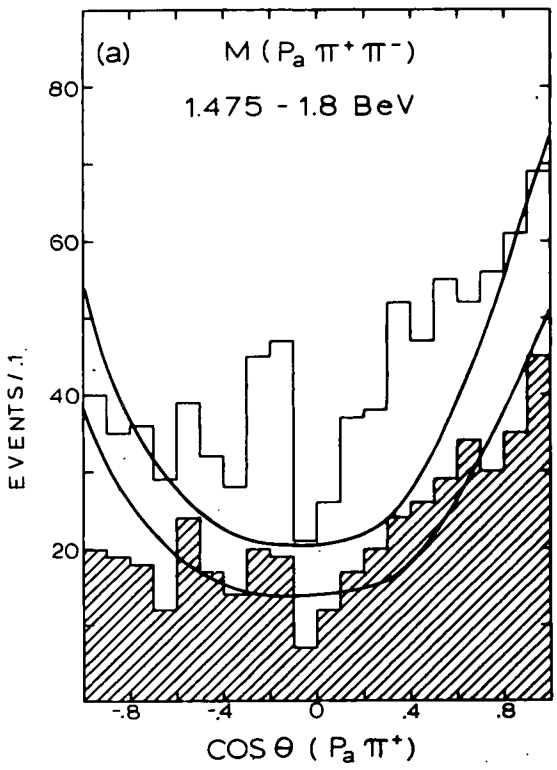
(a)
M ($P_a \pi^+ \pi^-$)
1.475 - 1.8 BeV
EVENTS/.1
80
60
40
20
-.8
-.4
0
.4
.8
COS Θ ($P_a \pi^+$)

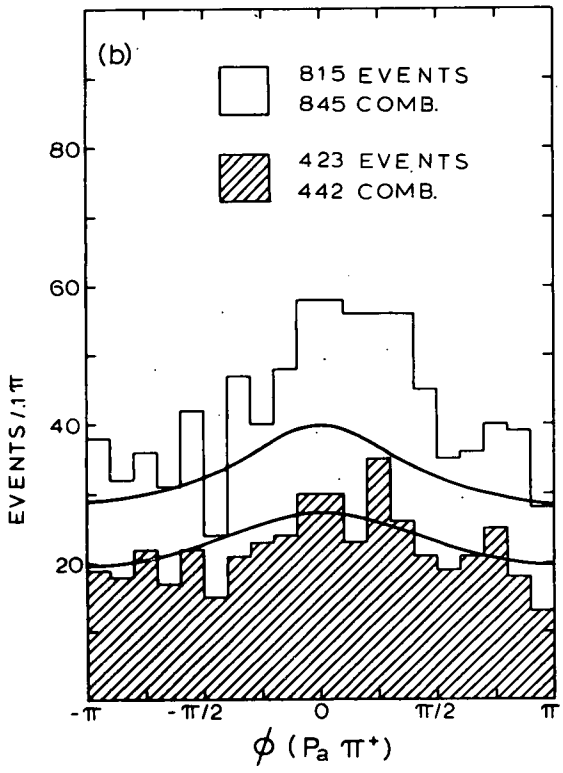
(b)
815 EVENTS
845 COMB.
423 EVENTS
442 COMB.
EVENTS/.1π
80
60
40
20
-π
-π/2
0
π/2
π
φ ($P_a \pi^+$)

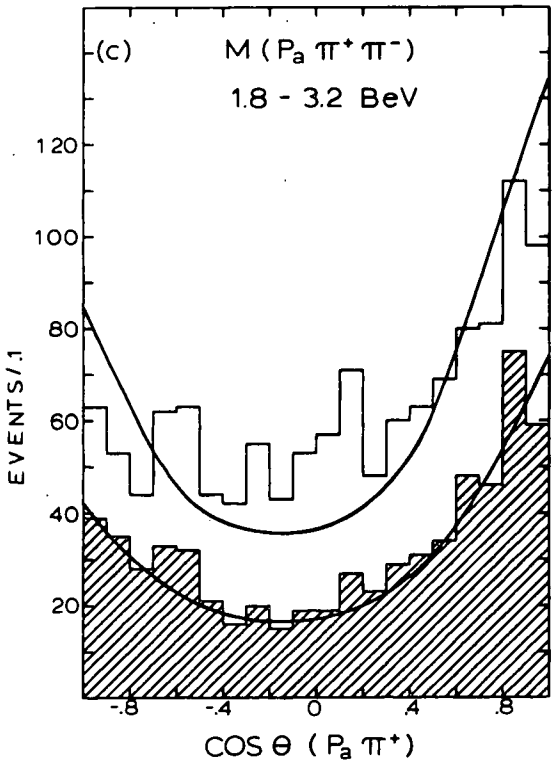
(c)
M ($P_a \pi^+ \pi^-$)
1.8 - 3.2 BeV
EVENTS/.1
120
100
80
60
40
20
-.8
-.4
0
.4
.8
COS Θ ($P_a \pi^+$)

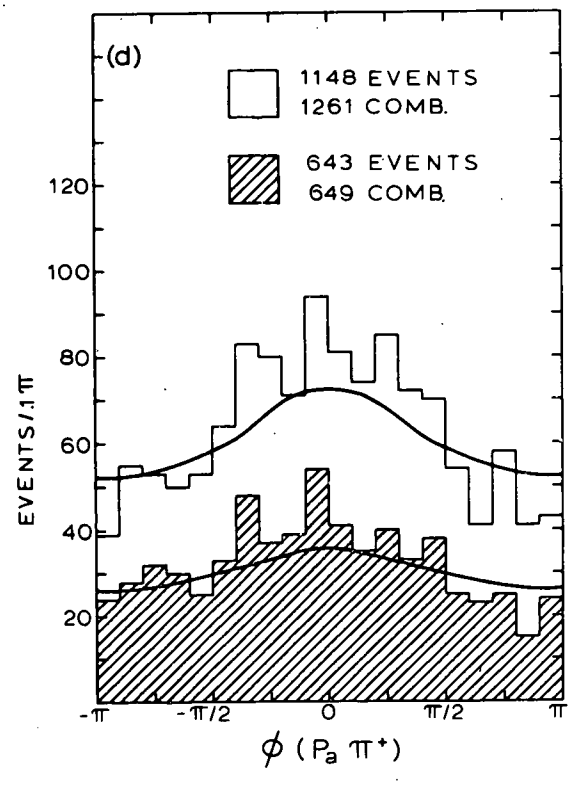
(d)
1148 EVENTS
1261 COMB.
643 EVENTS
649 COMB.
EVENTS/.1π
120
100
80
60
40
20
-π
-π/2
0
π/2
π
φ ($P_a \pi^+$)

any large contribution from resonance production. In contrast, for the 1350 - 1475 region the cos θ distribution shows a large accumulation of events between .4 and 1.0, in disagreement with the OPEM prediction. As discussed above, disagreement with the model is consistent with the interpretation of resonance production in the 1425 MeV region. We note that the cut on production cosine does not improve the agreement between the data and the model. This behavior is consistent with that of the enhancement in the mass distribution. That is, the 1425 MeV enhancement appears above the OPEM prediction both with and without the cut on production cosine. The accumulation in cos θ is not consistent with the OPEM prediction, but neither is it consistent with the cos θ distribution expected from the decay* of a N^{*++} formed in a pure state from the decay of a N^{*+}. For such a N^{*++} parity conservation requires that the contribution to cos θ be symmetric about zero. Thus it appears that if a resonance is being produced it interferes with some other process, perhaps with one pion exchange. For the mass region

---

*In Section IV, D, 2 we show that any resonance contribution to the 1425 MeV enhancement has the principal decay $N^{*++} \pi^-$.

1475 - 1800 MeV (Figure 17a and b) the cut on production cosine improves the agreement between the data and model but the agreement in cos θ is not as good as for the above 1800 MeV region (Figure 17c). As a possible explanation we note that the 1475 - 1800 MeV region no doubt has some contribution from the resonance(s) at 1700 MeV even for the cut on production cosine. In addition, contributions may come from the N*(1525) as well as the tail of the enhancement at 1425 MeV.

Our examination of the N^{*++} π^- system has shown that discrepancies in the OPEM variables $\phi(p_b\pi^-)$ and cos $\theta(p_a\pi^+)$ are associated with enhancements at 1700 MeV and around 1425 MeV in the N^{*++} π^- mass distribution. Especially for the cut on the production cosine to the N^{*++} the discrepancies are associated with the 1425 MeV peak. We thus interpret this enhancement as possibly resulting from resonance production in addition to (or perhaps interfering with) a one pion exchange background.

2. The 1425 MeV Enhancement

The interpretation of the 1425 MeV enhancement as possibly resulting from resonance production suggests that the properties of the enhancement be compared

to those of the N*(1470), the P_{11} wave resonance deduced from π^-p phase shift analysis. It is attractive to suppose that the N*(1470) should be observed in quasi-elastic scattering reactions of the type

$$X\,N \rightarrow X\,N^*(1470)$$

where N is a nucleon and X any strongly interacting particle. That is, since the N*(1470) has the quantum numbers of the nucleon it can be produced by the exchange of the quantum numbers of the vacuum. In the language of "diffractive dissociation",[19,20] the initial nucleon may exist as a virtual N*(1470) state. Transfer of four-momentum from X to the virtual state would place it on the mass shell. In a related concept, Morrison[21] has suggested that the production of the N*(1470) would proceed via a "Pomeranchukon" exchange similar to that associated with Regge Pole analyses of elastic scattering. Indeed, enhancements near 1400 MeV have been observed in the N π and N π π invariant mass distributions in reactions induced by a variety of strongly interacting particles. For most of these reactions, if the enhancement is interpreted as a resonance then the reaction is of the quasi-elastic scattering type.

For a comparison to the enhancement in our experiment we briefly review the properties of the P_{11} resonance and the enhancements observed in other reactions.

Beginning with Roper[22] a number of phase shift analyses (see Rosenfeld et al.[16] for a list of references) have indicated the existence of a resonance in the P_{11} wave. The parameters of the resonance quoted earlier from Rosenfeld et al.[16] (mass of 1470 MeV, width of 210 MeV) are essentially rounded off versions of the parameters determined in the recent phase shift analysis of Donnachie et al.[17] In this analysis the mass is taken as the point of maximum absorption in the partial wave. In a recent analysis by Bareyre et al.[23] two masses and widths are given. A mass of 1470 MeV and width of 255 MeV are determined from the P_{11} wave total cross section; a mass of 1505 MeV and width of 205 MeV from the velocity of the amplitude in the complex plane (the mass is taken as the point of maximum velocity). Earlier analyses gave mass values as low as 1370 MeV. This latter value was determined by Bransden et al.[24] from the point of maximum velocity of the amplitude. The analyses of Donnachie et al. and Bareyre et al. agree that the P_{11} resonance decays inelastically about 35% of the time.

Several analyses have been made of the inelastic decay modes of the P_{11} resonance.[25,26,27] These analyses are essentially of data for the reaction $\pi^- p \rightarrow N \pi \pi$. Various assumptions are made for the inelastic decay modes of the partial waves contributing to a $\pi^- p$ invariant mass region. Calculations corresponding to these assumptions are then compared primarily to distributions of the $N \pi \pi$ internal variables. The analyses agree that in the region of the N*(1470) the inelastic decay $N^{*-}(1236)\ \pi^+$ for the P_{11} wave cannot explain the data for $\pi^- p \rightarrow n \pi^+ \pi^-$. Instead the decay σ n is found to be dominant. Thurnauer[25] takes the σ to be a $\pi \pi$ resonance of mass 490 MeV and width 110 MeV. Namyslowski et al.[26] takes the σ as a T = 0, J = 0 $\pi \pi$ resonance of mass 400 MeV and width 50 MeV. Morgan[27] allows σ to represent a T = 0, J = 0 $\pi \pi$ state, not necessarily a resonance.* For completeness we mention that according to these analyses the D_{13} wave N*(1525)), whose inelastic decay contributes to the same general mass region as the P_{11}, has the dominant inelastic decay $N^{*-}(1236)\ \pi^+$.

---

*Whether the $\pi \pi$ system does resonate as a σ meson is a matter of some debate. See our reference 16 for a list of references.

Over a wide range of incident momenta, missing mass spectrometer experiments show a peak around 1400 MeV in the missing mass spectra of the reactions $p\ p \rightarrow p$ + missing mass and $\pi^{\pm}\ p \rightarrow \pi^{\pm}$ + missing mass. Table 2 summarizes the properties of the 1400 MeV enhancement as determined in the experiments of Anderson et al.,[28] Blair et al.,[29] and Foley et al.[30] References to earlier experiments may be found in our reference 8. In Table 2 the parameter "b" is from fits of the data to

$$\frac{d\sigma}{dt} = Ae^{-bt} \tag{4}$$

where t is the square of the four momentum transfer. A variety of production experiments with the final particles identified have observed $N\pi$ and $N\pi\pi$ enhancements around 1400 MeV. Table 3 lists the properties of the observed enhancement from experiments that attribute it to the $N^*(1470)$. The particles in the enhancement are indicated by parentheses.

Several comments on the reactions listed in Tables 2 and 3 are in order. With the exception of $\pi^-\ p \rightarrow \pi^o(p\ \pi^-)$, for a resonance interpretation of the enhancement each of the reactions is of the quasi-elastic scattering type in which the resonance could be

TABLE 2

REACTION	BEAM MOM. (BeV/c)	MASS (MeV)	WIDTH (MeV)	b $(BeV/c)^{-2}$	CROSS SECTION (mb)	REFERENCE
$p\ p \rightarrow p\ +$ MM	10	1405 ± 15	180 ± 50	22.3 ± 3.4	$.544 \pm .09$	Anderson[28]
	15			15.9 ± 2.3	$.602 \pm .106$	
	20			14.4 ± 2.5	$.660 \pm .15$	
	30			23.5 ± 5.1	$.744 \pm .35$	
$p\ p \rightarrow p\ +$ MM	4.55	1410 ± 15	125 ± 20	14.0 ± 1.3	$.63 \pm .08$	Blair[29]
	6.06			20.7 ± 2.7	$.65 \pm .18$	
	7.88			22.1 ± 4.1	$.45 \pm .09$	
$p\ p \rightarrow p\ +$ MM	9.86 - 20.24	1400 ± 30	150	$18. \pm 2.$	-	Foley[30]
$\pi^- p \rightarrow \pi^- +$ MM	13.98 - 26.23			$12. \pm 2.$	-	
$\pi^+ p \rightarrow \pi^+ +$ MM	10.02, 16.02			$16. \pm 4.$	-	

TABLE 3

REACTION	BEAM MOM. (BeV/c)	MASS (MeV)	WIDTH (MeV)	SPIN PARITY*	CROSS SECTION (mb)	REFERENCE
$p\,p \rightarrow p\,(p\,\pi^+\,\pi^-)$	10	1450 ± 15	-	-	$.18 \pm .04$	Almeida[8]
$p\,(n\,\pi^+)$		-	-	-	$.18 \pm .12$	
$p\,p \rightarrow p\,(p\,\pi^+\,\pi^-)$	8.1	-	-	x	$.35 \pm .15$**	Guyader[6]
$p\,p \rightarrow p\,(n\,\pi^+)$	5.5	-	-	-	$.80 \pm .16$	Alexander[4]
$p\,(p\,\pi^o)$					$.36 \pm .06$	
$\pi^+\,p \rightarrow \pi^+\,(n\,\pi^+)$	6	1405 ± 30	100	-	.034	Bell[31]
$\pi^-\,p \rightarrow \pi^o\,(p\,\pi^-)$		1436 ± 20	50		.008	
$K^+\,p \rightarrow K^+\,(n\,\pi^+)$	3	1385 ± 20	42 ± 22	-		Dodd[32]
$\pi^-\,p \rightarrow \pi^-\,(p\,\pi^+\,\pi^-)$	8	1412 ± 9	$49\ ^{+30}_{-20}$	x		Lamsa[38]
$K^-\,p \rightarrow K^-\,(p\,\pi^o)$	1.45	1470	40	-		Fridman[34]
$K^-\,P \rightarrow K^-\,(p\,\pi^+)$	1.425	1400 - 1450	50 - 100	x		Adelman[35,36]
$K^-\,(p\,\pi^o)$						

* "x" indicates that the spin-parity is consistent with $1/2^+$.

** Combined cross section for N*(1470) and N*(1525).

produced by the exchange of the quantum numbers of the vacuum. (π^- p $\rightarrow \pi^o$(p π^-) requires the exchange of at least one unit of Ispin.) The appearance of an enhancement around 1400 MeV in such reactions induced by a variety of incident particles over a wide range of momenta supports the ideas expressed above concerning the production of the N*(1470). However, an alternative explanation of the enhancements may be offered. Each of the reactions either has a three body final state or could have a quasi-three body final state in which the "quasi-particle" is the N^{*++}(1236). Each (again, with the exception of π^- p $\rightarrow \pi^o$(p π^-)) may then have the enhancement explained as a kinematic effect (Deck effect) arising from exchange diagrams similar to the one used for our OPEM*. As discussed previously, Gellert et al.[5] interpret the enhancement in p p $\rightarrow$ p (p π^+ π^-) at 6.6 BeV/c as kinematic in origin. Walker et al.[37] favor a kinematic interpretation of the enhancement in the reactions π^- p $\rightarrow \pi^-$ (π^o p), π^- (n π^+), and π^- (p π^+ π^-) at 7.0 BeV/c. For the two K^- p reactions listed in Table 3, the upper limit of N π phase space is at roughly

---

*See, for example, the diagrams discussed by Ross and Yam in reference 20.

1500 MeV. The Deck effect is usually associated with enhancements at the low end of invariant mass distributions and thus may not be an appropriate explanation of the enhancement in these reactions. However, as pointed out by Fridman et al.,[34] these experiments could be observing the tail of the N*(1525).

Interpretation of the various enhancements as the N*(1470) is complicated not only by the Deck effect. The widths listed in Tables 2 and 3 are all smaller than the values given by phase shift analyses; only the value of Anderson et al.[28] is consistent, within the quoted error, with the widths given by Donnachie et al.[17] and Bareyre et al.[23] The masses vary considerably (1385 ± 20 MeV to 1450 ± 15 MeV). Although several of the experiments[6,33,36] have reported decay angular distributions that are consistent with a spin-parity of $1/2^+$, none of them have ruled out other assignments. All of the three body enhancements listed are in p π^+ π^-. If these enhancements are the N*(1470) the decay p σ ($\sigma \rightarrow \pi^+ \pi^-$) might be expected since this decay would differ only in the z component of Ispin from the n σ decay favored by the analyses of the inelastic decay modes of the P_{11} wave.[25,26,27] Both Almeida et al.[7]

and Lamsa et al.[33] report that their data are consistent with the decay mode N*(1236) π.

We assert that the evidence for the identity of the N*(1470) of phase shift analysis and the enhancements observed in production experiments is not conclusive. We now show that the 1425 MeV enhancement in our experiment may not be understood as simply an incoherent sum of one pion exchange and production of the N*(1470).

The 1425 MeV enhancement was examined earlier in the $p_a\pi^+\ \pi^-$ mass distribution for the selection of $p_a\pi^+$ in the $N^{*++}(1236)$ mass band. As mentioned in that earlier examination, because of the low mass of the enhancement our selection neither guarantees the decay N*(1236) π nor eliminates the decay p σ for the portion of the enhancement that might result from resonance production. We examine the decay mode via the Dalitz plot (Figure 18) for $p_a\pi^+\ \pi^-$ combinations in the mass region of the enhancement ($1.35\ \text{BeV} \leq M(p_a\pi^+\ \pi^-) \leq 1.475\ \text{BeV}$). For this plot there is no restriction on the $p_a\pi^+$ mass. The solid curves on the projections are the predictions of the OPEM normalized to the number of combinations in the mass region 1800 - 2400 MeV of the overall $p\ \pi^+\ \pi^-$ distribution and are our estimate of the one pion exchange

Figure 18

Dalitz plot and projections for $1.35 \leq M(p_a \pi^+ \pi^-) \leq 1.475$ BeV. The solid and dashed curves on the projections are explained in the text.

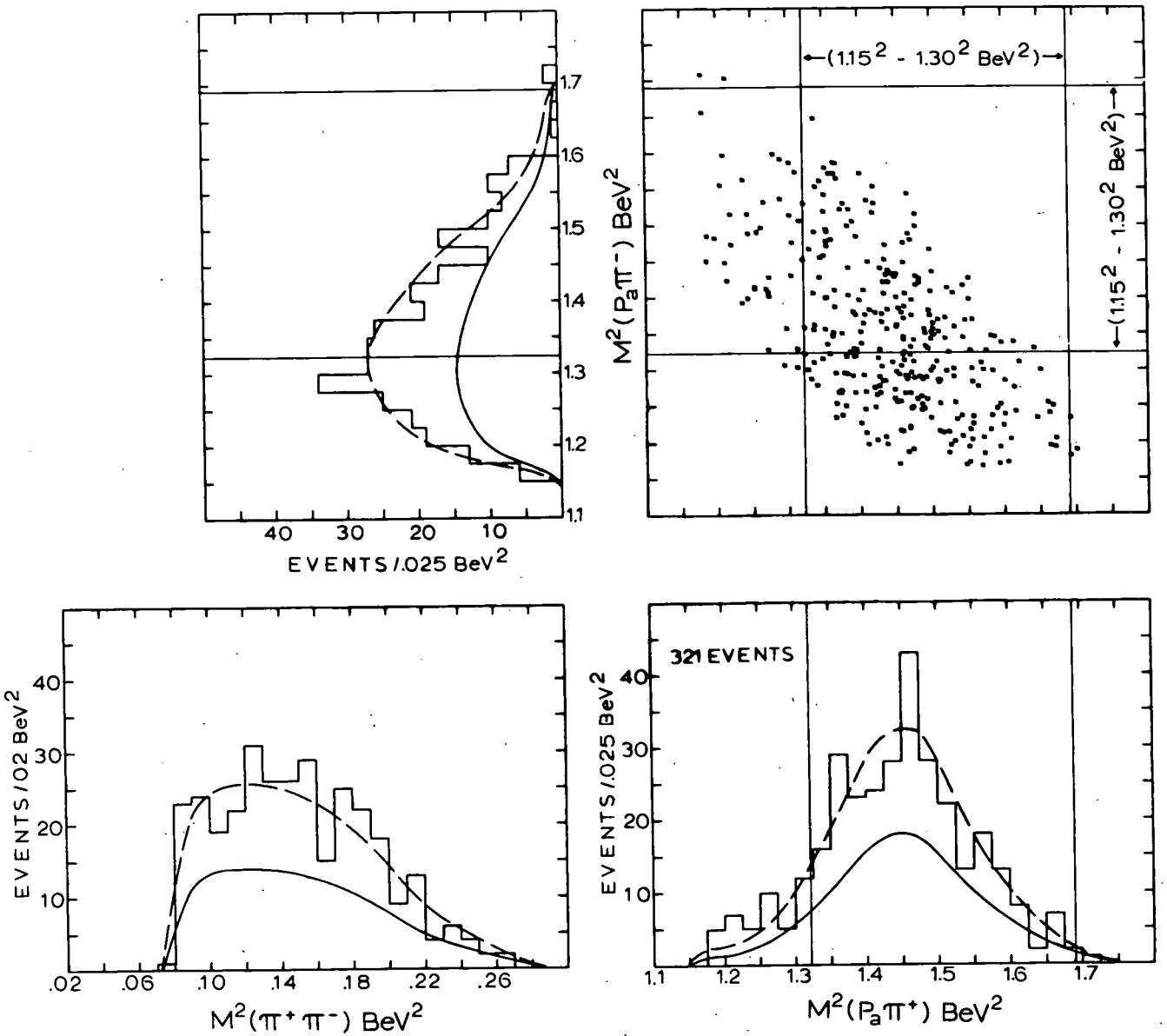
1.7
1.6
1.5
1.4
1.3
1.2
1.1
40
30
20
10
EVENTS/.025 BeV²
←(1.15² - 1.30² BeV²)→
M²(PaπT⁻) BeV²
←(1.15² - 1.30² BeV²)→
EVENTS/02 BeV²
40
30
20
10
.02
.06
.10
.14
.18
.22
.26
M²(π⁺π⁻) BeV²
321 EVENTS
EVENTS/.025 BeV²
40
30
20
10
1.1
1.2
1.3
1.4
1.5
1.6
1.7
M²(Paπ⁺) BeV²

background. The dashed curves are for the OPEM normalized to the number of events in the plot. These dashed curves agree quite well with the data, showing that any contribution from resonance production gives projections of the Dalitz plot of about the same shape as the model. Both the data and the model show a strong N^{*++} in the $p_a\pi^+$ distribution and no indication of N^{*o} production in the $p_a\pi^-$ distribution. (For ease of comparison the limits of our N*(1236) mass band are shown on the plot and projections.) The $\pi^+ \pi^-$ distribution shows no indication of a narrow resonance that could correspond to the σ. A broad σ resonance or T = 0, J = 0 state could go undetected in the $\pi^+ \pi^-$ distribution. However for such a resonance or state the $p_a\pi^+$ and $p_a\pi^-$ distributions in excess of the OPEM background should be similar and they are not.

Since the projections of the Dalitz plot in Figure 18 are well described in shape by the OPEM, it is of interest to consider whether a resonance decaying into N*(1236) π^- could give similar projections to those of the model. The dominance of the N^{*++} over N^{*o} is expected both for a Ispin = 1/2 resonance and for a kinematic effect. For the resonance the branching ratio from Clebsch - Gordan coefficients is

$$\text{Ratio} \quad \frac{(N^{*++}\ \pi^-)}{(N^{*o}\ \pi^+ \rightarrow p\ \pi^-)} = \frac{9}{1}$$

For the kinematic effect consider Diagram a of Figure 4. The contribution to low $p\ \pi^+\ \pi^-$ mass will come from N^{*++} (N^{*o}) production at one vertex and $\pi^-\ p$ ($\pi^+\ p$) elastic scattering at the other vertex. In section IV, D, 1 we showed that double Isobar production (N^{*++} at one vertex, $N^{*o}(1236)$ at the other) does not contribute significantly to the 1425 MeV enhancement. Above the $N^*(1236)$ region the $\pi^-\ p$ and $\pi^+\ p$ differential cross sections are roughly the same.[38] Thus we expect

$$\text{Ratio} \frac{(N^{*++}\ \pi^-)}{(N^{*o}\ \pi^+ \rightarrow p\ \pi^-)} \sim \frac{|\langle \pi^+\ p \mid N^{*++} \rangle|^2}{|\langle \pi^-\ p \mid N^{*o} \rangle|^2} \sim \frac{9}{1}$$

Given the dominance of the $N^{*++}\ \pi^-$ contribution for either resonance production or a kinematic effect, the $p_a\pi^-$ and $\pi^+\ \pi^-$ distributions will be essentially reflections of the N^{*++} decay. In particular, the $p_a\pi^-$ and $\pi^+\ \pi^-$ masses may be thought of as depending on the angle in the N^{*++} rest frame between the outgoing proton and the line of flight of the N^{*++} from the $N^{*++}\ \pi^-$ rest frame

(θ_2 of Figure 19). As discussed below, a resonance decaying into $N^{*++}\ \pi^-$ will (in the absence of interference) give a distribution of this angle that depends on the spin - parity of the resonance. Thus a resonance could yield similar $p_a\pi^-$ and $\pi^+\ \pi^-$ distributions to those predicted by the OPEM if the model predicts a similar distribution of the above angle as the resonance. We conclude that the projections of the Dalitz plot could be consistent with the decay of a resonance into $N^{*++}\ \pi^-$ but not into p σ.

Given the $N^{*++}(1236)\ \pi^-$ decay mode of any resonance contribution to the 1425 MeV enhancement, we refer to the discussion at the end of Section IV, D, 1. In that discussion we showed that if the resonance decayed $N^{*++}\ \pi^-$ then the resonant amplitude apparently interfered with some other process. Without a detailed understanding of the interference a determination of the spin-parity is not possible. However Guyader et al.[6] in the reaction $p\ p \rightarrow p\ p\ \pi^+\ \pi^-$ at 8.1 BeV/c, and Lamsa et al.[33] in $\pi^-\ p \rightarrow \pi^-\ p\ \pi^+\ \pi^-$ at 8.0 BeV/c have reported angular distributions that are consistent with $J^P = 1/2^+$. Thus, with particular reference to the experiment of Guyader et al., we examine angular distributions appropriate

Figure 19

Definition of the sequential decay angles discussed in the text. "in" and "out" refer to the incident and outgoing protons. "N*" refers to the intermediate resonance. $\overrightarrow{(N^* \pi)}$ specifies the direction of transformation from the overall center of mass to the $N^* \pi$ rest frame.

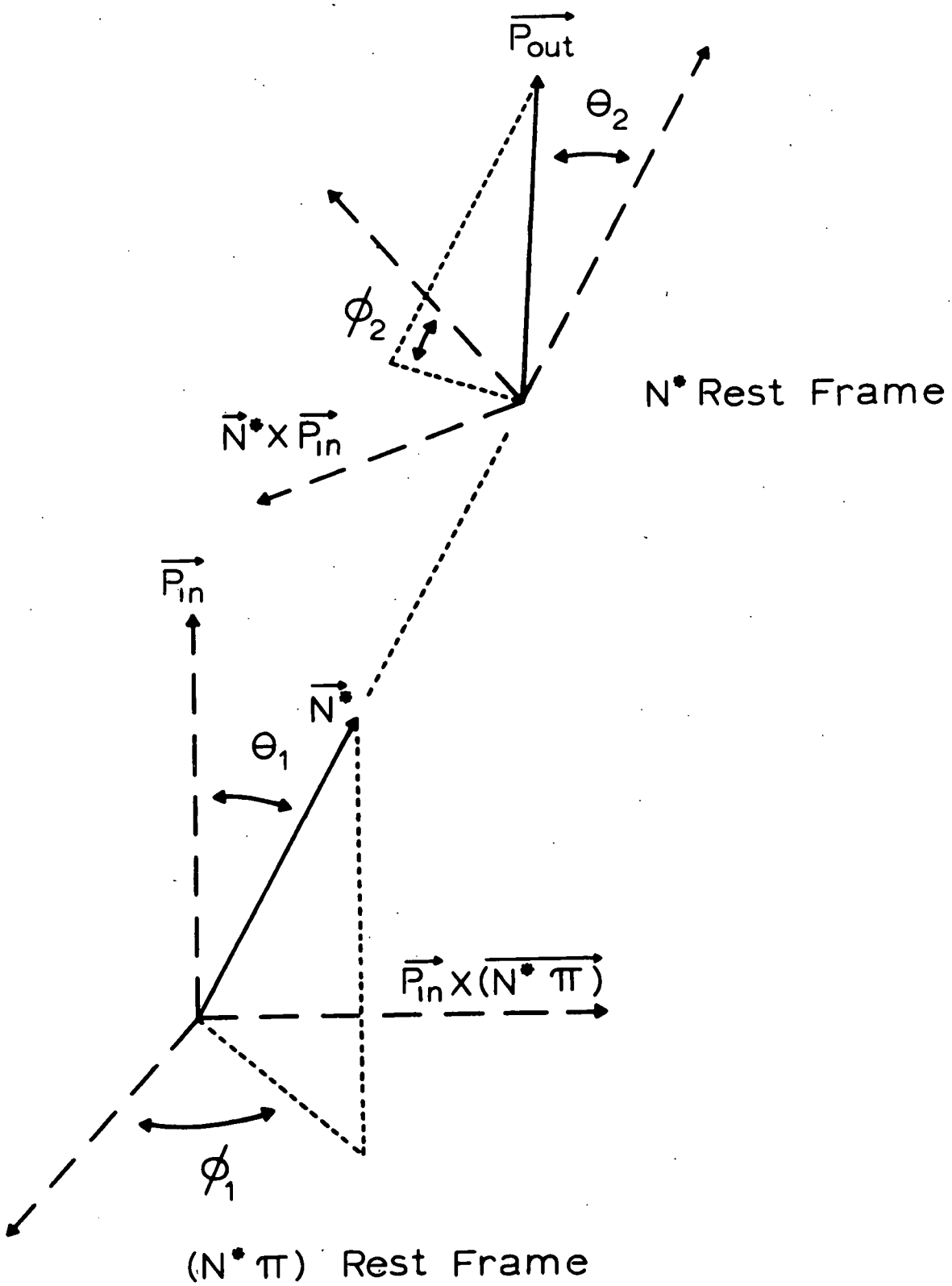
$\vec{P}_{out}$
θ_2
ϕ_2
N* Rest Frame
$\vec{N}^* \times \vec{P}_{in}$
$\vec{P}_{in}$
$\vec{N}^*$
θ_1
$\vec{P}_{in} \times (\vec{N^*\pi})$
ϕ_1
$(N^*\pi)$ Rest Frame

for the sequential decay

$$N^{*+} \rightarrow N^{*++}(1236)\ \pi^- \qquad N^{*++} \rightarrow p_a \pi^+$$

We show that although some of the distributions could be consistent with $J^P = 1/2^+$, others are not but rather reflect the apparent interference.

We consider the decay angles defined in Figure 19. (θ_1, ϕ_1) are for the initial decay, (θ_2, ϕ_2) for the final decay. The distributions of these angles are shown in Figure 20 for the selection $1.35 \leq M(N^{*++}\ \pi^-) \leq 1.475$ BeV. The shaded histograms are for the additional requirement that $|\text{prod. cos}\ (N^{*++}\ \pi^-)| \geq .98$. This latter selection criterion tends to isolate the 1425 MeV enhancement (Figure 21) like the cut on production cosine to the N^{*++} (Figure 13b) but is more appropriate for the current discussion. Shown for comparison are the predictions of the OPEM (A = 3), normalized to the 1800 - 2400 MeV region of the appropriate $N^{*++}\ \pi^-$ mass distributions. Consider the initial decay. In the absence of interference the parity conserving decay of a spin one-half particle will be isotropic. As shown in Figure 20a, the cos θ_1 distribution is relatively flat. Particularly

Figure 20

Sequential decay angles as defined in Figure 19 for the decay

$$N^{*+} \rightarrow N^{*++}\ \pi^- \quad (N^{*++} \rightarrow p_a \pi^+)$$

The shaded histograms are for $|\text{prod. cos}\ (N^{*++}\ \pi^-)| \leq .98$. The solid curves are the OPEM predictions normalized as discussed in the text.

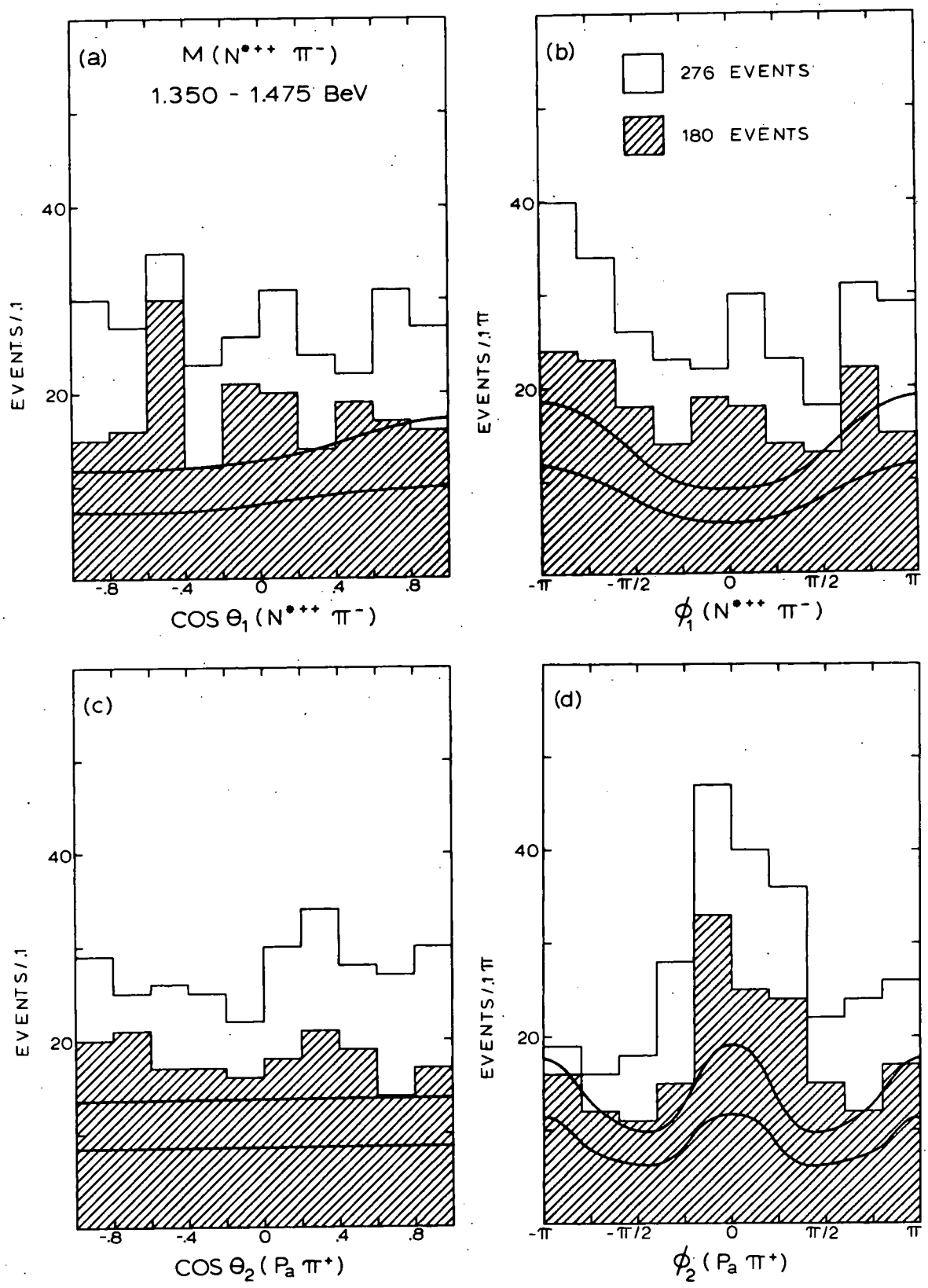
(a)
M (N*++ π⁻)
1.350 - 1.475 BeV
EVENTS/.1
40
20
-.8
-.4
0
.4
.8
COS θ1 (N*++ π⁻)
(b)
276 EVENTS
180 EVENTS
EVENTS/.1 π
40
20
-π
-π/2
0
π/2
π
φ1 (N*++ π⁻)
(c)
EVENTS/.1
40
20
-.8
-.4
0
.4
.8
COS θ2 (Pa π+)
(d)
EVENTS/.1 π
40
20
-π
-π/2
0
π/2
π
φ2 (Pa π+)

for the cut on production cosine, subtraction of the OPEM prediction would leave a relatively flat distribution. The ϕ_1 distribution shows to some extent the tendency of the OPEM to peak at $\pm \pi$. Subtraction of the OPEM would give a distribution that might be consistent with isotropy. We do not investigate the initial decay angular distributions in more detail since the final decay angles (θ_2, ϕ_2) are more revealing. For these latter angles Jackson[39] shows that for any J^P of the N^{*+} if one assumes that only the lowest L value contributes (for J = 1/2, there is only one L value) the distribution is given by:

$$W(\theta_2,\phi_2) \propto 1 + C_{J,P} \cdot P_2 (\cos \theta_2)$$

The distribution is independent of the production mechanism of the N^{*+}. The $C_{J,P}$ are tabulated in reference 39 for $J \leq 11/2$. In particular, for J = 1/2 (either parity)

$$W(\theta_2,\phi_2) \propto 1 + 3\cos^2\theta_2$$

The data show no indication of this distribution. The $\cos \theta_2$ distribution agrees well in shape (as expected from the above discussion of the Dalitz plot) with the flat prediction of the OPEM. The ϕ_2 distribution is quite markedly not flat. This latter distribution is strongly

Figure 21

Mass of $N^{*++}(1236)\ \pi^-$ for

$|$ prod. cos $(N^{*++}\ \pi^-)| \geq .98.$

The smooth curves are defined in the text.

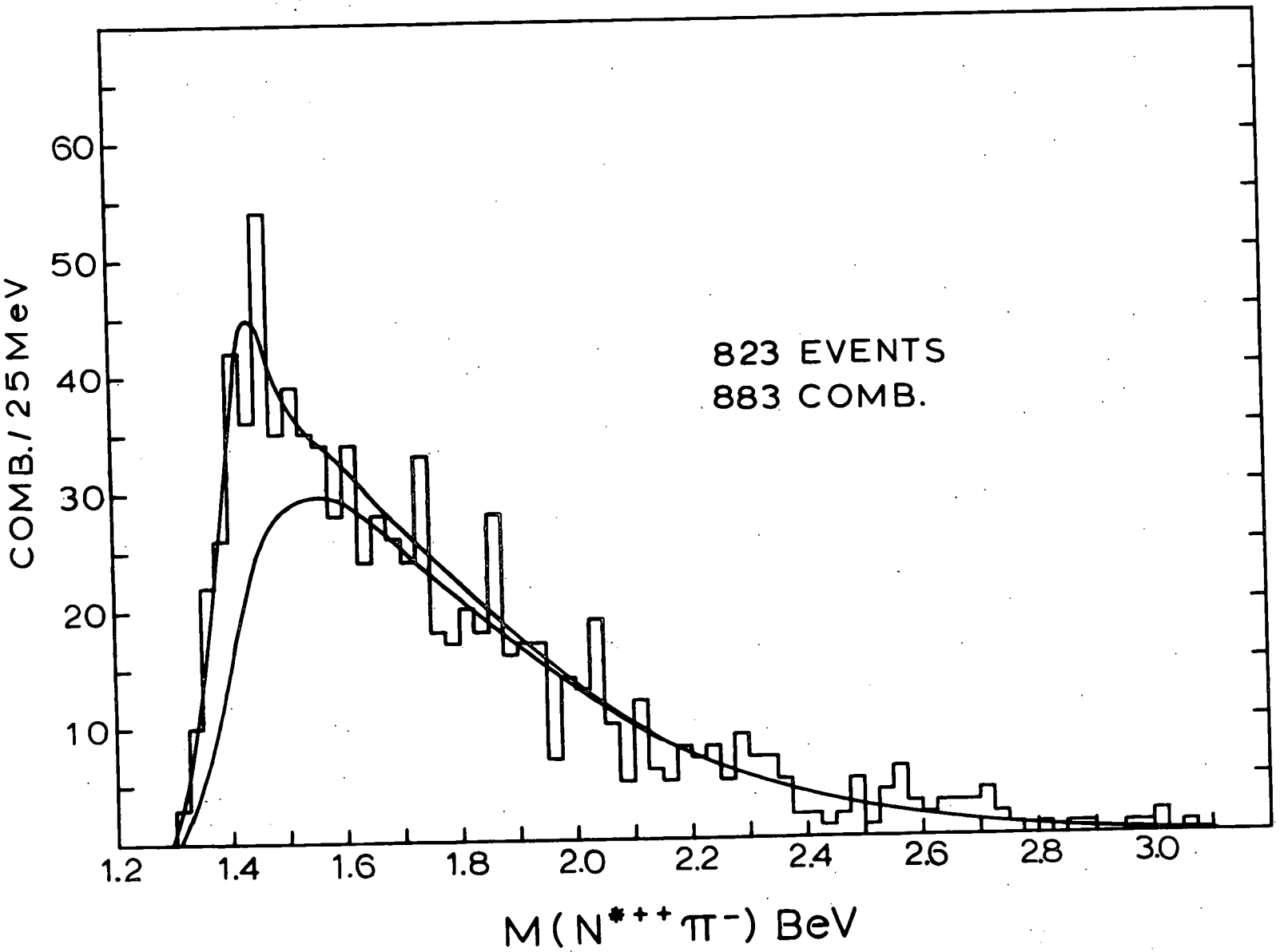
823 EVENTS
883 COMB.
COMB./25 MeV
60
50
40
30
20
10
1.2
1.4
1.6
1.8
2.0
2.2
2.4
2.6
2.8
3.0
M(N*++π-) BeV

peaked towards $\phi_2 = 0$; subtraction of the OPEM background would result in a distribution that would be even less consistent with isotropy. Moreover, the ϕ_2 distribution reflects the apparent interference since parity conservation requires for a pure state that $W(\phi) = W(\phi + \pi)$. Thus the final decay angles are not consistent with any spin-parity assignment for a non-interfering N^{*+}. We conclude that the 1425 MeV enhancement in our data may not be readily identified as the N*(1470) on the basis of angular distributions.

From the above discussion of angular distributions, we are not able to identify the 1425 MeV enhancement as an incoherent sum of resonance production and one pion exchange background. However when treated as such a sum, the mass and width of the "resonance" part are of interest for comparison to the values obtained in the production experiments listed in Tables 2 and 3. We determine a mass and width from the $N^{*++}\ \pi^-$ mass distribution with $|\text{prod. cos } (N^{*++}\ \pi^-)| \leq .98$ (Figure 21). This latter selection isolates the 1425 MeV enhancement like the selection $|\text{prod. cos } (N^{*++})| \leq .96$ (Figure 13b) but is more appropriate for a $N^{*++}\ \pi^-$ resonance. In Figure 21 the lower of the two solid curves

is the OPEM (A = 3) prediction for the background normalized to the 1.8 - 2.4 BeV mass region. The upper curve is the sum of the OPEM background and a simple Breit-Wigner to represent the resonance contribution. The parameters of the Breit-Wigner were determined as follows. The amount of Breit-Wigner resonance in the mass region 1.3 - 1.6 BeV was set equal to the excess of events above the OPEM curve in the same mass region. The mass and width were then obtained via a fit (maximum likelihood) to the histogram in the 1.3 - 1.6 BeV region. This method allowed a reasonable fit to the shape of the experimental distribution in the region of the enhancement while eliminating any effects of the tail of the Breit-Wigner. The results (with statistical errors) were $M = 1.42 \pm .01$ BeV, $\Gamma = .11 \pm .01$ BeV. To examine the dependence of the mass and width on the background, we obtained in the same manner values for the OPEM background with A = 1 and with no form factor. The results were $M = 1.41 \pm .01$ BeV, $\Gamma = .10 \pm .02$ BeV and $M = 1.44 \pm .01$ BeV, $\Gamma = .13 \pm .02$ BeV respectively. Taking the values obtained for A = 3 but allowing for the uncertainty in background (as well as statistical errors) we estimate $M = 1.42 \pm .03$ BeV, $\Gamma = .11 \pm .03$ BeV. Within the error

estimates, our values are consistent with those of the missing mass spectrometer experiments (Table 2). Our value for the mass is fairly consistent (again, within the errors) with most of the values obtained in other bubble chamber experiments (Table 3). Our value for the width is somewhat larger than the 40 - 50 MeV obtained in several of these experiments.

We conclude the discussion of the 1425 MeV enhancement by examining the t (square of the four momentum transfer) distribution for the protons recoiling against the p π^+ π^- combinations in the enhancement. Figure 22 shows the distribution for $1.35 \leq M(p\ \pi^+\ \pi^-) \leq 1.475$ BeV. A maximum likelihood fit for the events with $.025 \leq t \leq .25$ $(BeV/c)^2$ (215 events) to equation (4) gave $b = 11 \pm 1$. (Essentially the same result is obtained if the p π^+ combination is restricted to the N^{*++} mass band.) The OPEM predicts a value of b that ranges from 12 (no form factor) to 13 (form factor with A = 1). Since the value for the data is about the same as predicted we can assign a value of about 11 to events in excess of the number predicted by the model.

The value for b of 11 $(BeV/c)^{-2}$ is smaller than the 18 - 22 $(BeV/c)^{-2}$ obtained for the enhancement near 1400

MeV in the proton-proton missing mass spectrometer experiments at nearby beam momenta (Table 2). The difference between our value and those of the missing mass experiments is perhaps not meaningful because of the different experimental conditions. For these experiments the 1400 MeV region may be populated by any three or four body final state containing a proton. In addition, the missing mass experiments obtain $d\sigma/dt$ by finding the cross section for the enhancement above a (usually arbitrary) background at various values of t. We do not have access in our experiment to other final states and have insufficient data to simulate the technique to obtain $d\sigma/dt$ of the missing mass experiments. We have, however, examined the possibility that experimental biases against small values of t could explain our smaller value of b.

One source of such a bias is the finite (measuring) errors on t which have a tendency to spread out a narrow t distribution. In the 1.35 - 1.475 BeV mass region the errors are typically 1 - 5% of the value; 82% of the events have an error less than 10%. To examine the effect of such errors we generated by a Monte-Carlo method a set of t's that satisfied equation (4) with b = 18. We then assigned an error of 20% to each of the t and

Figure 22

"t" distribution to the protons recoiling against those p π^+ π^- combinations with mass between 1.35 and 1.475 BeV. The smooth curve is for b = 11 $(\text{BeV/c})^{-2}$.

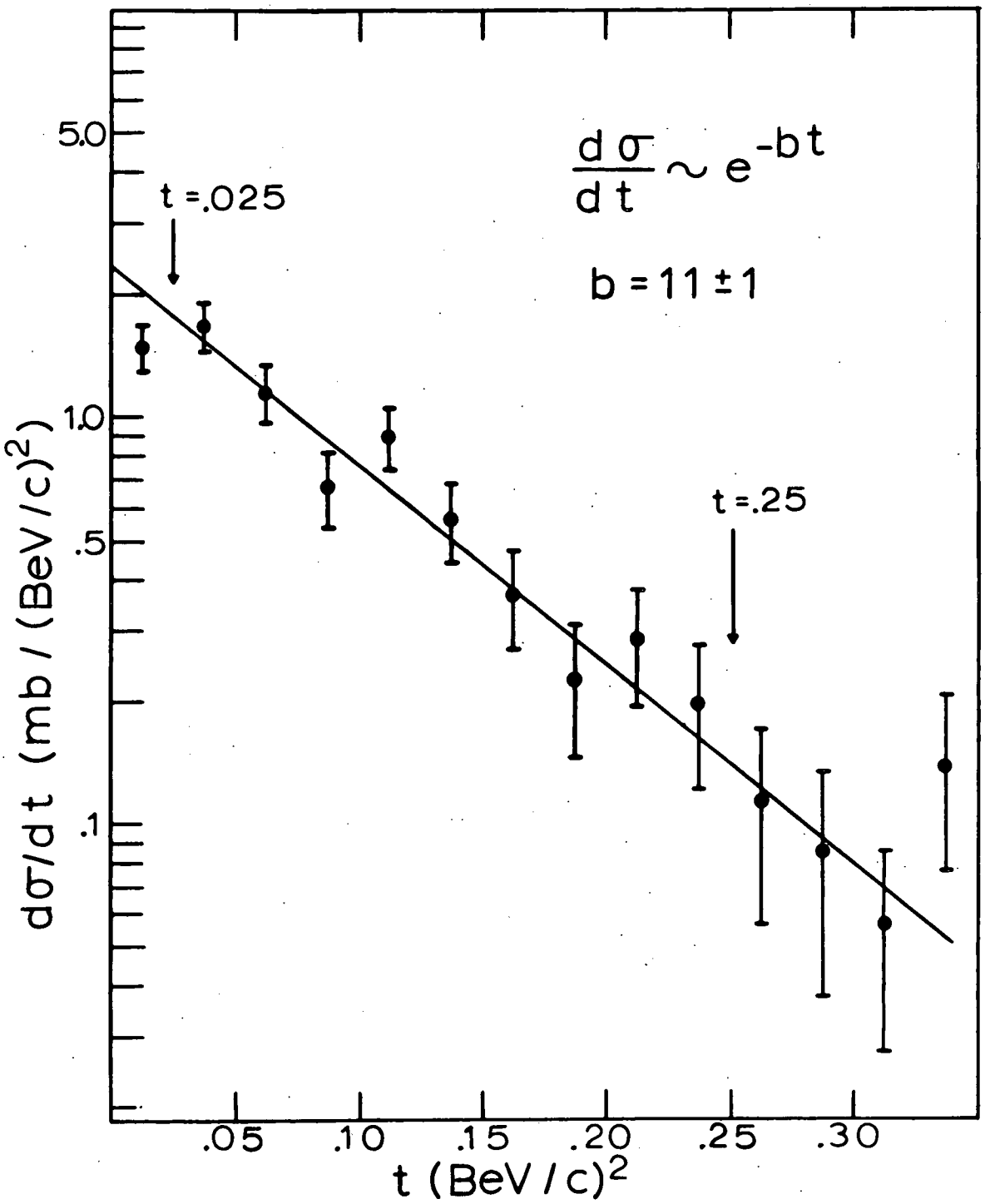
$\frac{d\sigma}{dt} \sim e^{-bt}$
b = 11 ± 1
t = .025
t = .25
5.0
1.0
.5
.1
dσ/dt (mb / (BeV/c)²)
.05
.10
.15
.20
.25
.30
t (BeV/c)²

distributed (Gaussian distribution) each t about the original value according to the error. The distributed t gave a value of b that was essentially indistinguishable from 18 for $.025 \leq t \leq .25$ $(\text{BeV/c})^2$. Thus the errors in t could not have reduced a higher value of b down to 11. A second possibility is that we have lost events with small t values in the scanning - measuring - reconstructing phase of the experiment. That such a loss could occur may be understood by considering those events in which a high momentum secondary proton in combination with the $\pi^+ \pi^-$ has small invariant mass and the proton recoiling against the combination has a small value of t. For the recoiling proton (which we identify as the target proton)

$$t = 2MT \approx P^2$$

where M is the mass of a proton and T and P are the kinetic energy and momentum of the proton in the lab. Protons of momentum less than about 100 MeV will usually be undetected in the bubble chamber and hence we will lose events with $t \lesssim .01$ $(\text{BeV/c})^2$. This loss does not effect our value of b since it was determined for $.025 \leq t \leq .25$ $(\text{BeV/c})^2$. However in this t range it would still be possible for scanners to miss or for the reconstruction program to reject selectively events with protons of small

lab momentum (and hence small values of t). To examine this possibility we take advantage of the forward-backward symmetry in the overall center of mass expected for a proton-proton experiment. We may obtain a value of b for forward recoil protons (fast in the lab) and backward recoil protons (slow in the lab). The values are 12 ± 2 $(\text{BeV/c})^{-2}$ for 99 events and 10 ± 2 $(\text{BeV/c})^{-2}$ for 116 events respectively. We conclude that our value for b does not appear to be particularly effected by experimental biases.

In summary, we are not able to identify the 1425 MeV enhancement in this experiment as the N*(1470). Any resonance contribution to the enhancement has the principal decay $N^{*++}(1236)$ π^- rather than the p σ decay favored by the analyses of π^- p inelastic scattering. The decay angular distributions do not allow a determination of the spin-parity of the presumed resonance but rather reflect an apparent interference process. The mass and width of the enhancement, treated as a non-interfering resonance, agree fairly well with the values obtained in the missing mass spectrometer experiments; the width is larger than the values obtained in some other bubble chamber experiments. The t distribution of the events in the region of the

enhancement is wider than that of the missing mass experiments. This wider distribution does not appear to be explained by experimental biases in our data but could reflect the difference in experimental conditions.

E. The p p , p p π^+ , and p p π^- Systems

As evidenced by the absence of discussion in a recent review of resonances[16] there are no established resonances with Baryon number = 2. However the possibility has been mentioned[40] that such resonances might exist and be members of an SU_3 multiplet of which the deuteron would be a stable member. A candidate for this multiplet has been submitted by Kidd et al.[3] A peak is observed at a mass of 2520 MeV with a width of 120 MeV in the p p π^+ mass distribution from the p p π^+ π^- final state at an incident momentum of 4.0 BeV/c. More recently Brunt et al.[41] report a possible resonance in the d π^+ mass distribution in the reaction p d $\rightarrow$ p d π^+ π^- at incident momenta of 1.825 and 2.110 BeV/c. The mass and width are 2130 MeV and 50 MeV respectively. Given the possibility of resonance production the Baryon number = 2 systems merit at least a cursory examination.

The overall p p mass distribution is shown in Figure 23, the overall p p π^+ distribution in Figure 24a, and the

Figure 23

Mass distribution for all p p combinations. The solid curve is the OPEM (A = 3) prediction; the dashed curve is phase space. Both curves are normalized to the number of events.

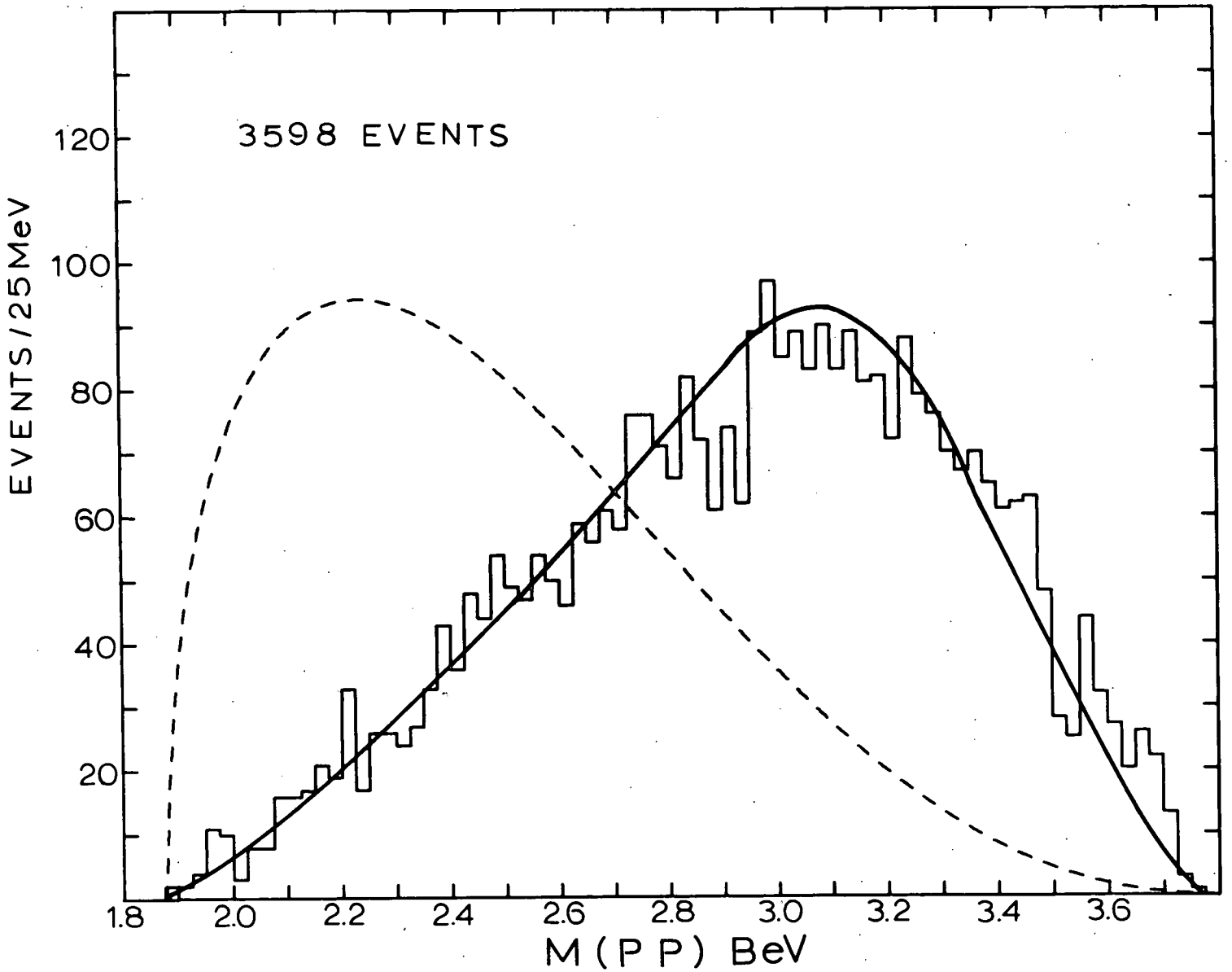
3598 EVENTS
EVENTS/25MeV
120
100
80
60
40
20
1.8
2.0
2.2
2.4
2.6
2.8
3.0
3.2
3.4
3.6
M(PP) BeV

Figure 24

p p π^+ mass distributions. The dashed curve is phase space. The solid curves are the OPEM (A = 3) predictions normalized to the number of events in each histogram.

(a) All events.

(b) Unshaded. Those events for which at least one p π^+ combination is in the $N^{*++}(1236)$ mass band. Shaded. Those events for which at least one p π^+ combination is in the $N^{*++}(1236)$ mass band and has $|\text{prod. cos } (p\ \pi^+)| \leq .96$.

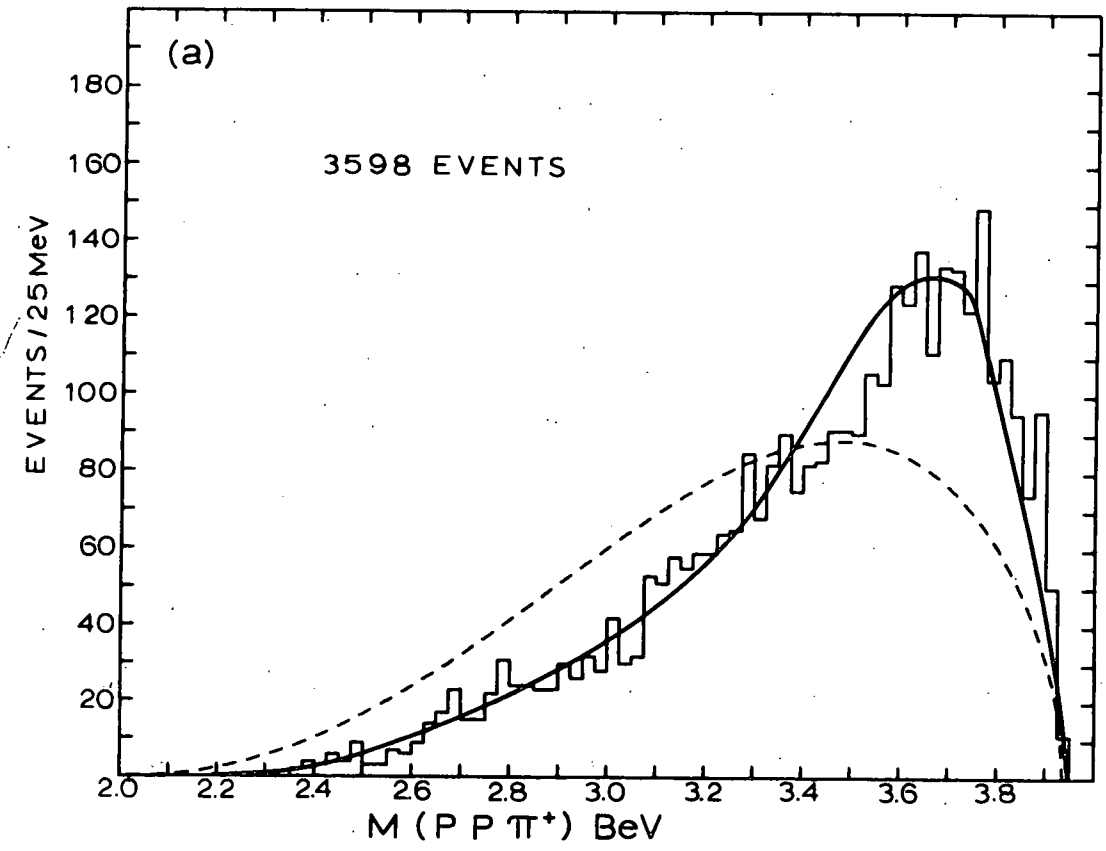
(a)
3598 EVENTS
EVENTS / 25 MeV
180
160
140
120
100
80
60
40
20
2.0
2.2
2.4
2.6
2.8
3.0
3.2
3.4
3.6
3.8
M (P P π⁺) BeV

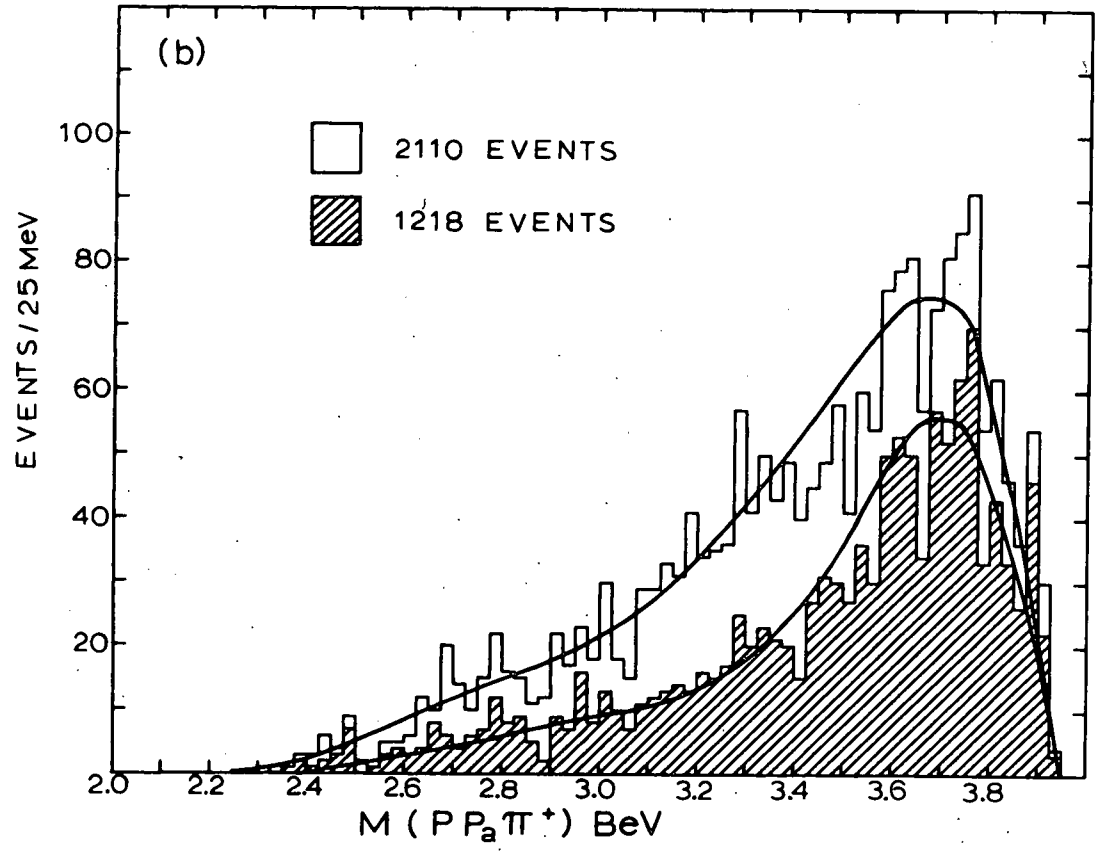
(b)
2110 EVENTS
1218 EVENTS
EVENTS / 25 MeV
100
80
60
40
20
2.0
2.2
2.4
2.6
2.8
3.0
3.2
3.4
3.6
3.8
M (P Pa π⁺) BeV

Figure 25

p p π^- mass distributions. The dashed curve is phase space. The solid curves are the predictions of the OPEM (A = 3) normalized to the number of events in the overall distribution.

(a) All events.

(b) Those events for which at least one p π^+ π^- combination has a mass less than 1800 MeV.

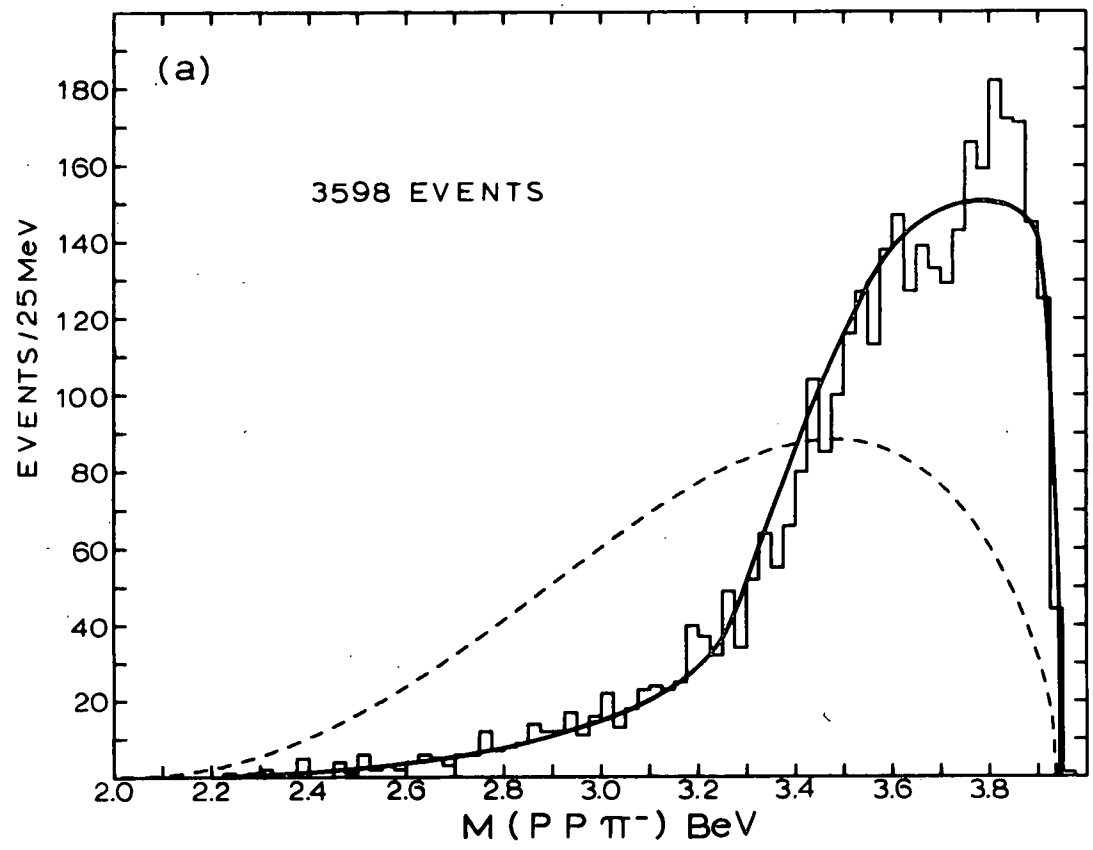
(a)
3598 EVENTS
EVENTS/25 MeV
180
160
140
120
100
80
60
40
20
2.0
2.2
2.4
2.6
2.8
3.0
3.2
3.4
3.6
3.8
M (P P π⁻) BeV

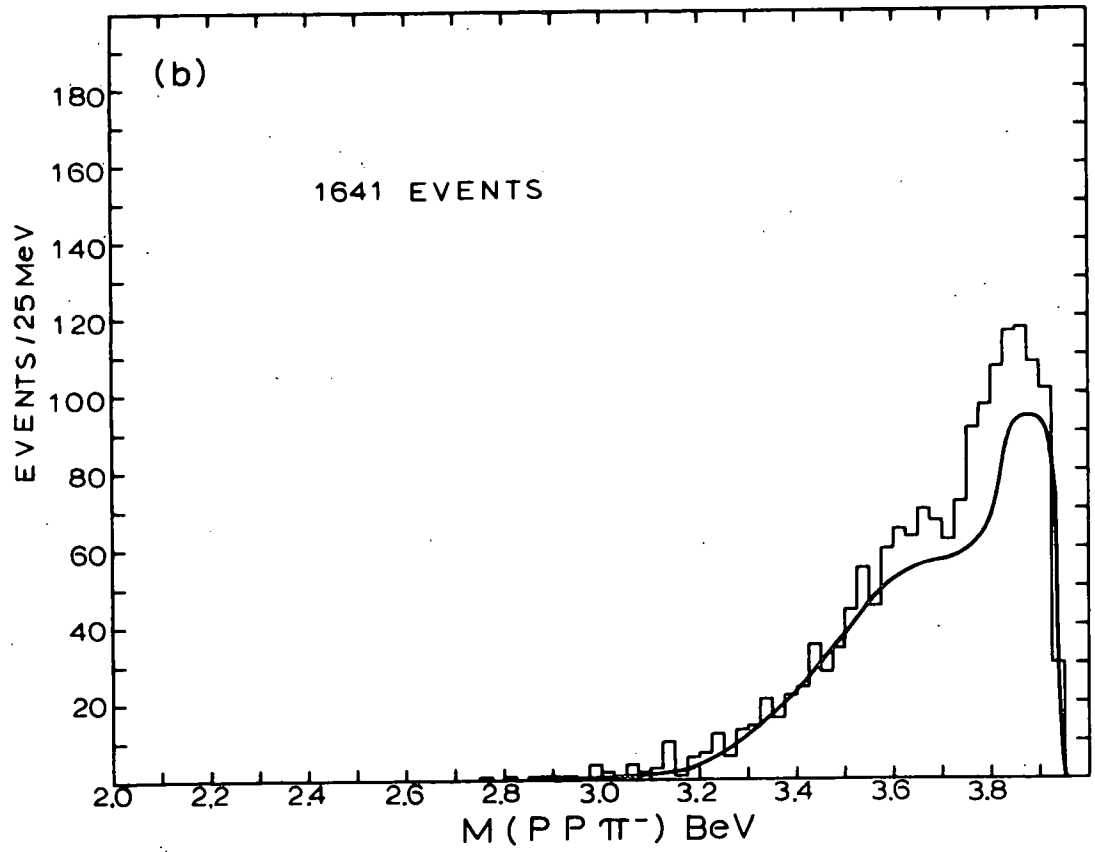
(b)
1641 EVENTS
EVENTS/25 MeV
180
160
140
120
100
80
60
40
20
2.0
2.2
2.4
2.6
2.8
3.0
3.2
3.4
3.6
3.8
M (P P π⁻) BeV

overall p p π^- distribution in Figure 25a. Displayed for comparison are the OPEM and phase space predictions, both normalized to the number of events. All three mass distributions show a shifting towards high invariant mass relative to the phase space prediction, consistent with the peripheral nature of the protons and proton-pion combinations. The p p and p p π^+ distributions seem particularly well described by the OPEM. We observe no significant enhancements above the OPEM curve or the general shape of the distributions. In particular there is no evidence for the resonance suggested by Kidd et al.[3] at a p p π^+ mass of 2520 MeV. Alexander et al.[4] at an incident momentum of 5.5 BeV/c and Almeida et al.[7] at 10 BeV/c also observe no evidence for a resonance at this mass. The resonance at 2130 MeV reported by Brunt et al.,[41] if real, has Ispin = 1. Without violating Ispin it could be produced in our experiment and, depending on the production mechanism, decay into p p or p p π^-. Neither the p p nor the p p π^- mass distribution show an enhancement at 2130 MeV. However, the absence of an effect in a p p experiment does not necessarily constitute evidence against a resonance in a p d experiment since the production mechanisms would presumably be quite different (Baryon

exchange in the p p experiment as opposed to meson exchange in the p d experiment.

The decay of resonances with Baryon number = 2 into N^{*++} p may be at least contemplated. Thus we show the N^{*++} p mass distribution in Figure 24b. This mass distribution has a broad peaking centered roughly at 3700 MeV. However the OPEM curve peaks at about the same mass as the data, making a resonance interpretation of the peak unlikely. Further evidence against a resonance interpretation is provided by the presence of the peak in the distribution with the cut on the production cosine to the N^{*++} (shaded histogram). That is, the decay of a relatively high mass N^{*++} p resonance would not be expected to yield peripheral N^{*++} 's. We conclude that the peak is kinematic in origin.

The p p π^- mass distribution (Figure 25a) generally agrees with the OPEM prediction but does show an enhancement above the OPEM curve at the upper limit of phase space, centered at about 3800 MeV. The probable origin of this enhancement may be understood in terms of the previously discussed resonance production at low p π^+ π^- mass. Figure 25b shows the p p π^- mass for the restriction that at least one p π^+ π^- combination has a mass less than

1800 MeV. This latter p p π^- mass distribution is narrower than the overall distribution and peaks at about the same high mass. Thus we attribute the enhancement in the p p π^- distribution to the excess of events (relative to the OPEM) at low p π^+ π^- mass. As further evidence against a resonance interpretation we refer to the p p π^- mass distribution of Almeida et al. at 10 BeV/c.[7] This distribution shows a similar peak above the prediction of a similar OPEM calculation. However, the center of the peak is shifted to roughly 4225 MeV, consistent with the higher phase space limit of the 10 BeV/c experiment but not consistent with the production of a resonance.

F. The π^+ π^- System

The overall π^+ π^- invariant mass distribution is shown in Figure 26a together with the predictions of the OPEM and phase space. The model describes the general shift towards low mass relative to phase space. Noticeable enhancements appear above the OPEM curve at about 700 MeV and between roughly 350 and 600 MeV. An excess of events (above the OPEM curve) at low mass is expected kinematically as a result of resonance production at low p π^+ π^- mass. To demonstrate that the excess between 350 and 600 MeV may be attributed to such resonance production we

Figure 26

$\pi^+ \pi^-$ mass distributions. The dashed curve is phase space. The solid curves are the predictions of the OPEM (A = 3) normalized to the number of events in the overall distribution.

(a) All events.

(b) Those events for which at least one p $\pi^+ \pi^-$ combination has a mass less than 1800 MeV.

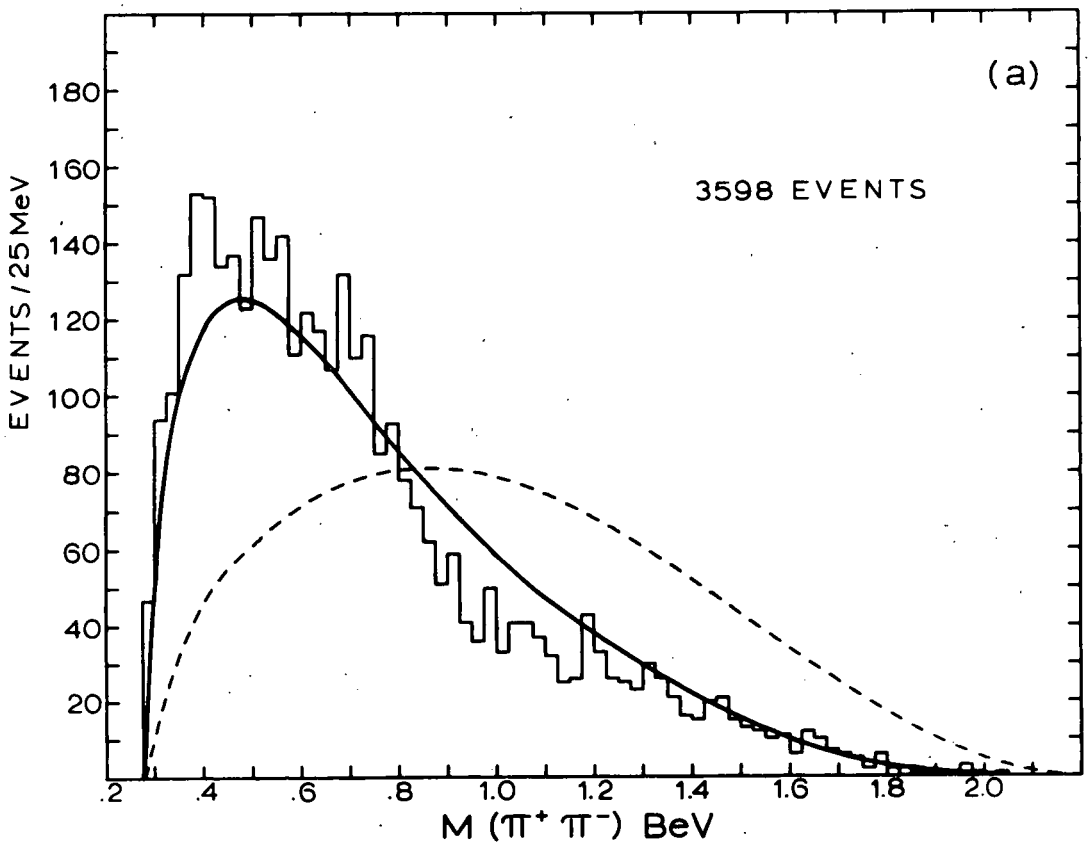
(a)
3598 EVENTS
EVENTS / 25 MeV
180
160
140
120
100
80
60
40
20
.2
.4
.6
.8
1.0
1.2
1.4
1.6
1.8
2.0
M (π⁺ π⁻) BeV

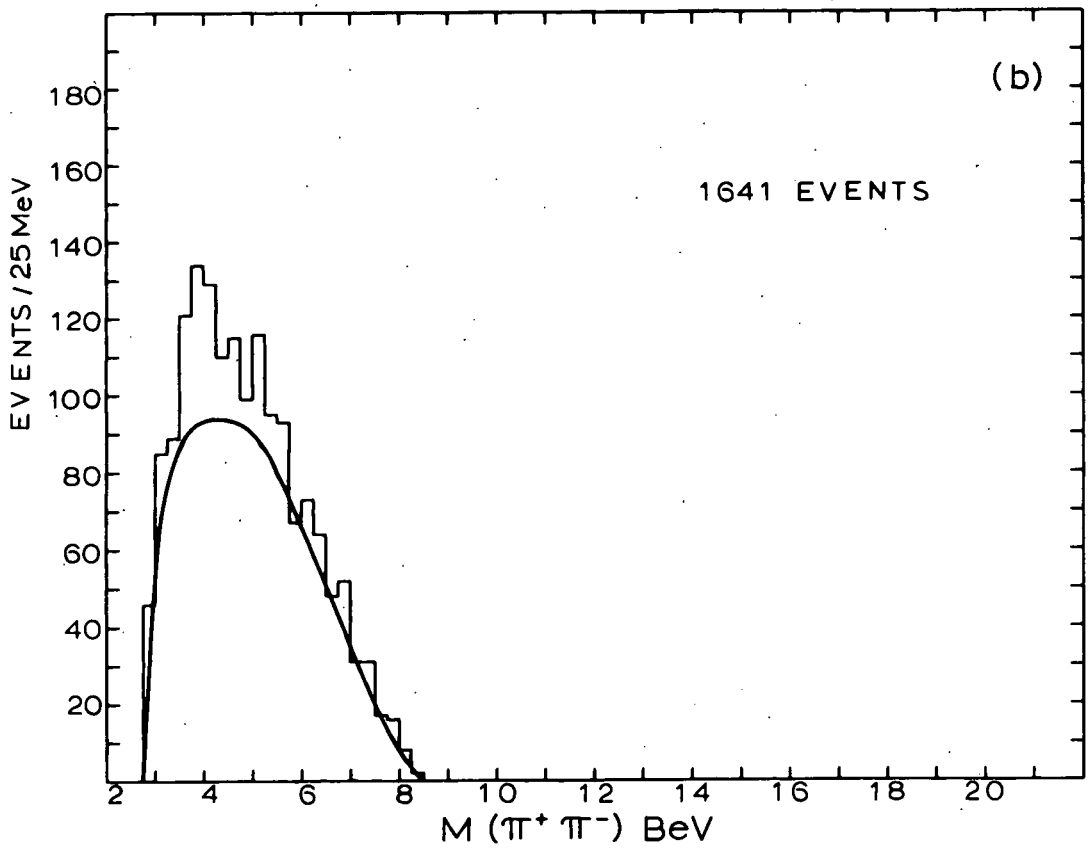
(b)
1641 EVENTS
EVENTS / 25 MeV
180
160
140
120
100
80
60
40
20
2
4
6
8
10
12
14
16
18
20
M (π⁺ π⁻) BeV

show, in Figure 26b, the $\pi^+ \pi^-$ mass distribution for events with at least one p $\pi^+ \pi^-$ combination with a mass less than 1800 MeV. For this distribution the excess of events above the OPEM curve between 350 and 600 MeV is seen to correspond roughly to the excess in the overall distribution.

Consider the enhancement at 700 MeV. Taking only the events in the three bins from 675 - 750 MeV, the enhancement is roughly a three standard deviation effect above the OPEM background (normalized to the number of events in the histogram, as shown in Figure 26a). While of limited statistical significance, the enhancement could be evidence for the production of the ρ meson or of the elusive[42,43] ϵ^o (also called S^o). If it exists, the ϵ^o would be a $T = 0$, $J^P = 0^+$ resonance of positive G-parity at about the same mass as the ρ. As explained below, the ϵ^o could be produced by a certain "double peripheral" mechanism while the ρ could not. The absence, in our data, of a large signal at the mass of the ρ is characteristic of the p p $\pi^+ \pi^-$ final state; other studies report[4,6,7] little or no evidence for the ρ.

Given the enhancement at 700 MeV and some understanding of the background (via the OPEM), we examine

possible production mechanisms in an attempt to increase any ρ (or ϵ^o) signal relative to the background. For ρ production we hypothesize

$$p\ p \rightarrow p\ N^{*+}$$
$$\qquad\qquad\quad \lfloor\!\rightarrow p\ \rho$$
$$\qquad\qquad\qquad\quad \lfloor\!\rightarrow \pi^*\ \pi^-$$

That such a hypothesis might be relevant is suggested by the work of Chinowsky et al.[44] In a study of p p interactions at 6.0 BeV/c, enhancements are observed at about 2.0 BeV in the mass distributions of the particles in parentheses in the final states n ($p\ \pi^+\ \pi^+\ \pi^-$), p ($p\ \pi^+\ \pi^-\pi^o$), p ($\Lambda\ \pi\ K$), and n ($\Lambda\ \pi^+\ K^+$). In an analysis of the neutron final states the enhancements (in the neutron states) are interpreted as a $T = 3/2$ resonance with the N*(1950) of π^+ p scattering as the likely candidate. Chinowsky et al. isolate the decay $N^{*++}(1236)\ \rho^o$ and suggest that N ρ should be one of the major inelastic decay modes. If the enhancement in the proton final states indicates production of the same resonance then we might expect to observe the decay p ρ^o in the p ($p\ \pi^+\ \pi^-$) final state.

Consider the angles defined in Figure 27a. For the hypothesized mechanism (and in the absence of interference)

Figure 27

(a) Definition of angles θ_1 and θ_2 and the $\cos\theta_1$ distribution.

(b) $\cos\theta_2$ distribution for $\cos\theta_1 \leq 0$.

(c) Mass distribution for both $p\,\pi^+$ combinations for those events with at least one $p\,\pi^+\,\pi^-$ combination having $\cos\theta_1 \leq 0$ and $\cos\theta_2 \geq 0$.

The solid curves are the predictions of the OPEM (A = 3) normalized to the overall number of combinations.

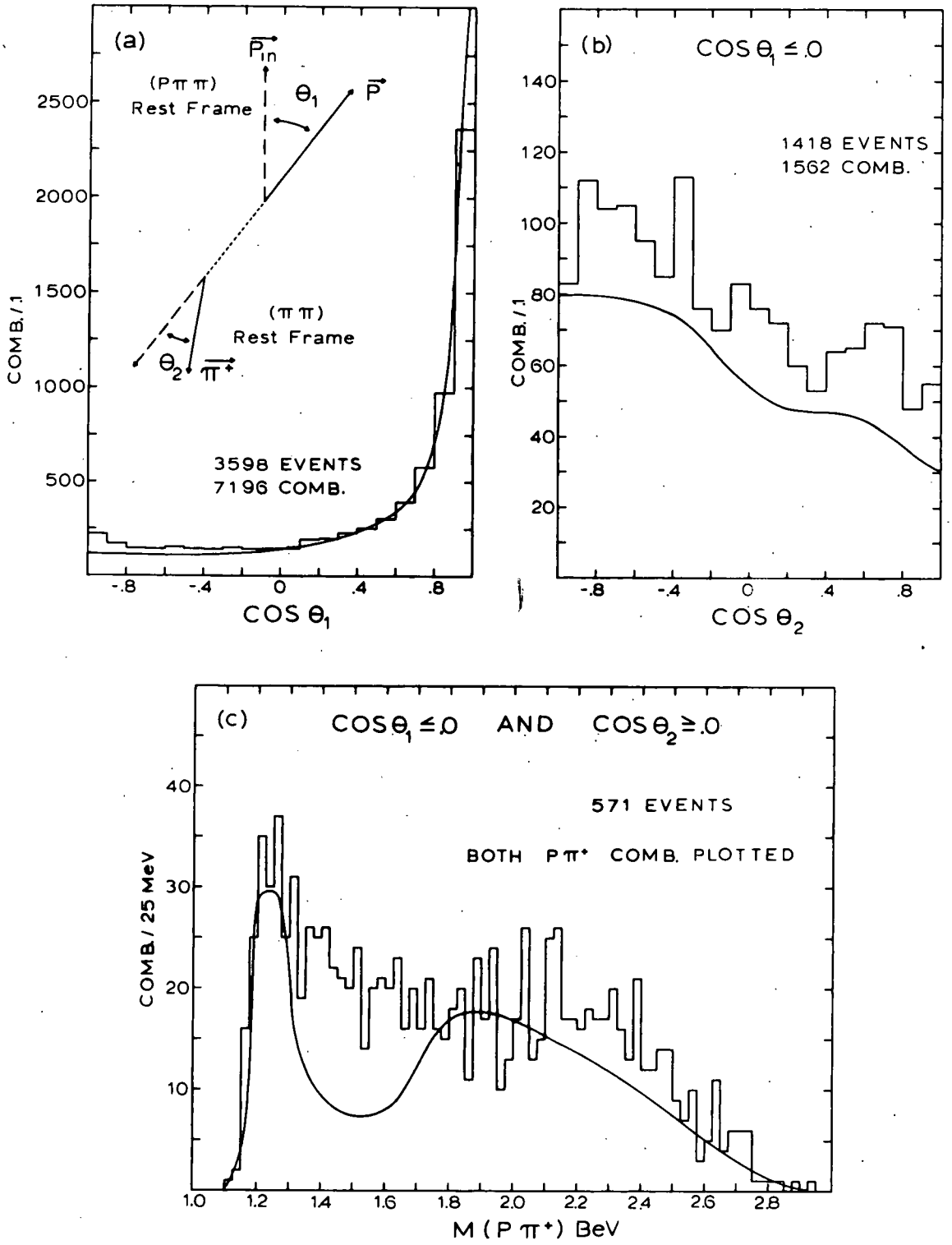
(a)
$\vec{P}_{in}$
(Pππ)
Rest Frame
θ_1
$\vec{P}$
(ππ)
Rest Frame
θ_2
$\vec{\pi}^+$
3598 EVENTS
7196 COMB.
COMB./.1
COS θ_1
(b)
COS $\theta_1 \leq .0$
1418 EVENTS
1562 COMB.
COMB./.1
COS θ_2
(c)
COS $\theta_1 \leq .0$ AND COS $\theta_2 \geq .0$
571 EVENTS
BOTH $P\pi^+$ COMB. PLOTTED
COMB./25 MeV
M ($P\pi^+$) BeV

the distributions of cos θ_1 and cos θ_2 will be symmetric about zero. Figure 27a shows the cos θ_1 distribution for all p π^+ π^- combinations. As predicted by the OPEM (solid curve) the distribution peaks strongly towards +1. We should then enhance any contribution from the above mechanism (relative to the one pion exchange background) by selecting those p π^+ π^- combinations with cos $\theta_1 \leq 0$. For this selection, Figure 27b shows the cos θ_2 distribution. This distribution is skewed somewhat to negative values. For such values the π^+ will be traveling more or less in the same direction as the proton and we thus associate the skewing with $N^{*++}(1236)$ production. The selection cos $\theta_2 \geq 0$ (in addition to the selection on cos θ_1) may then be expected to further enhance the relative contribution from the hypothesized mechanism. Figure 27c shows the mass distribution for both p π^+ combinations for those events satisfying the above selection criteria. The N^{*++} peak has been considerably reduced compared to the overall distribution (Figure 5a); an excess of combinations (relative to the OPEM curve) in the mass region 1.35 - 1.7 BeV, seen to some extent in the overall distribution, has been emphasized. Having reduced the N^{*++} contribution and perhaps the one pion exchange

contribution, we plot in Figure 28 the $\pi^+ \pi^-$ mass versus the mass of those p $\pi^+ \pi^-$ combinations satisfying the above selection criteria. The shaded histograms show the contribution to the projections from the events that have both combinations satisfying the criteria. The excess of combinations (relative to the OPEM curve) at $\pi^+ \pi^-$ mass less than 600 MeV is, as discussed above, seen to be associated with the p $\pi^+ \pi^-$ resonances with mass less than 1800 MeV. The 700 MeV enhancement appears relatively clearly above the OPEM curve, but at a mass somewhat lower than generally accepted for the ρ (for comparison, a nominal ρ band of mass = 770 MeV and width = 120 MeV is shown). The $\pi^+ \pi^-$ combinations in the region of the enhancement are distributed (on the scatter plot of Figure 28) rather uniformly between, roughly, a p $\pi^+ \pi^-$ mass of 1650 and 2100 MeV. Correspondingly, the p $\pi^+ \pi^-$ mass projection shows a broad excess (above the OPEM curve) of events in that mass region. With the exception of the peak at 1700 MeV, no real resonant-like structure is observed. The 1700 MeV peak does not show a particularly strong concentration of events in the region of the 700 MeV $\pi \pi$ enhancement. We conclude that if the enhancement corresponds to the ρ, our data show no strong indication that the ρ results from the decay of a N*.

Figure 28

$\pi^+ \pi^-$ mass versus mass of p $\pi^+ \pi^-$ combinations with $\cos \theta_1 \leq 0$ and $\cos \theta_2 \geq 0$. The smooth curves on the projections are the predictions of the OPEM (A = 3) normalized to the overall number of combinations. The shaded distributions show the contribution to the projections from events with both combinations satisfying the restrictions on $\cos \theta_1$ and $\cos \theta_2$.

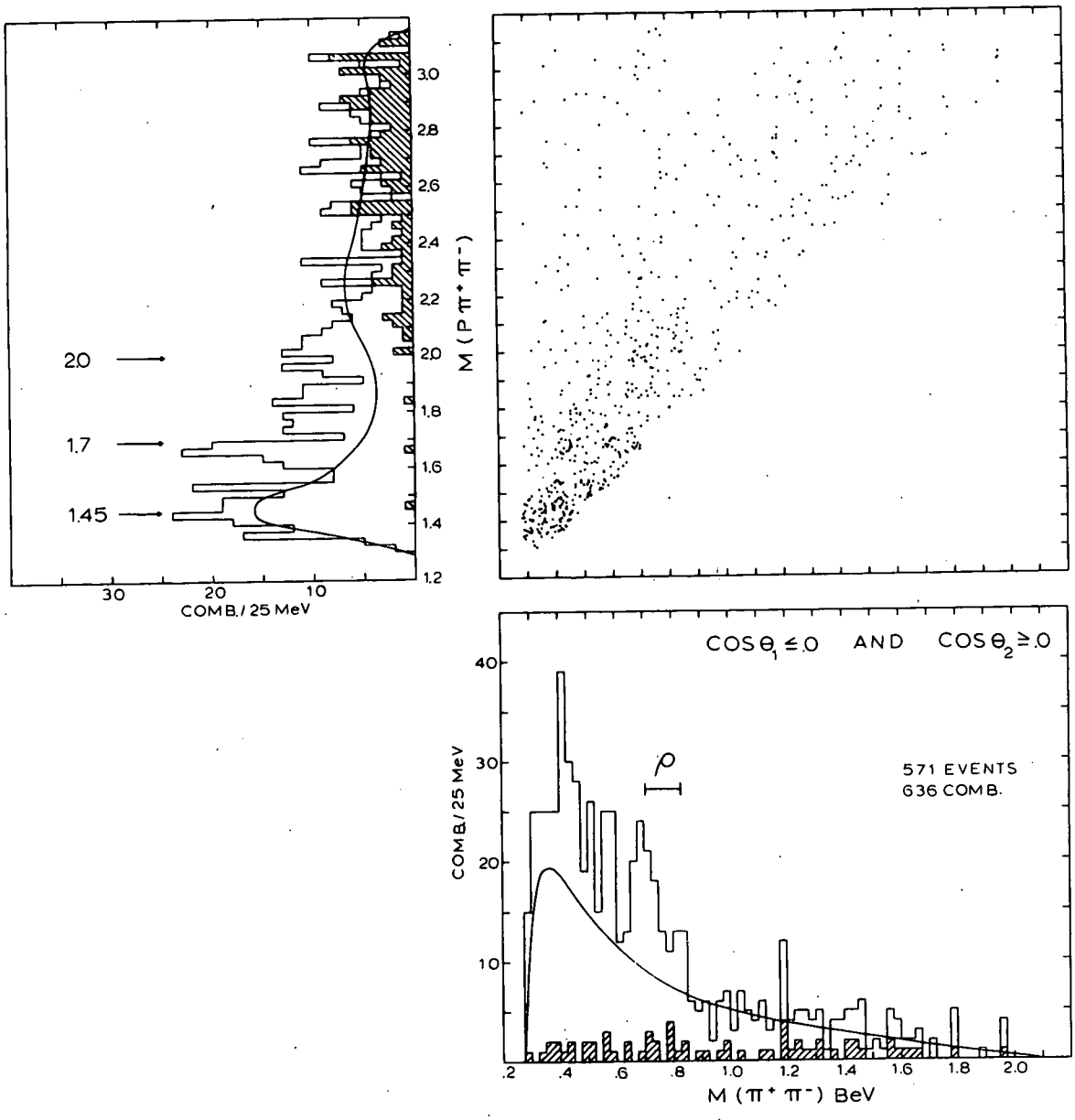
20
1.7
1.45
30
20
10
COMB./25 MeV
3.0
2.8
2.6
2.4
2.2
2.0
1.8
1.6
1.4
1.2
M(Pπ⁺π⁻)
COSθ₁≤0 AND COSθ₂≥0
ρ
571 EVENTS
636 COMB.
40
30
20
10
COMB./25 MeV
.2
.4
.6
.8
1.0
1.2
1.4
1.6
1.8
2.0
M(π⁺π⁻) BeV

An alternative explanation for the 700 MeV enhancement could be production of the ϵ^o. That the ϵ^o might be produced by a mechanism that excluded ρ production may be understood by considering the "double peripheral" exchange diagram in Figure 29a. (In this figure $(\pi\pi)$ designates a $\pi\ \pi$ resonance). Saperstein and Shrauner[46] have performed an absorption model calculation corresponding to this diagram with the ρ as the resonance. They suggest that such a diagram should be the dominant source of ρ production in $N\ N \rightarrow N\ N\ \pi\ \pi$ reactions. In our particular reaction the exchanged pions would be π^o's. Since the ρ does not couple to $\pi^o\ \pi^o$, it could not be produced in this experiment by such a diagram. However, the ϵ^o, if it exists, does couple to $\pi^o\ \pi^o$ and thus could be produced.

To examine the possibility of ϵ^o production by the diagram of Figure 29a, we exploit the spinless character of this meson. Let θ be the angle in the $\pi^+\ \pi^-$ rest frame between one of the hypothetical exchanged π^o's and the outgoing π^+. As predicted by the OPEM, the cos θ distribution* for all events peaks towards +1 (Figure 29b). Since any contribution from the ϵ^o will be isotropic we

---

*Since one may not distinguish between the two exchanged pions, the distribution has been folded about zero.

Figure 29

(a) "Double peripheral" exchange diagram.

(b) Distribution of cos θ. The angle θ is defined in the text.

(c) Unshaded. $\pi^{\pm}$ π^- mass distribution for cos $\theta \leq .5$. Shaded. π^+ π^- mass distribution for cos $\theta \leq .5$ and π^+ π^- longitudinal momentum in the overall center of mass less than 300 MeV.

The smooth curves are the predictions of the OPEM (A = 3) normalized to the overall number of combinations.

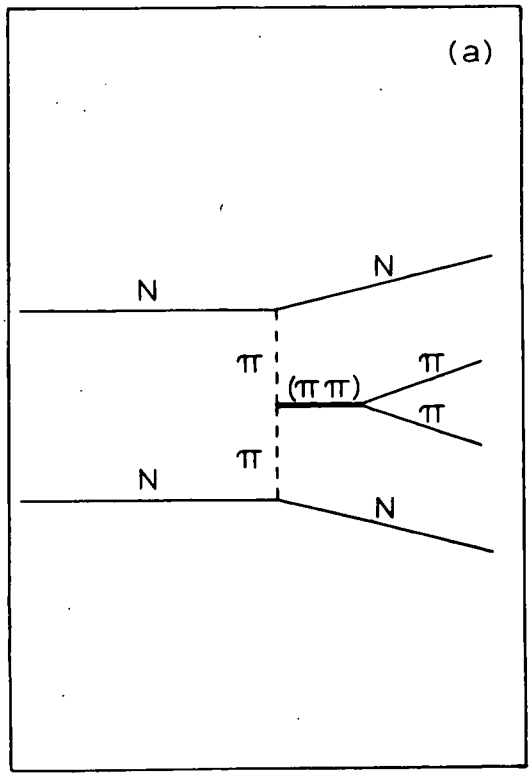
(a)
N
N
π
(π π)
π
π
π
N
N

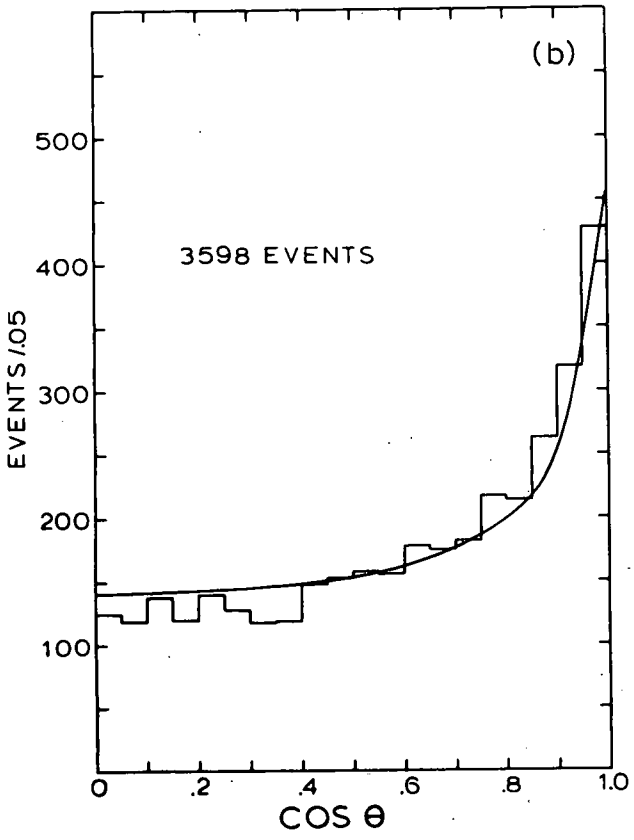
(b)
3598 EVENTS
EVENTS/.05
500
400
300
200
100
0
.2
.4
.6
.8
1.0
COS θ

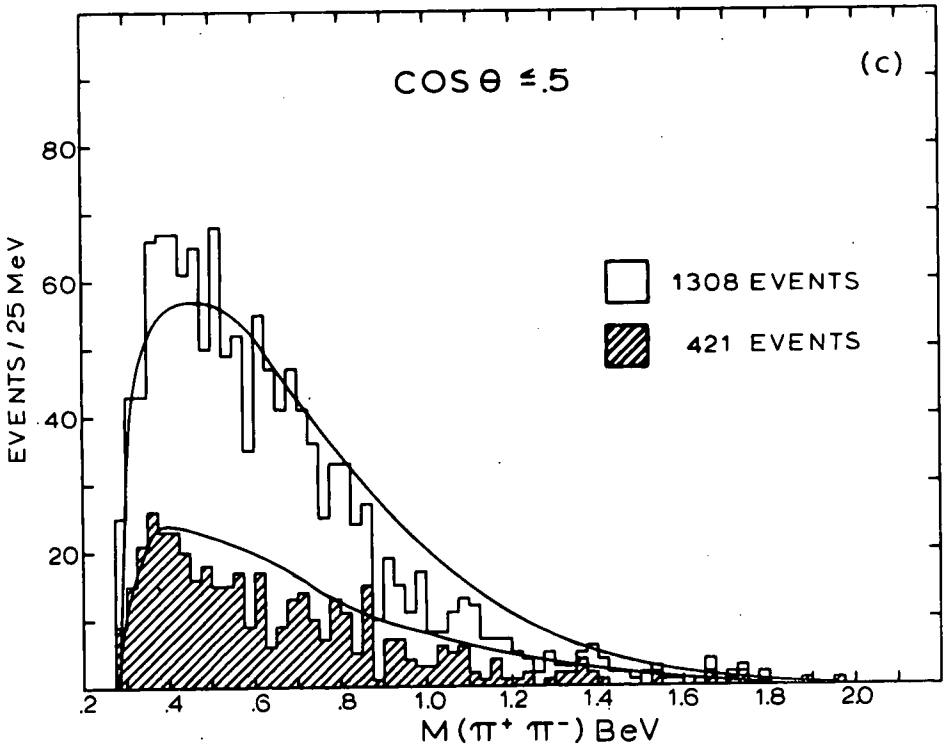
COS θ ≤.5
(c)
1308 EVENTS
421 EVENTS
EVENTS / 25 MeV
80
60
40
20
.2
.4
.6
.8
1.0
1.2
1.4
1.6
1.8
2.0
M (π⁺ π⁻) BeV

should increase the signal to background by selecting events with $\cos\theta \leq .5$. The unshaded histogram of Figure 29c shows the $\pi^+ \pi^-$ mass distribution and the corresponding OPEM prediction for this selection. The shaded histogram is for an additional restriction designed to take advantage of the double peripheral character of the proposed mechanism. Specifically, the restriction is that the longitudinal momentum of the $\pi^+ \pi^-$ combination in the overall center of mass be less than 300 MeV/c. The distributions of Figure 29c show that the above selection criteria have not produced an isolation of the 700 MeV enhancement relative to the general shape predicted by the OPEM. We conclude that there is no indication that the 700 MeV enhancement corresponds to the production of the ϵ^o by a double peripheral process.

LIST OF REFERENCES

1. M. W. Firebaugh, "Strange Particle Production in 8 BeV/c Proton-Proton Interactions", (Ph.D. Thesis), University of Illinois (1966).

2. M. Firebaugh, G. Ascoli, E. L. Goldwasser, R. D. Sard, and J. Wray, "Strange-Particle Production in 8 BeV/c Proton-Proton Interactions", (To be Published in Physical Review).

3. J. Kidd, L. Mandelli, V. Pelosi, S. Ratti, A. Sichirollo, L. Tallone, F. Conte, and G. Tomasini, Phys. Letters 16, 75 (1965).

4. G. Alexander, O. Benary, G. Czapek, B. Haber, N. Kidron, B. Reuter, A. Shapira, E. Simopoulou and G. Yekutieli, Phys. Rev. 154, 1284 (1967).

5. E. Gellert, G. A. Smith, S. Wojcicki, E. Colton, P. E. Schlein, and H. K. Ticho, Phys. Rev. Letters 17, 884 (1966).

6. J. Le Guyader, G. Kayas, M. Sene, T. P. Yiou, J. Allitti, N. T. Diem, G. Smadja, J. Ginestet, D. Manesse, and T. H. Anh, "PP to PP$\pi^+\pi^-$ Interactions at 8.1 GeV/c", Submitted to Heidelberg International Conference on Elementary Particles (1967).

7. S. P. Almeida, J. G. Rushbrooke, J. H. Scharenguivel, M. Behrens, V. Blobel, T. Borecka, H. C. Dehne, J. Diaz, G. Knies, R. Schafer, and W. P. Swanson, "Four-Prong Events in 10-GeV/c PP Interactions", Submitted to Berkeley International Conference on High Energy Physics (1966).

8. S. P. Almeida, J. G. Rushbrooke, J. H. Scharenguivel, M. Behrens, V. Blobel, H. C. Dehne, J. Dias, R. Schafer, and W. P. Swanson, Nuovo Cimento 50, 1000 (1967).

9. R. W. Hanft, "Strange Particle Production in π^-p and π^+n Interactions at 2.5 GeV/c" (Ph.D. Thesis), University of Illinois (1967).

10. W. Galbraith, E. W. Jenkins, T. F. Kycia, B. A. Leontic, R. H. Phillips, A. L. Read, and R. Rubenstein, Phys. Rev. 138, B913 (1965).

11. E. Ferrari, Nuovo Cimento 30, 240 (1963).

12. E. Ferrari and F. Selleri, Nuovo Cimento Suppl. 24, 453 (1962).

13. E. Ferrari and F. Selleri, Nuovo Cimento 27, 1450 (1963).

14. F. Selleri, Nuovo Cimento 40, 236 (1965).

15. J. D. Jackson, Nuovo Cimento 34, 1644 (1964).

16. A. H. Rosenfeld, N. Barash-Schmidt, A. Barbaro-Galtieri, L. R. Price, P. Soding, C. G. Wohl, M. Roos, and W. J. Willis, Rev. Mod. Phys. 39, 1 (1968).

17. A Donnachie, R. G. Kirsopp, and C. Lovelace, Phys. Letters 26B, 161 (1968).

18. R. T. Deck, Phys. Rev. Letters 13, 169 (1964).

19. M. L. Good and W. D. Walker, Phys. Rev. 120, 1857 (1960).

20. M. Ross and Y. Y. Yam, Phys. Rev. Letters 19, 546 (1967).

21. D. R. O. Morrison, Phys. Rev. 165, 1699 (1968).

22. L. D. Roper, Phys. Rev. Letters 12, 340 (1964).

23. P. Bareyre, C. Bricman and G. Villet, Phys. Rev. 165, 1730 (1968).

24. B. H. Bransden, P. J. O'Donnell, and R. G. Moorhouse, Phys. Rev. 139, B1566 (1965).

25. P. G. Thurnauer, Phys. Rev. Letters 14, 965 (1965).

26. J. M. Namyslowski, M. S. K. Razmi, and R. G. Roberts, Phys. Rev. 157, 1328 (1967).

27. D. Morgan, Phys. Rev. 166, 1731 (1968).

28. E. W. Anderson, E. J. Bleser, G. B. Collins, T. Fujii, J. Menes, F. Turkot, R. A. Carrigan Jr., R. M. Edelstein, N. C. Hien, T. J. McMahon, and I. Nadelhaft, Phys. Rev. Letters 16, 855 (1966).

29. I. M. Blair, A. E. Taylor, W. S. Chapman, P. I. P. Kalmus, J. Litt, M. C. Miller, D. B. Scott, H. J. Sherman, A. Astbury, and T. G. Walker, Phys. Rev. Letters 17, 789 (1966).

30. K. J. Foley, R. S. Jones, S. J. Lindenbaum, W. A. Love, S. Ozaki, E. D. Platner, C. A. Quarles, and F. H. Willen, Phys. Rev. Letters 19, 397 (1967).

31. R. B. Bell, D. J. Crennel, P. V. Hough, U. Karshon, K. W. Lai, J. M. Scarr, T. G. Schumann, I. O. Skillicorn, R. C. Strand, A. H. Bachman, P. Baumel, R. M. Lea, and A. Montwill, Phys. Rev. Letters 20, 164 (1968).

32. W. P. Dodd, R. B. Palmer, and N. P. Samios, "Observation of the N*(1400) Resonance in K^+p Interactions at 3.0 GeV/c", Brookhaven National Laboratory Preprint (1968).

33. J. W. Lamsa, N. M. Cason, N. N. Biswas, I. Derado, T. H. Groves, V. P. Kenney, J. A. Poirer, and W. D. Shepard, Phys. Rev. 166, 1395 (1968).

34. A Fridman, G. Maurer, A. Michalon, B. Schiby, R. Strub, C. Zeck, and P. Cuer, Phys. Letters 23, 386 (1966).

35. S. L. Adelman, Phys. Rev. Letters 13, 555 (1964).

36. S. L. Adelman, Phys. Rev. Letters 14, 1043 (1965).

37. W. D. Walker, M. A. Thompson, W. J. Robertson, B. Y. Oh, Y. Y. Lee, R. W. Hartung, A. F. Garfinkel, A. R. Erwin, and J. D. Davis, Phys. Rev. Letters 20, 133 (1968).

38. M. N. Focacci and G. Giacomelli, "Pion-Proton Elastic Scattering", Cern Report 66-18 (1966).

39. J. D. Jackson in High Energy Physics Les Houches, Edited by De Witt and Jacob (Gordan-Breach, 1965, p. 326).

40. F. U. Dyson and N. H. Xuong, Phys. Rev. Letters 13, 815 (1964).

41. D. C. Brunt, M. J. Clayton, and B. A. Westwood, Phys. Letters 26B, 317 (1968).

42. G. Goldhaber in Proceedings of the XIII International Conference on High Energy Physics, Berkeley, 1966 (University of California, 1967, p. 103).

43. I. Butterworth in Proceedings of the Heidelberg International Conference on Elementary Particles, 1967 (North-Holland, 1968, p. 11).

44. W. Chinowsky, P. Condon, R. R. Kinsey, S. Klein, M. Mandelkern, P. Schmidt, J. Schultz, F. Marting, M. L. Perl, and T. H. Tan, "Rare Decay Modes of N*(1950)", UCRL-17651 Rev. (1968).

45. A. M. Saperstein and E. Shrauner, Phys. Rev. 163, 1559 (1967).

46. L. Ferretti, E. Manaresi, G. Puppi, A. Ranzi, and G. Quareni, Nuovo Cimento 1, 1238 (1955).

47. J. Ashkin, J. P. Blaser, F. Feiner, and M. O. Stern, Phys. Rev. 101, 1149 (1956).

48. J. Ashkin, J. P. Blaser, F. Feiner, and M. O. Stern, Phys. Rev. 105, 724 (1957).

49. P. M. Ogden, D. E. Hagge, J. A. Helland, M. Banner, J. Detoeuf, and J. Teiger, Phys. Rev. 137, B1115 (1965).

50. J. A. Helland, T. J. Devlin, D. E. Hagge, M. J. Longo, B. J. Moyer, and C. D. Wood, Phys. Rev. 134, B1062 (1964).

51. V. Cook, B. Cork, W. R. Holley, and M. L. Perl, Phys. Rev. 130, 762 (1963).

52. M. L. Perl, L. W. Jones, and C. C. Ting, Phys. Rev. 132, 1252 (1963).

53. Aschen-Berlin-Birmingham-Bonn-Hamburg-London (I.C.)-Munich Collaboration, Phys. Letters 10, 248 (1961).

54. Y. A. Budagov, S. Wiktor, V. P. Dzhelepov, P. F. Yermolov, and V. I. Moskalev, Nucl. Phys. 22, 226 (1961).

55. H. R. Rugge and O. T. Vik, Phys. Rev. 129, 2300 (1963).

56. J. A. Helland, T. J. Devlin, D. E. Hagge, M. J. Longo, B. J. Moyer, V. Perez-Mendez, and C. D. Wood, Phys. Rev. 134, B1079 (1964).

57. F. Grard, G. Macleod, L. Momtanet, M. Cresti, R. Barloutaud, C. Choquet, J. M. Gaillard, J. Heughebaert, A. Leveque, P. Lehmann, J. Meyer, and D. Revel, Nuovo Cimento 22, 193 (1961).

58. L. Bertanza, R. Carrara, A. Drago, P. Franzini, I. Mannelli, G. V. Silverstrini, and P. H. Stoker, Nuovo Cimento 19, 467 (1961).

59. R. J. Easterling, R. E. Hill, Norman E. Booth, S. Suwa, and A. Yokosawa, "π^- p Elastic Scattering Between 1.7 and 2.5 GeV/c", EFINS 66-29 (1966).

APPENDIX. OPEM INPUT DATA

We discuss briefly the method used to express the π^+ p and π^- p elastic differential cross sections in a form suitable for input to the Monte-Carlo computer program. With the notation of Section IV, B the differential cross section may be written

$$\frac{d\sigma}{d\Omega}(\omega,\Omega) = \sigma(\omega)\cdot G(\omega,\cos\theta)/2\pi$$

with $$\int_{-1}^{+1} G(\omega,\cos\theta)\,d\cos\theta = 1$$

$\sigma(\omega)$ is the total elastic π p cross section. $G(\omega, \cos\theta)$ gives, at a particular ω, the scattering angular distribution in the π p center of mass.

Focacci and Giacomelli[38] have plotted experimental values for the total elastic cross sections together with a smooth curve drawn thru the experimental points. To express $\sigma(\omega)$, the smooth curves were reduced to tabular form with values of ω closely (widely) spaced in regions of rapidly (slowly) varying cross section.

References 46 - 59 give π p elastic differential cross sections at values of ω spanning the phase space limits of our experiment. From these references, differential cross sections were selected at values of ω closely (widely) spaced when the angular part of the cross section was rapidly (slowly) varying with ω. A selected differential cross section at a given ω was reduced to tabular form (typically from a smooth curve drawn thru experimental points) and normalized to express $G(\omega, \cos\theta)$ at that value of ω.

The computer program used the tables for $\sigma(\omega)$ and $G(\omega, \cos\theta)$ in a manner equivalent to obtaining $d\sigma/d\Omega(\omega,\Omega)$ at arbitrary ω and $\cos\theta$ by linear interpolation of the tables.

VITA

Donald Frank Grether was [redacted] He graduated from Fairview High School in Dayton, Ohio in June, 1958. He attended Miami University in Oxford, Ohio from September, 1958 to his graduation in June, 1962 with a Bachelor of Arts with Honors degree in Physics.

He began his graduate studies in September, 1962 at the University of Illinois. He received a Master of Science degree in Physics in February, 1964. During his studies he has held teaching and research assistantships in the Department of Physics.